Crack Closure Measurement by the Optical Method of Caustics

Thesis

CRACK CLOSURE MEASUREMENT BY THE OPTICAL METHOD OF CAUSTICS

A THESIS SUBMITTED TO THE
MATERIALS DISCIPLINE OF
THE OPEN UNIVERSITY
FOR THE DEGREE OF
DOCTOR OF PHILOSOPHY

by

IAN WALLHEAD

(BSc CPhys MInstP)

November 1994

Date of submission : 15th November 1994
Date of award : 14th March 1995

I.R. Wallhead
The Open University

PhD Thesis
November 1994

ABSTRACT

This work presents an investigation into the applicability of the optical method of caustics as a tool to study the role of crack closure in fatigue crack propagation. The technique has been applied to centre-cracked panel specimens of 2024-T3 aluminium alloy under a range of fatigue loading conditions which are expected to induce crack closure to varying degrees.

The optical method of caustics is an experimental technique which is primarily applied to the measurement of stress intensity factors by quantifying out of plane surface deformations local to the crack tip. In this work the technique has been used to measure stress intensity factors throughout various fatigue cycles so as to quantify the range of stress intensity factors actually experienced by the crack tip, and thus determine ΔK_{eff}. In order to accomplish this the technique has required substantial development both to measure low stress intensity factors where closure effects are known to predominate, and to measure them with sufficient resolution to quantify ΔK_{eff}.

These improvements comprise the application of an accurately collimated laser (with output beam wavefront error of approximately $\lambda/5$ at 633nm), the specification of optically flat specimen surfaces (with a surface form error of approximately $\lambda/4$ at 633nm over the measurement area), together with the use of a CCD camera image processing system for recording and measuring the caustics. Most importantly, however, the experimental arrangement of the technique has been dramatically modified for this study to produce a "split beam caustics" set-up which has been found to substantially increase the accuracy of the technique.

Using these developments it has been shown that the method of caustics can detect premature material contact in the wake of a fatigue crack. This is manifest as an increased tensile stress field ahead of the crack which can exist even under a small far field compressive loading. However, the quantification of crack closure using this technique is not in agreement with other experimental evidence or theoretical models. Furthermore, in stark contradiction with contemporary theory, fatigue crack growth rate is found to be independent of the stress field range around the crack tip (conventionally described in terms of a stress intensity factor range, ΔK) under certain conditions, such following a single tensile overload.

Close observation of the crack tip stress field under conditions of closure has revealed that its spatial function is such that it cannot truly be expressed in terms of a stress intensity factor which assumes the stress field to vary as $K/\sqrt{2\pi r}$. Consequently, it is concluded that successful application of ΔK_{eff} as the fatigue crack driving force is derived on phenomenological rather than physical grounds.

ACKNOWLEDGEMENTS

I would like to express my sincere gratitude to my supervisor, Dr. Lyndon Edwards, for his invaluable guidance and support throughout this project. Without his motivation (not to mention optimism!) this thesis, I'm sure, would have taken years to complete. I would also like to thank Dr. Peter Poole for valuable and inspiring discussions on the subjects of fatigue and fracture mechanics. Special thanks are also due to Dr. Salih Güngör whose friendship and patient assistance throughout the early part of the project undoubtedly accelerated my learning curve in this field of research. My thanks are also due to Dr. Hayder Ahmad for his friendship and discussions on subjects too numerous to mention.

I would like to offer my gratitude to Professor Bill Plumbridge for provision of the laboratory facilities, and to the Defence Research Agency (Farnborough) and the Department for Trade and Industry for financial support for this project.

I would also like to thank the research, technical and secretarial staff of the Materials Discipline for their varied assistance throughout this project.

Lastly, my deepest thanks go to my future wife, Dr. Karen Littleton, for her continual love and support over the years and without whom this research would never have begun, let alone finished.

Ian Wallhead

November 1994

PREFACE

This thesis is submitted for the degree of Doctor of Philosophy of The Open University. It is an account of the research performed in the Materials Discipline of the Faculty of Technology between August 1991 and October 1994 under the supervision of Dr. Lyndon Edwards. The work reported is original and has been performed without collaboration. None of this work has been submitted for a degree or other qualification at this or any other university. Where the work of other authors has been included in the text, this has been acknowledged and its source given in the List of References at the end of the thesis.

Certain parts of the research conducted for this thesis have been published (or accepted for publication) in academic journals as the following articles, or presented at (and published in the proceedings of) the following conferences:

Journal Articles

1. I. R. Wallhead and L. Edwards. "Letter to the Editor: Comments on 'Techniques of Optical Caustics Photography' by D.A. Meyn". Engineering Fracture Mechanics, Vol 46, No 3, pp 537-540, 1993.

2. I. R. Wallhead, S. Güngör and L. Edwards. "Optimisation of the Optical Method of Caustics for the Determination of Stress Intensity Factors". Optics and Lasers in Engineering, Vol 20, pp 109-133, 1994.

3. I. R. Wallhead and L. Edwards. "High Accuracy Stress Intensity Factor Measurement Using the Optical Method of Reflected Caustics". Engineering Fracture Mechanics, Vol 49, No 5, pp 699-709, 1994.

Conference Publications and Presentations

1. I. R. Wallhead, S. Güngör and L. Edwards. "Characterisation of fatigue crack growth by the optical method of caustics". Fatigue 93, the Fifth International Conference on Fatigue and Fatigue Thresholds, Vol 3, pp 1863-1868, May 3-7, 1993, Montréal,Quebec, Canada, EMAS (Publ) Ltd., Warley, England.

2. I. R. Wallhead, P. Poole and L. Edwards. "On The Measurement Of The Crack Tip Stress Field As A Means Of Determining ΔK_{eff} Under Conditions Of Fatigue Crack Closure". FAA/NASA International Symposium on Advanced Structural Integrity Methods For Airframe Durability And Damage Tolerance, Vol 2, pp 933-946, May 4-6, 1994, Hampton, Virginia, USA, (NASA Conference Publication 3274).

In addition, the results and findings detailed in this thesis have contributed to the following journal and conference papers:

Journal Article

H. Y. Ahmad, I. R. Wallhead and L. Edwards, Technical Note: "Measurement of Mixed Mode Stress Intensity Factors by the Optical Method of Caustics". Fatigue and Fracture of Engineering Materials and Structures, In Press.

Conference Publication and Presentation

S. Güngör, I. R. Wallhead and L. Edwards, "Application of the optical method of caustics to fatigue crack growth". Int. Symposium on Non-Destructive Testing & Stress-Strain Measurement, & FENDT '92, Vol 2, pp 598-603, October 12-14, 1992, Tokyo, Japan.

TABLE OF CONTENTS

LIST OF FIGURES

LIST OF TABLES

LIST OF SYMBOLS

A	coefficients of Newman's (1984) equation (suffixed with 0,1,2 and 3)
a	crack length (half crack length for a central crack). Used by Dugdale (1960) as the crack length plus the extent of plasticity ahead of the crack tip
a_2	constant
Δa	fatigue crack extension from an electro-discharge machined notch
α	constraint factor used to account for a range of stress state conditions between plane stress and plane strain
α	angle between a ray and the normal to the specimen surface
b	lens-to-specimen distance
δb	uncertainty in lens-to-specimen distance measurement
C	empirical constant
c	constant
D	caustic transverse diameter (planar specimen)
D_c	caustic transverse diameter for a beam incident on the concave surface of a deformed specimen
D_v	caustic transverse diameter for a beam incident on the convex surface of a deformed specimen
D'	transverse diameter of the caustic real image
d	specimen thickness
δD	error introduced to caustic diameter as a result of a specimen surface deformation
$\delta D'$	uncertainty in diameter measurement of the caustic real image
Δ	angle between a non-collimated beam ray and the specimen normal
E	Young's modulus
ε	incident beam wavefront error
ε_z	strain component normal to the plane of the specimen
f	lens focal length
ϕ	polar angle
ϕ	diameter of a deformed specimen (i.e. twice the radius of curvature)

grad	gradient of a scalar function
γ	angle between a deformed specimen surface and the x,y plane
h	sagittal height of a deformed specimen (over the incident beam diameter)
J	Jacobian determinant
K	stress intensity factor (subscripts of I, II or III refer to the loading mode)
K_c	critical stress intensity factor
K_{caus}	stress intensity factor determined from a caustic measurement
K_{cl}	stress intensity factor at the point of crack closure
K_{max}	maximum stress intensity factor of a fatigue cycle
K_{min}	minimum stress intensity factor of a fatigue cycle
K_{op}	stress intensity factor at the point of crack opening
K_{theo}	stress intensity factor determined analytically
ΔK	stress intensity factor range
ΔK_{eff}	effective stress intensity factor range
ΔK_{th}	threshold stress intensity factor range
δK	uncertainty in stress intensity factor measurement
l	half length of a central crack as used by Dugdale (1960)
λ	wavelength of incident beam (633nm)
M	imaging lens magnification
m	empirical constant
m	non-collimated beam caustic scaling factor
ν	Poisson ratio
P	load
P_s	period of the specimen surface form error
π	constant, 3.14159
R	stress ratio (K_{min}/K_{max})
R	radius of curvature of an incident beam wavefront
r	radial distance from crack tip
r_0	initial curve radius

r_p	the distance ahead of the crack tip to which the plastic zone extends
r_y	radius of the plastic zone
δr	virtual beam deviation at the caustic reference plane as a result of a specimen surface deformation
S_o	stress at which a fatigue crack first opens (as used by Newman (1984))
S_{max}	maximum stress of a fatigue cycle (as used by Newman (1984))
s	extent of plasticity ahead of the crack tip as used by Dugdale (1960)
σ	stress
σ_o	material flow stress (average between the yield stress and ultimate tensile strength)
σ_y	material yield stress
σ_{UTS}	material ultimate tensile strength
Δs	change in optical path length
θ	polar angle ahead of crack tip
θ	angle to the optical axis of a non-collimated beam ray
U	a measure of the portion of the fatigue cycle over which crack closure occurs ($\Delta K_{eff}/\Delta K$)
U_{caus}	U-factor determined from caustic measurements
U_{CMOD}	U-factor determined from compliance measurements
U_{Elber}	Elber's (1971) prediction of closure based on empirical data
U_{Newman}	Newman's (1984) semi-empirical closure prediction
u	lens-to-caustic reference plane distance
v	lens-to-screen distance
δv	uncertainty in lens-to-screen distance measurement
W	specimen width
w	ray deviation vector in the plane of the caustic
Y	dimensionless geometrical scaling factor to account for finite specimen dimensions
Y_{max}	position of the caustic transverse diameter in the 0,X,Y coordinate system
z_0	caustic reference plane distance

z_1	location of the focus of a non-collimated beam ray in the 0,x,y,z coordinate system
$z_{1(eff)}$	equivalent non-collimated beam focus distance for a collimated beam incident on a deformed specimen surface
z_a	amplitude of the specimen surface deformation
δz_1	uncertainty in the focus location of a non-collimated beam ray
0,X,Y	cartesian coordinate system in the plane of the caustic
0,x,y,z	cartesian coordinate system with the origin at the crack tip on the surface of the specimen. z direction is normal to the plane of the specimen

Chapter 1: INTRODUCTION

The need to design lightweight airframe structures which are durable and damage tolerant has historically provided much motivation for fracture mechanics research. This, together with the more recent demands to extend the lives of ageing aircraft has led to the requirement to improve structural life prediction methodologies.

At the centre of many analytical and numerical life prediction techniques is the concept of fatigue crack closure. Elber's (1970) observation that fatigue crack surfaces contact even under tension-tension cyclic loading has been used to explain many crack growth characteristics, particularly variable amplitude loading and load sequencing effects. Over the years since Elber's discovery of plasticity induced crack closure additional mechanisms have been identified which account for a range of other fatigue phenomena such as environmental effects. Undoubtedly, the crack closure concept has made a significant contribution to the understanding of the mechanics of fatigue crack growth.

This conceptually simple phenomenon, however, has been notoriously difficult to reliably and easily quantify. Various experimental techniques have been developed but correlation between them has not been completely successful under all loading conditions. Consequently, a universal consensus of opinion on how to best measure the effective crack driving force in fatigue remains elusive.

During the 1960's a technique was developed to remotely analyse the stress field in the vicinity of a crack and in doing so provide a direct measure of Irwin's (1958) stress intensity factor, K. This technique, referred to as the optical method of caustics, is centred around the the use of the non-contact and non-destructive properties of an optical beam to evaluate the stress induced out-of-plane displacements around a crack tip. Whilst the technique has been used in a multitude of fracture applications it has rarely been applied to fatigue. The main objective of this work is to utilise the technique to facilitate a thorough study of the crack tip stress field variations during fatigue so as to investigate its applicability to the determination of ΔK_{eff}, universally considered, today, to be the effective crack driving force in fatigue macrocracks. The material used for this work was 2024-T3 aluminium alloy (an aluminium, copper, magnesium alloy widely used in the construction of aircraft wing-skins) configured into centre-cracked panel specimens. This material in such a configuration is of interest to the aerospace industry since it models the common problem of a crack propagating from a fastener hole.

It was recognised during this work that to investigate stress field variations during fatigue would extend the technique beyond its current limits. A significant improvement of the method has been necessary to enable perceived changes in K to be resolvable.

The following chapter provides a background to the principles of fatigue and fracture mechanics. Chapter 3 describes the crack closure concept in detail covering its historical development and its physical significance in fatigue, particularly under variable amplitude loading. In addition, various techniques are outlined which have been developed to attempt to quantify the crack driving force based on the crack closure concept. Finally in this chapter the mathematical modelling of Newman (1981) is described in which the principles of crack closure have been used to predict crack growth rates under constant and variable amplitude loading.

Chapter 4 provides a thorough qualitative and quantitative description of the optical method of caustics from the basics of the optical phenomenon to the derivation of the caustic formula for the application to opaque engineering materials in fracture mechanics. The historical background and the development of the technique spanning three decades is covered together with an illustration of the wide range of conditions to which the method has

been applied. Although this chapter chiefly presents the work of other researchers found in the open literature a section of original analysis is also presented which serves to illustrate how the technique is applied in different optical situations.

Chapter 5 presents the bulk of the original caustic work in the development of the technique for the application to fatigue. The technique is thoroughly analysed from the point of view of improving its experimental accuracy. From this analysis a series of conclusions was drawn which were then put into practice to produce an optimised caustic experimental set-up. This set-up was then used to conduct the experiments presented in Chapter 6.

In Chapter 7 the experimental results are interpreted and compared with other contemporary work in this field. Chapter 8 presents the conclusions drawn from this study.

Chapter 2: THE MECHANICS OF FATIGUE AND FRACTURE

2.1 INTRODUCTION

Fracture Mechanics is the study of components containing some sort of flaw or defect. The subject arises from the fact that most engineering failures are the result of a defect which is either initially present in the component or generated by fatigue damage.

The development of Fracture Mechanics has produced a natural separation of the subject into two categories: Linear Elastic Fracture Mechanics (LEFM) and Elastic Plastic Fracture Mechanics (EPFM). LEFM is concerned with the fracture of cracked bodies made from linear elastic materials (i.e. homogeneous, isotropic and obeying Hooke's Law). EPFM is applied to conditions where material yielding is considered to be excessive. This may be due to the material properties, the applied load, or when the extent of the yielding is large compared with the crack length.

Most engineering applications of Fracture Mechanics are concerned with relatively long cracks in high strength elastic materials; i.e. within the LEFM regime. This thesis will be limited to such conditions.

2.2 THE CRACK TIP STRESS FIELD AND THE STRESS INTENSITY FACTOR

The fracture of flawed components is widely analysed by a stress analysis based on the concepts of elastic theory. Following the initial work of Westergaard (1939), Irwin (1958) produced solutions of the crack tip stress distribution for the three main modes of loading shown in Figure 2.1.

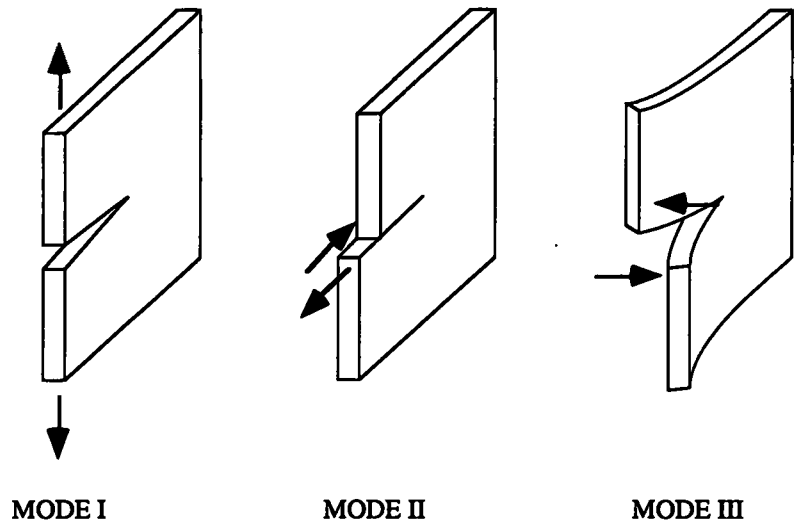

Figure 2.1 : The three modes of loading: Mode I - opening or tensile mode; Mode II - in-plane shear mode; Mode III - tearing or antiplane shear mode

The work in this thesis is limited to Mode I loading since this is by far the most commonly encountered engineering problem. Under such loading the crack tip stresses are found to be

$$\sigma_{ij}(r,\theta) = \frac{K_I}{\sqrt{2\pi r}} f_{ij}(\theta) \qquad (2.1)$$

where r and θ are the radius from the crack tip and polar angle respectively within a polar coordinate system (Figure 2.2). The term f_{ij} is a dimensionless function of θ.

An important feature of equation (2.1) is that the stress distribution around any crack is similar and depends only on r and θ. The difference between one cracked component and another is the magnitude of the parameter K_I, which is termed the *stress intensity factor* (or, more specifically in this case, the mode I stress intensity factor). Thus, the parameter K

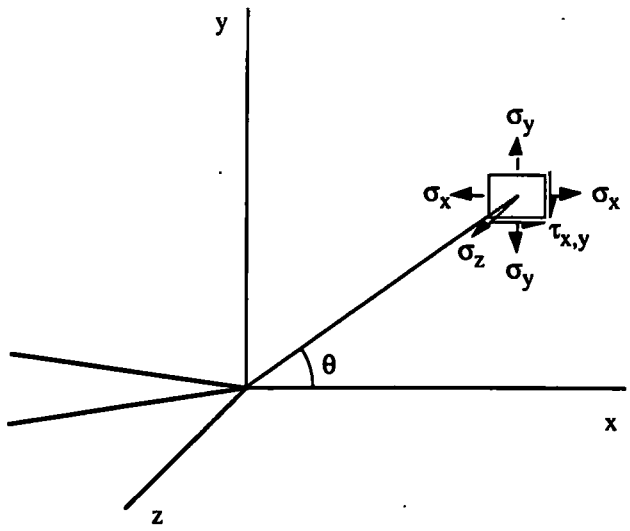

Figure 2.2 : Crack tip stresses

provides a unique description of the local stress field ahead of a linear elastic crack. The stress intensity factor can be expressed as

$$K_I = Y\sigma\sqrt{\pi a} \qquad (2.2)$$

where Y is a dimensionless geometrical scaling factor (Y=1 for an infinite plate), σ is the nominal applied stress, and a is the crack length for an edge crack (or half crack length for a central crack).

Irwin's characterisation of a linear elastic crack in terms of K was undoubtedly a momentous leap forward in Fracture Mechanics, supported by the discovery that there is a material dependent limiting value of K beyond which a component exhibits rapid fracture. The impact of the stress intensity factor concept from an engineering point of view is evident from equation (2.2). Given the factor Y, a crack can be characterised by the readily measurable parameters of applied stress and crack length. Values of Y for a wide variety of crack and specimen configurations have been determined and catalogued (Sih, 1973; Rooke and Cartwright, 1976).

Equation (2.1) is, in fact, only the first term in an infinite series expansion of r. However, provided the region considered is close to the crack tip (i.e. r is small), this first term dominates. The region where this is the case is often referred to as the K-dominant

zone within which the stress field is described as being an inverse square root singularity or K-field.

The stress field is described as a singularity because, as equation (2.1) shows, stresses tend to infinity as r tends to zero. In practice, however, such stresses are limited by local crack tip yielding which occurs over a region ahead of the crack tip known as the plastic zone. The resulting stress field (in the absence of any strain hardening) is therefore given by equation (2.1) up to the material yield stress, σ_y, and is shown schematically in Figure 2.3.

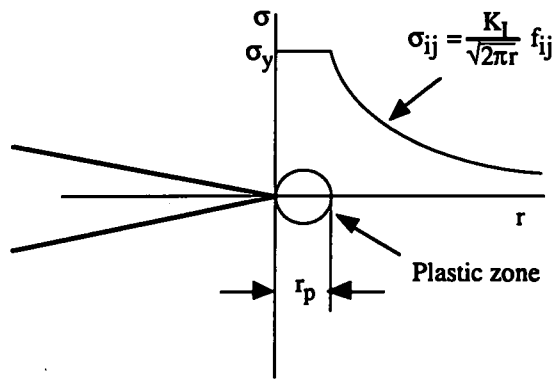

Figure 2.3 : The crack tip stress field showing the plastic zone

2.3 THE CRACK TIP PLASTIC ZONE

Crack tip plasticity plays an essential role in the fracture process and to the applicability of LEFM. Despite the fact that plasticity and non-linear effects are unavoidably prevalent in and around the fracture process zone, the principles of LEFM can be applied provided the plastic zone is small compared with the extent of the K-field and the overall dimensions of the body. This condition, known as small scale yielding, points to the fact that the stress intensity factor will describe the crack tip stress field despite local plastic deformation. To conform with the small scale yielding criterion the plastic zone size must not exceed one-fifteenth of the in-plane dimensions of crack length and remaining ligament.

The size of the plastic zone can be estimated using equation (2.1). For $\theta=0$, σ reaches σ_y when r becomes r_p according to

$$\sigma_y = \frac{K_I}{\sqrt{2\pi r_p}} \tag{2.3}$$

hence, the distance the plastic zone extends from the crack tip is given by

$$r_p = \frac{1}{2\pi}\left(\frac{K_I}{\sigma_y}\right)^2 \tag{2.4}$$

However, the presence of the plastic zone leads to a redistribution of the local stresses. The crack tip is said to effectively extend into the plastic zone to some extent. Irwin (1958) estimated the size of the plastic zone to be twice that of the initial approximation, viz

$$r_p = \frac{1}{\pi}\left(\frac{K_I}{\sigma_y}\right)^2 \tag{2.5}$$

The plastic zone size is often quoted as a radius, r_y, which is therefore given by

$$r_y = \frac{1}{2\pi}\left(\frac{K_I}{\sigma_y}\right)^2 \tag{2.6}$$

Equations (2.5) and (2.6) refer to the plane stress plastic zone size. For conditions of plane strain, the triaxial stress field suppresses the plastic zone. For the general case the plastic zone size is given by

$$r_p = \frac{1}{\alpha\pi}\left(\frac{K_I}{\sigma_y}\right)^2 \tag{2.7}$$

where α carries the value 1 for plane stress and 3 for plane strain. Equation (2.7) shows that the plastic zone is largest at the two free surfaces where plane stress conditions prevail and smallest at the midplane.

The actual shape of the plastic zone shown in Figure 2.3 is rather simplistic. The edge of the yield zone at a range of θ can be estimated using the Tresca or Von Mises yield criterion. For further details of plastic zone shapes under plane stress and plane strain conditions see Broek (1974).

It is worth mentioning at this point another model of crack tip plasticity proposed by Dugdale (1960) for the case of plane stress. In this model, Dugdale considers plastic regions at each tip of a central crack of length 2l to be narrow strips extending over a distance s from the tips (Figure 2.4). When loaded, the crack is allowed to extend elastically to a length of 2a (where a=l+s). It is shown that an internal stress equal to the yield strength

of the material is required to reclose the crack implying the region s represents local plasticity. The extent of plasticity calculated from this model is in good agreement with that calculated from equation (2.5).

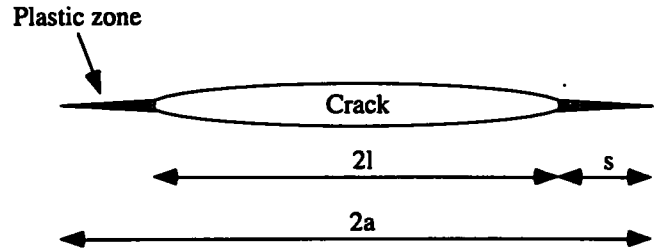

Figure 2.4 : Dugdale strip yield model

2.4 FATIGUE

2.4.1 Introduction

Fatigue is the progressive, irreversible structural change that can occur in a material when it is subjected to fluctuating strains. The important, and unfortunate, characteristic of fatigue is that material damage can occur at stress levels well below the tensile strength. The complete fatigue process can be subdivided into the following stages:

(i) Crack initiation

(ii) Crack propagation

(iii) Final catastrophic failure

In certain circumstances, such as in welded and riveted joints, pre-existent macroscopic flaws result in the first stage being by-passed; the life of a component then being determined by only crack propagation.

2.4.2 Crack Initiation

Fatigue failures almost always initiate at the surface of a component. This can be caused by surface stress concentrations as a result of, for instance, scratches, dents, machining marks, corrosion etc. In addition, the presence of surface discontinuities caused by cyclic slip has

been well known for some time (Thompson *et al*, 1956). In a nominally defect free material, cyclic strains can produce irreversible slip giving rise to surface intrusions and extrusions (Figure 2.5) which will promote crack initiation.

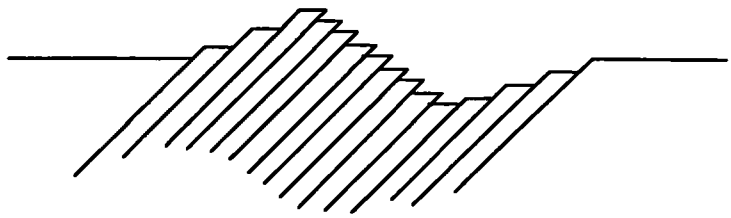

Figure 2.5 : Cyclic strain induced slip bands producing surface intrusions and extrusions

Furthermore, when these bands form, this region seems to have suffered permanent damage; further fatigue after surface polishing causes new surface damage at the same sites. It has been demonstrated that these "persistent slip bands" have undergone cyclic softening relative to the matrix (Hertzberg, 1989).

2.4.3 Fatigue Crack Propagation

The main body of this thesis is concerned with the propagation of long cracks (say, 10-50mm in length). Such macrocracks lie firmly within the LEFM regime and so the stress intensity factor concept is widely applied to correlating fatigue crack growth.

During the 1960s efforts to find a fatigue crack propagation correlating parameter centred on the stress intensity factor range, ΔK, following the work of Paris and Erdogan (1963). The stress intensity factor range is defined as

$$\Delta K = K_{max} - K_{min} \qquad (2.8)$$

where the extremes of applied stress are used in equation (2.2) to determine K_{max} and K_{min}. The crack growth rate, da/dN, is found to be constant at all combinations of a and σ giving the same ΔK, and is also found to exhibit a power law relationship over a range of ΔK.

Crack propagation data are usually presented as log da/dN against log ΔK giving the sigmoidal curve shown in Figure 2.6.

This curve demonstrates a threshold ΔK (ΔK_{th}) below which macrocracks remain dormant. At the other extreme a very rapid increase in growth rate is observed as K_{max} approaches the critical stress intensity factor, K_c.

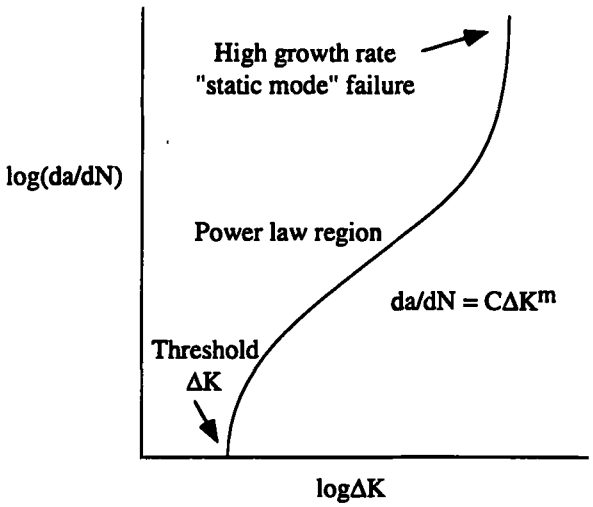

Figure 2.6 : Variation of fatigue crack growth rate with ΔK

At intermediate ΔK levels crack growth rate follows the now familiar Paris-Erdogan Law:

$$da/dN = C\Delta K^m \qquad (2.9)$$

where the constants C and m are empirically determined.

During fatigue cycling the monotonic plastic zone generated during uploading is compressed by the surrounding elastic material as the load is reduced from K_{max}. This leads to a residual compressive stress at the crack tip which will reach the yield stress producing a reverse plastic zone. Under constant amplitude fatigue this region of reverse plasticity repeatedly yields and so is often referred to as the *cyclic* plastic zone (Figure 2.7).

Outside the plastic zone (but within the K-dominant zone) the stress field is still expected to follow the general $1/\sqrt{r}$ form characteristic of a K-field except, that is, for the small equilibrating tensile stress field resulting from the compression of the monotonic plastic zone.

Rice (1967) showed that on load reduction from K_{max}, subtraction of the elastic stress distribution from the truncated K_{max} stress field leads to a reverse plastic zone size which

can be estimated by substituting $2\sigma_y$ for σ_y and ΔK for K in the plastic zone equations (2.5)-(2.7). This gives the reverse plastic zone size as

$$r_{p(reverse)} = \frac{1}{\alpha\pi}\left(\frac{\Delta K_I}{2\sigma_y}\right)^2 \qquad (2.10)$$

For zero to tension loading the reverse plastic zone is, therefore, estimated to be one-quarter of the monotonic plastic zone.

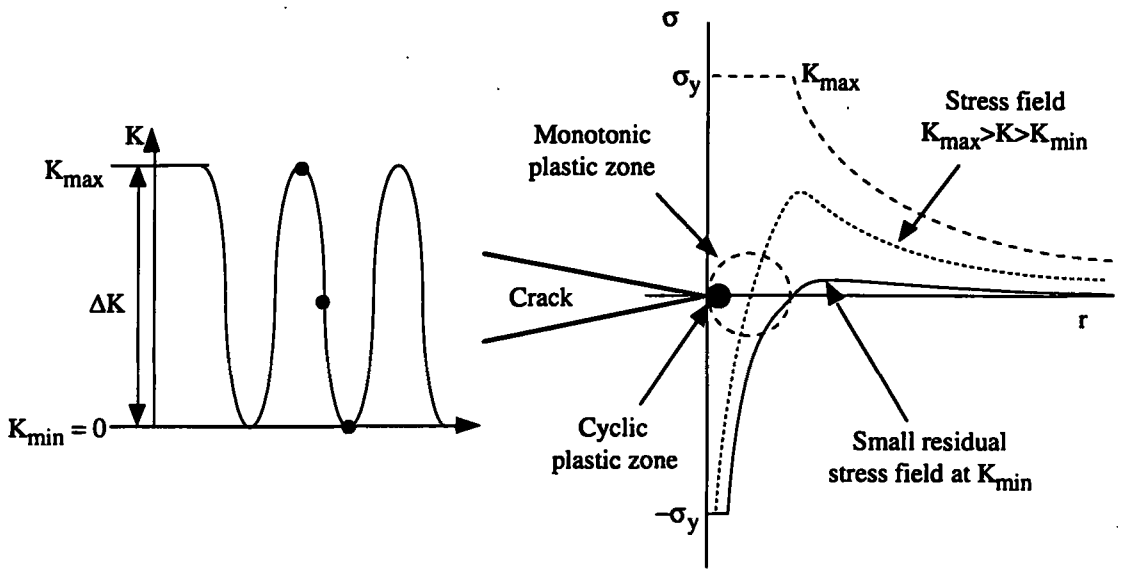

Figure 2.7 : Crack tip stress fields for zero to tension cycling

2.5 CONCLUSIONS

The use of the stress intensity factor concept in the characterisation of fatigue and fracture has been very successful. Crack propagation, be it dynamically in rapid fracture or incrementally in fatigue, has been empirically correlated in a multitude of materials and specimen configurations using the stress intensity factor approach.

The fact that the crack tip, which is in a region of extreme plastic strain, can be characterised by the elastic stress field around the crack tip means that the concept of K carries with it an implicit assumption; there is a unique relationship between the crack tip stress field (outside the plastic zone but within the K-dominant zone) and the complex state actually at the tip. An ability to measure this stress field eliminates the need to model the

crack tip condition. Furthermore, since the stress distribution is always of the $K/\sqrt{(2\pi r)}$ form, the single parameter, K, which itself can be determined from the crack length and applied stress, uniquely describes the crack tip and so eliminates the need to measure the actual stress distribution.

Chapter 3: FATIGUE CRACK CLOSURE

3.1 INTRODUCTION

Equation (2.9) ($da/dN = C\Delta K^m$) demonstrates how fatigue crack growth rate varies with ΔK. However, it takes no account of the effects of mean stress which are most noticable when part of the fatigue cycle involves a period of compression. In tension-compression fatigue, crack growth rates are found to correlate with K_{max}; that is, when only the tension part of the fatigue cycle is considered (Hudson, 1969). It was concluded from this finding that only that part of the fatigue cycle where the crack is open is effective in contributing to fatigue crack propagation.

This understanding was extended in 1970 when Elber (1970) discovered that, in 2024-T3 aluminium alloy sheet, cracks can close whilst still under a tensile load. Elber attributed this to being a result of the plastic stretch of material in the wake of a propagating fatigue crack.

Immediately, the crack closure concept was found to explain (qualitatively, at least) a range of anomalous fatigue crack growth characteristics; irregular short crack growth, mean stress effects, overload induced crack growth retardation and other variable amplitude fatigue phenomena.

Since Elber's initial discovery a multitude of papers has been published reporting crack closure in numerous materials, variations with different loading conditions, measurement methods, numerical and analytical predictions, and so forth. Today, fatigue crack closure is almost universally accepted* as having a major influence on the growth of fatigue cracks and is now firmly embedded within the understanding of the mechanics of fatigue.

3.2 MECHANISMS OF CRACK CLOSURE

3.2.1 Plasticity Induced Crack Closure

Elber's original discovery was attributed to a plasticity effect. The local yielding at the crack tip causes a region of material - the monotonic plastic zone - to be stretched parallel to the loading direction. As the crack propagates it is continually creating, and then growing through, such a zone leaving behind it a wake of stretched material - the so called plastic wake (Figure 3.1).

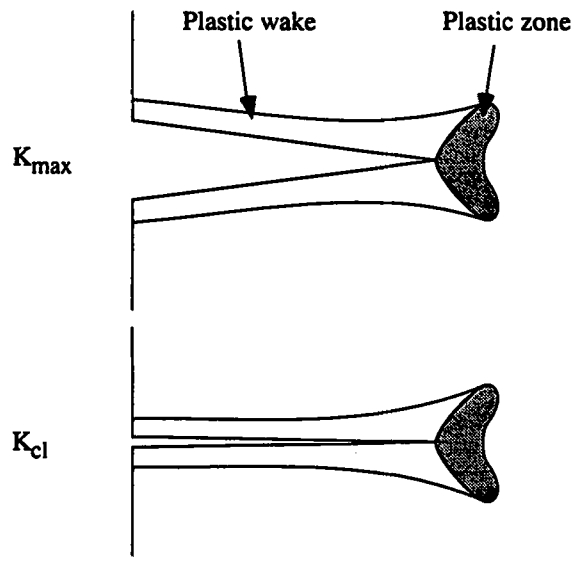

Figure 3.1 : Fatigue crack closure caused by a stretched plastic wake

---

* *Some established researchers (Vasudevan et al, 1993 and Sadananda et al, 1993) have recently suggested that crack closure under cyclic tension either does not exist or has an insignificant effect in fatigue.*

Because this material is stretched it will come into contact before the minimum in the load cycle is reached. At the minimum load the wake is then necessarily under compression. Using the principle, described in Section 3.1, that only the portion of the fatigue cycle in which the crack is open will contribute to fatigue crack growth, Elber modified equation (2.8) to produce

$$\Delta K_{eff} = K_{max} - K_{cl} \qquad (\text{for } K_{cl} > K_{min}) \qquad (3.1)$$

where ΔK_{eff} becomes the crack driving force in fatigue and K_{cl} is the stress intensity factor at the load where the crack closes (Figure 3.2). Equation (3.1) produces a modified Paris-Erdogan Power Law given by

$$da/dN = C(\Delta K_{eff})^m \qquad (3.2)$$

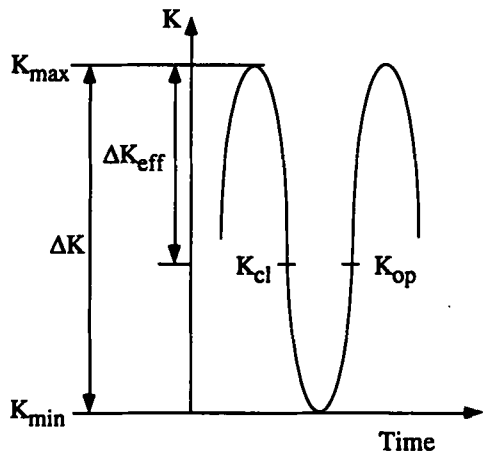

Figure 3.2 : Schematic of fatigue crack closure

There is some debate as to whether the effective minimum of the fatigue cycle is the crack opening point of the loading half of the cycle (K_{op}) or the closing point of the unloading half (K_{cl}). However, in most practical cases these two points are likely to be indistinguishable (Fleck, 1982; Banerjee, 1984; Abdel Mageed *et al*, 1992).

Since Elber's discovery significant research has been conducted to ascertain the precise mechanism of plasticity induced closure. In thick components there is a well known transition from plane strain conditions at the midplane of the crack front to plane stress conditions at the free surfaces. As described in Section 2.3, this leads to a larger surface plastic zone size compared to the midplane. It follows from this (which is supported by

three-dimensional finite element results (see, for example, Chermahini *et al* (1988))) that plasticity induced closure should predominate in the surface region and may be the cause of observed crack front curvature (Schijve, 1988). Indeed, some researchers consider plasticity induced closure to only operate under plane stress conditions (Ritchie and Suresh, 1982; McEvily, 1988). A further consequence of the stress state is the formation of fracture surface shear lips. Fretting debris observed on the lips provides evidence for prominent contact in this region (Schijve, 1988).

3.2.2 Roughness Induced Crack Closure

Some time after Elber's plasticity model the concept of crack closure arising from the fracture surface morphology began to emerge (Halliday and Beevers, 1979; Minakawa and McEvily, 1981; Suresh and Ritchie, 1982). Given the inherently rough morphology of fracture surfaces, it is difficult to imagine the two crack flanks mating perfectly as the crack closes (Figure 3.3). Only a small amount of mode II or III loading will induce premature contact of rough surfaces, which can be significant if the size of the asperities is comparable to the crack opening displacement (COD).

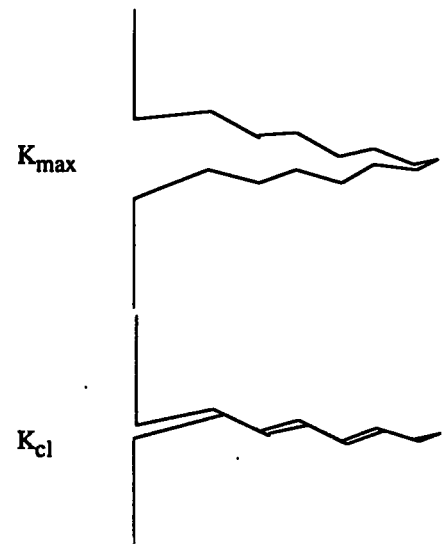

Figure 3.3 : Closure caused by a rough surface morphology

Due to the subtle difference between this "propping open" mechanism and that of plasticity induced closure, roughness is often said to induce crack "non-closure". Some researchers seem to be intrigued as to how these apparently opposing mechanisms produce identical

effects. Banerjee (1984), for instance, considers roughness induced closure to produce a residual *tensile* stress at the crack tip (since the tip is open) whereas a plastic wake produces a residual compressive stress. In the absence of an applied load, however, the stress at the crack tip must always be compressive (with or without closure); the existence of a reverse plastic zone is evidence of this. Any closure mechanism simply has the effect of reducing the crack tip strain amplitude and, likewise, the cyclic plastic zone size. The characteristic of roughness induced closure is that the compressive stress behind the crack occurs at discrete locations in the wake rather than continually distributed along it.

Experimental confirmation of roughness induced closure in 2024-T3 has been provided by Bowles and Schijve (1983) who developed a vacuum infiltration method which identified that crack closure occurred at specific locations on the fracture surface.

3.2.3 Oxide Induced Crack Closure

A further closure mechanism arises from the possible formation of an oxide layer on the freshly formed fracture surface (Figure 3.4). It is interesting to note that this concept seems first to have been realised by Endo *et al* (1969) before Elber discovered the plastic wake effect. In explaining reduced crack growth rate in salt water, the formation of an oxide layer was considered to reduce the crack tip strain amplitude during the fatigue cycle.

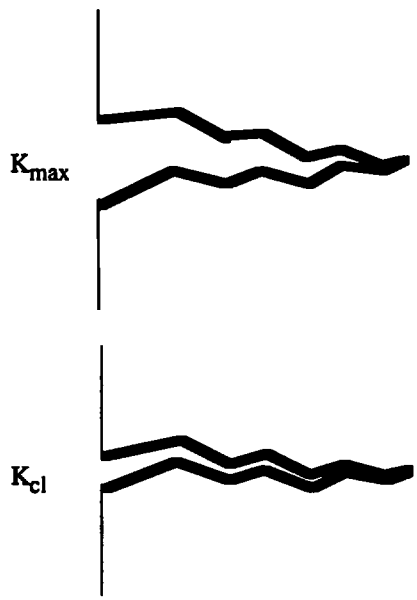

Figure 3.4 : Closure resulting from oxide deposits on the fracture surface

Crack closure produced from oxidation was established as a viable closure mechanism in the early 1980s when it was postulated by Ritchie *et al* (1980) and Suresh *et al* (1981;1982) as a cause for crack growth rate fluctuations in a range of atmospheres.

3.3 CLOSURE RELATED FATIGUE PHENOMENA

Since Elber's initial discovery, closure has been able to explain a wide range of fatigue characteristics. This is illustrated by the fact that all crack growth analyses are now performed with at least some consideration of closure. The following details some previously anomalous fatigue observations for which the closure concept has been central to the understanding of their mechanisms.

The curve in Figure 2.6 from which the Paris-Erdogan Law is taken is, in fact, a limited illustration in that it represents only a single stress ratio, R (defined as K_{min}/K_{max}), over the range of ΔK. It is now well known that at the same ΔK, different stress ratios (i.e. different mean stresses) often yield different growth rates. The effects, however, are not universal for all materials at all stress intensity factor ranges. For instance, Frost (1971) found no stress ratio dependence in pure aluminium, copper, titanium or mild steel.

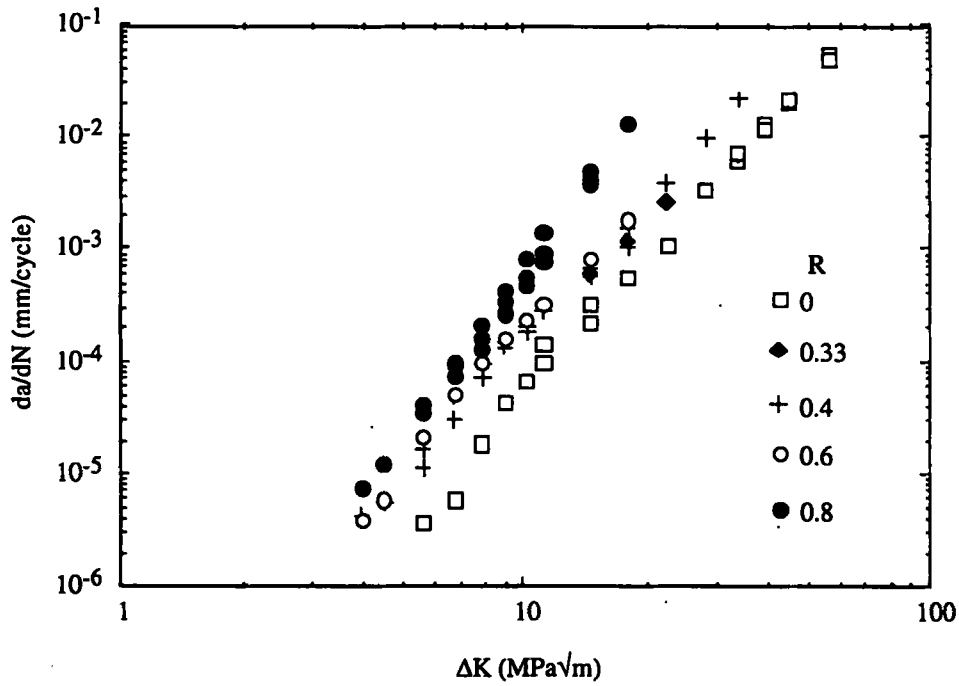

Figure 3.5 : The stress ratio effect on growth rate in 2024-T3 aluminium alloy (after Gallagher (1983))

Elber used the widely researched 2024-T3 aluminium alloy in his original work (using a thickness of 5mm). Over the 'power law' region this material exhibits the stress ratio effect shown in Figure 3.5.

By determining ΔK_{eff} over a range of ΔK and stress ratios ($-0.1<R<0.7$), Elber was able to collapse the above data into one line on a da/dN versus ΔK_{eff} plot, arriving at the empirical relation

$$U = \frac{\Delta K_{eff}}{\Delta K} = 0.5 + 0.4R \qquad -0.1<R<0.7 \qquad (3.3)$$

Similar relations have been determined for other materials; see Schijve (1988) for a brief review.

The physical basis for the R effect is illustrated in Figure 3.6. Fatigue at a higher mean stress produces a larger plastic zone and so a larger closure level. However, the closure level does not increase proportionally with mean stress. The resulting ΔK_{eff} is therefore a higher percentage of the applied ΔK.

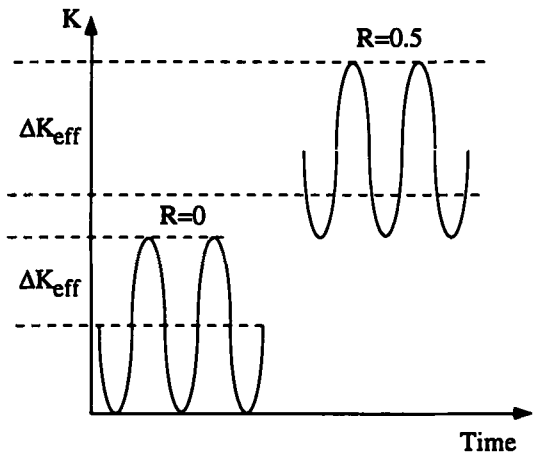

Figure 3.6 : Closure variations with stress ratio

There is evidence to suggest, however, that primary plastic flow is not the cause of the stress ratio effect. This is based on two observations (McEvily, 1988). Firstly, fine grained materials tend to exhibit a markedly reduced stress ratio effect. Secondly, there is a lack of firm evidence of a specimen thickness effect; surface regions are expected to provide the main contribution to plasticity induced closure due to the considerably higher plane stress plastic zone. These observations point towards crack surface roughness as the root of this

effect which is particularly apparent at load ranges around ΔK_{th}; coarse grained materials have higher thresholds than fine grained materials (Gray *et al*, 1983; Allen, 1988). In addition, crack growth around ΔK_{th} tends to be more crystallographically determined, leading to a more tortuous crack path, which is likely to result in closure from crack surface mismatch (Minakawa and McEvily, 1981; Ritchie and Suresh, 1982). Minakawa *et al* (1986) have found pronounced stress ratio effects in IN9021-T4 aluminium alloy (a fine grained material) but this occurs at relatively high ΔK due to static modes of fracture activated as K_{max} approaches K_c.

Zaiken and Ritchie (1985) found that compressive overloads increase ΔK_{eff} around ΔK_{th} by "flattening surface asperities" enabling subthreshold crack growth for a short period until the original closure level returned.

Variations in crack growth rate and threshold level have also been found in a range of atmospheres (Ritchie *et al*, 1980; Suresh *et al*, 1981;1982) and ambient temperatures (Liaw, 1988). This is attributed to variations in corrosion debris formed on the crack surfaces.

Plasticity induced closure has, however, been widely cited as the cause of load interaction or sequencing effects. Examples of such effects are the well known temporary crack growth retardation following tensile overloads, spurious growth rates following programmed block loading, and the interaction between overloads and underloads. For a recent review of such effects see Kumar (1992). Early models dealing with load interaction effects (eg Willenbourg *et al* (1971) and Wheeler (1972)) were based on residual stress variations. The retardation following an overload, for instance, was said to result from the crack having to grow through the enlarged monotonic plastic zone; material which is compressed by the surrounding elastic material. From the closure point of view, however, the relevance is the increased compressive forces *behind* the crack once the crack has grown (or is growing) through the enlarged plastic zone. The overload plastic zone produces a transient increase in the plastic stretch in the crack wake causing growth retardation due to the subsequent reduction in ΔK_{eff}. An observation supporting this concept is that of delayed retardation (von Euw *et al*, 1971) in which the crack decelerates following overload as the increased closure begins to take effect.

McEvily (1977) investigated the effect of overloads in aluminium alloys and found that crack growth retardation was greatly reduced by removing the surface layer immediately after overload. This, again indicates that plasticity induced closure is a predominantly surface phenomenon.

By measuring closure pre- and post-overload, Bertel *et al* (1981) and Clérivet and Bathias (1988) were able to collapse growth rate data on a da/dN versus ΔK_{eff} plot into one line as Elber had done for a range of stress ratios.

The anomalous growth rate of short cracks is also a much quoted phenomenon attributed to crack closure. It is well known that short cracks (of the order of the material grain size) can propagate faster than long cracks (at the same ΔK^*) and can also propagate at subthreshold ΔK when long cracks are dormant. Closure has been highlighted as a possible contributor to this phenomenon since, in short cracks, surface roughness is yet to develop (Ritchie and Suresh, 1982; Suresh and Ritchie, 1982).

3.4 MEASUREMENT METHODS

Despite crack closure being a remarkably elementary concept, accurate and repeatable quantification of ΔK_{eff} as the true fatigue crack driving force has been surprisingly elusive. To quote Newman (1988), "*After nearly 20 years of research, most researchers now agree that closure occurs. However, no concensus of opinion exists on how to best measure closure effects or crack-opening behaviour. Some numerical methods are now available to calculate crack-opening stresses, but they are complicated to use in practical applications.*" The following details some of the more widely used closure measurement techniques.

---

* *The stress intensity factor concept should be applied to short cracks with caution since the small scale yielding assumption may be violated; the plastic zone is likely to be a large proportion of the crack length.*

3.4.1 Mechanical Compliance Techniques

Mechanical compliance techniques are by far the most commonly used for closure measurement. Under LEFM conditions the strain at any point on a cracked specimen should vary linearly with applied load, the gradient of the resulting compliance curve being a function of the crack length. When closure occurs the crack undergoes an effective reduction in length producing a change in the compliance curve gradient. In practice, closure is a progressive process starting close to the tip resulting in a gradual change in gradient as shown in Figure 3.7 (a plot of a full fatigue cycle usually exhibits a hysteresis curve due to the crack tip plasticity). The precise stress at which closure occurs can be notoriously difficult to locate from such a compliance curve. This can be alleviated to some extent by using an offset procedure (see, for instance Fleck (1982)) whereby load is plotted against the change in displacement which essentially amplifies the load-displacement signal. A further complication is the lack of a unique definition of the closure point. Many researchers consider the first non-linearity point (P_1 in Fig. 3.7) as the closure load, thus assuming no crack tip damage occurs below P_1. Others take the load P_2, the intersection of the tangency lines, as the closure load (Allison *et al*, 1988). In this case it is assumed that damage occurs between P_1 and P_2 but that a steadily increasing level of crack tip shielding is occurring as P_2 is approached. This seems to be supported by Ohta *et al* (1978) who performed some fatigue studies in steel concluding that fatigue damage still occurred below the closure load (P_1).

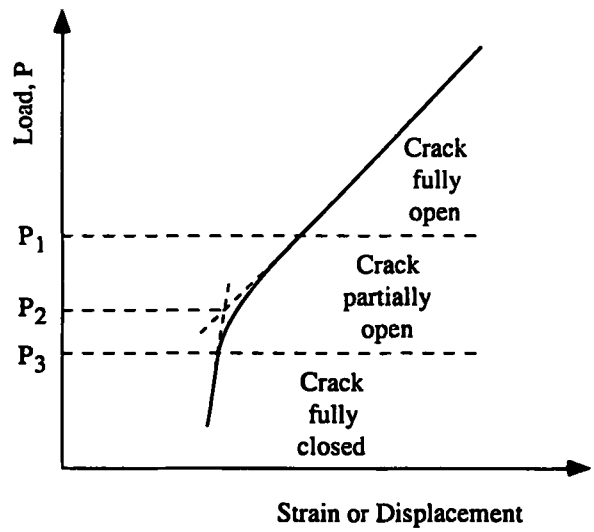

Figure 3.7 : A typical compliance curve indicating crack closure

A further variable in closure measurement from a compliance curve is the gauge position. In compact tension (CT) specimens back face strain (BFS) gauges or crack mouth clip gauges are most frequently used. In centre-cracked tension (CCT) specimens the crack mid-point may be used. However, a strain gauge or clip gauge placed near to the crack tip (or even straddling the crack) on the specimen surface (which was Elber's (1970) original method) is said to increase the sensitivity of measurement (Fleck, 1982; Schjive, 1988).

Unfortunately, several researchers have reported discrepancies in closure measurements between different gauge locations. Clerivet and Bathias (1988) found in a 2124-T351 aluminium alloy CT specimen that a crack mouth clip gauge yielded a lower crack opening stress than a gauge placed across the crack near the tip. Bertel *et al* (1981), using a 2024-T3 aluminium alloy CCT specimen, were able to correlate overload induced retardation with variations in closure determined from a near tip gauge despite no observed variation with a centre-crack clip gauge. Also, limiting the measurements to the crack tip region, Abdel Mageed *et al* (1992) found that the measured crack opening stress in CCT aluminium alloy sheets was a function of the clip gauge position (1 to 7 mm behind the crack tip). Jones *et al* (1978) had made a similar conclusion using Sharpe's interferometric strain/displacement gauge (Sharpe, 1982).

Inconsistencies between crack mouth and crack tip measurements have regularly been explained in terms of the local stress state at the surface. A crack tip gauge is clearly a surface measurement where plasticity induced closure is expected to predominate; this has been described as a 'local' closure measurement. A crack mouth gauge, on the other hand, has been described as a 'global' or 'bulk' closure measurement. This immediately raises the question of which measurement derives the ΔK_{eff} which governs crack growth rate. In addition, as Schijve (1988) points out, any non-linear compliance should be detectable, wherever it is occurring.

Whilst, then, mechanical compliance techniques are widely applied to closure measurement it is far from easy to obtain an unambiguous crack opening stress level.

3.4.2 Electrical Potential and Ultrasonic Methods

Electrical and acoustic resistance measurements have also been used to determine crack closure stresses. The basic principle behind these techniques is that the characteristic resistance of a specimen changes as the crack closes. That is, crack surfaces in contact will transmit electrical current and ultrasonic waves. Several investigators, however, have experienced inconsistencies between these and mechanical compliance techniques and the general consensus is that they should be used with caution (Schijve, 1988). Reasons cited include the effect of a tenacious oxide layer on the crack surfaces providing insulation indicating an electrically open crack when it is mechanically closed. Alternatively, grazing incidence contact between rough crack surfaces will provide negligible load bearing capability but may indicate electrical and acoustic closure. For a full review of these techniques see Fleck (1982) or Banerjee (1984).

3.4.3 Direct and Indirect Observation

Direct observation of the crack tip as well as observation of the effects of closure have also been used to assess the crack opening stress. The application of the electron microscope together with the development of novel crack loading devices have enabled material displacements around the crack tip to be observed even during fatigue cycling (Davidson and Lankford, 1979; Davidson 1988; Mouritsen and Karihaloo, 1993). Whilst these and similar techniques are obviously complex to use, they do conveniently illustrate the occurrence of closure. The drawback usually cited is the surface measurement limitation; they offer no indication of closure at the crack mid-plane.

Indirect observation methods involve measuring the effects of closure on crack growth rate (Schijve, 1988). Since ΔK_{eff} is considered to be the true fatigue crack driving force, it follows that cracks will not propagate under conditions where $\Delta K_{eff}=0$. By following a given constant amplitude load sequence with a lower amplitude block K_{cl} can be determined; the K_{max} of the lower block which just produces crack propagation corresponds to K_{cl}. This phenomenological determination of closure should yield a true ΔK_{eff} but will certainly be very labour intensive, particularly when measuring transient changes in closure, such as following an overload.

A further indirect closure measurement has been performed by Schijve and his co-workers (Schijve, 1988). It is assumed that crack growth under high stress ratios is in the absence of closure (cracks remain open for the whole fatigue cycle). Crack growth at, say, R=0.8 should therefore directly reveal ΔK_{eff} since $\Delta K_{eff}=\Delta K$. It may be assumed, then, that any other loading condition giving the same crack growth rate will be the result of the same ΔK_{eff}.

3.5 CRACK CLOSURE MODELLING

The mechanisms of crack closure are so entwined in the mechanics of fatigue that reliable prediction of fatigue life, particularly under variable amplitude loading conditions, will first require a reliable calculation of closure. Since the discovery of closure several researchers have produced analytical and finite element models to predict crack closure stresses and ΔK_{eff}. These models are reviewed briefly by Banerjee (1984).

The most comprehensive, and arguably successful, closure modelling has been performed by Newman and his coworkers at NASA (Newman, 1981; Newman *et al*, 1993). His (finite element) analysis is based on the 'modified Dugdale model' of crack tip plasticity described in Section 2.3; *modified*, since it includes the stretched plastic wake left behind the crack tip. One of the key features of Newman's model is the inclusion of a constraint factor, α, to accommodate conditions where a plane stress state cannot be assumed. The physical significance of Newman's α is identical to that in equation 2.7, i.e. α takes the value 1 for plane stress and 3 for plane strain. Under intermediate conditions α becomes more ambiguous and needs to be determined empirically. Newman does this by measuring crack growth rates under constant amplitude conditions at a range of ΔK and stress ratios producing a Paris-Erdogan plot analagous to Fig. 3.5. He then selects a value of α in his model which collapses the data onto a single curve of da/dN versus ΔK_{eff}. This may, in the first instance, seem a futile operation but once α is determined in this way for constant amplitude loading a multitude of variable amplitude loading conditions can be modelled using the same α.

By performing a polynomial fit to a series of results from his model, Newman has produced a convenient set of equations (equations (3.4)-(3.9)) for predicting closure level under constant amplitude loading (Newman, 1984). The equations provide a useful comparator for any experimental determination of closure under constant amplitude loading.

$$\frac{S_o}{S_{max}} = A_0 + A_1R + A_2R^2 + A_3R^3 \qquad \text{for } R \geq 0 \qquad (3.4)$$

and

$$\frac{S_o}{S_{max}} = A_0 + A_1R \qquad \text{for } -1 \leq R < 0 \qquad (3.5)$$

The coefficients are

$$A_0 = (0.825 - 0.34\alpha + 0.05\alpha^2)\left[\cos\left(\frac{\pi S_{max}}{2\sigma_o}\right)\right]^{1/\alpha} \qquad (3.6)$$

$$A_1 = (0.415 - 0.071\alpha)\left(\frac{S_{max}}{\sigma_o}\right) \qquad (3.7)$$

$$A_2 = 1 - A_0 - A_1 - A_3 \qquad (3.8)$$

$$A_3 = 2A_0 + A_1 - 1 \qquad (3.9)$$

where: S_o is the minimum stress required to open the crack

S_{max} is the maximum stress in the constant amplitude cycle

(Note S_o/S_{max} could equally be described as K_o/K_{max})

R is the stress ratio

α is the 'constraint factor'

σ_o is the material flow stress (average between the yield stress and ultimate tensile strength)

Equations (3.4) and (3.5) represent closure level as S_o/S_{max}. The commonly quoted U factor is determined using equation (3.10).

$$U = \frac{\Delta K_{eff}}{\Delta K} = \frac{1 - \frac{S_o}{S_{max}}}{1-R} \qquad (3.10)$$

Since Newman's equations can be applied to any material, it is interesting to compare his analysis with the experimental results of Elber (1971) which are summarised as equation (3.3); both researchers' work applies to centre-cracked tension specimens.

Firstly, a discrepancy is apparent due to equations (3.6) and (3.7). Newman's work clearly states S_o/S_{max} is a function of S_{max} whereas Elber's equation (3.3) indicates closure is only a function of stress ratio. By plotting Newman's equations against S_{max} (Figure 3.8), however, it can be seen that predicted closure is only a weak function of S_{max} and was therefore probably not apparent to Elber. Figure 3.9 compares Newman's and Elber's equations as a plot of U against R.

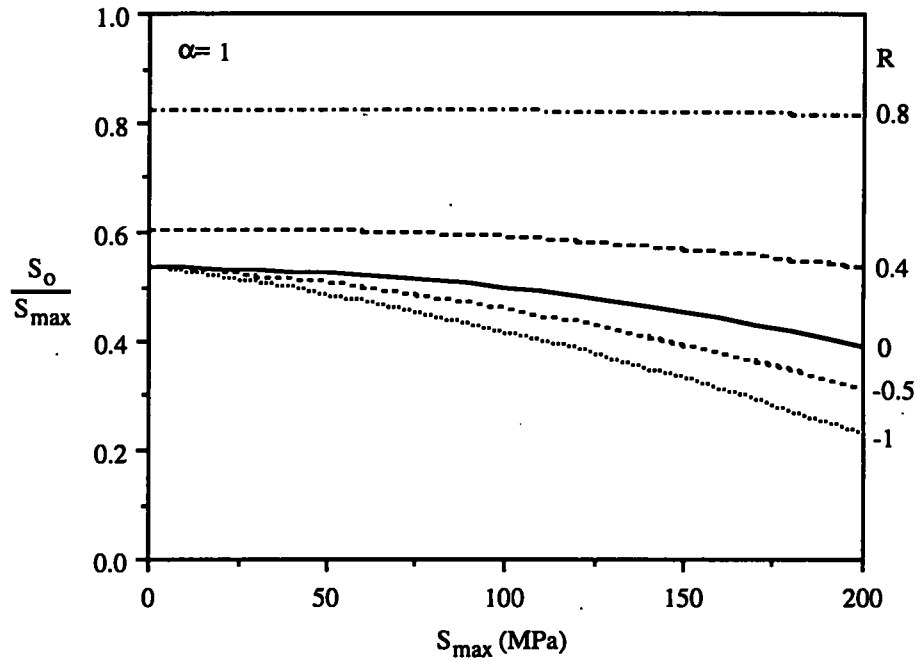

Figure 3.8 : Newman's closure prediction for 2024-T3 aluminium alloy as a function of S_{max} for α=1

It can be seen from Figure 3.9 that Newman's plane stress closure prediction agrees well with Elber's results. Elber's experiments were conducted on a 5mm thick specimen and at high ΔK (25-30MPa$\sqrt{m}$) and so a plane stress assumption is reasonable. Unfortunately, Newman's own correlation of constant amplitude growth rate data confuses the picture; for a 2.3mm thick 2024-T3 aluminium alloy specimen his model correlates growth rates when α=1.8 (Newman, 1984). Newman has recently stated (Newman, 1994) that an α of approximately 1.8 correlates growth rate data in 2024-T3 under virtually all specimen thicknesses and loading conditions. Only in very fine grained materials, for instance, does α approach a plain strain value.

This insensitivity of α points towards a microstructural effect. That is, a given level of roughness induced closure (the same for all specimen thicknesses) is indicating an α of 1.8

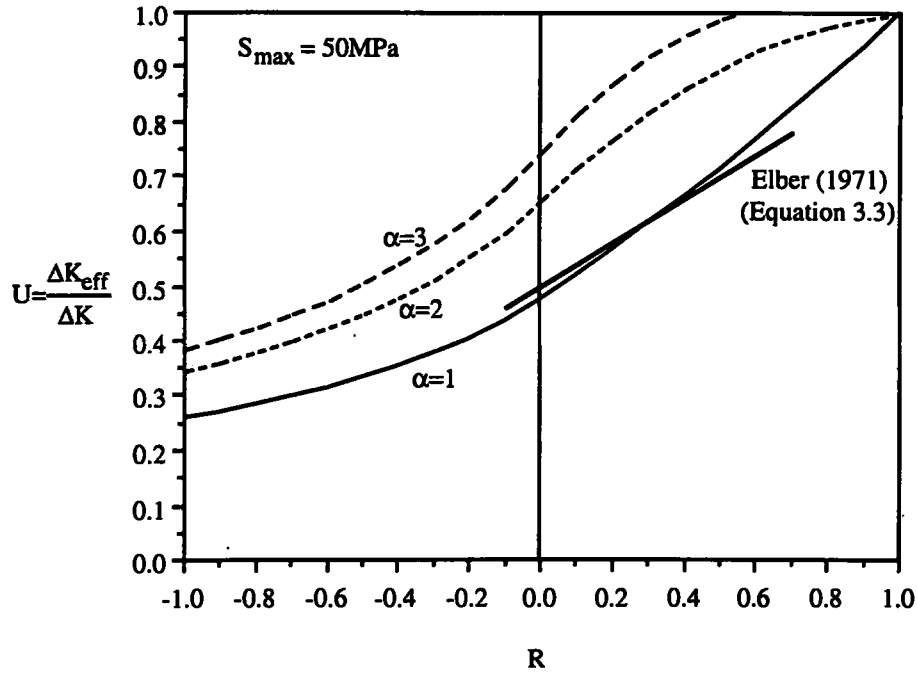

Figure 3.9 : Comparison between Newman's closure prediction and Elber's experimental results (for 2024-T3 aluminium alloy)

rather than the extent of plasticity (which is a function of thickness). After all, Newman has no independent microstructural parameter in his model. This would then be in agreement with the findings of McEvily (1988) and others, described in Section 3.3, that crack surface morphology is the root of closure in constant amplitude loading.

Despite Newman's model being widely acclaimed, its physical basis is therefore open to question. Although its lack of complete agreement with Elber's experiments may be due, to some extent, to Elber's limited early tests, it cannot be assumed that Newman's model is complete.

3.6 PRESENT STATE OF THE ART

In the 25 years since the discovery of crack closure, research into numerous materials, environments and loading conditions has clearly shown that it plays an important role in the mechanics of fatigue and in the governing of fatigue crack propagation rate. Closure has been found to be primarily caused by crack surface morphology (be it inherent in the material

or as a result of external effects) and crack tip yielding (particularly in circumstances where the extent of yielding fluctuates). Furthermore it has been possible, to a great extent, to identify the conditions in which the different mechanisms predominate.

However, despite the volume of research into crack closure there is still, today, substantial disagreement between researchers particularly with reference to quantifying closure. This has a subsequent effect in crack growth predictions; it is essential for closure to be accurately measured to provide a firm base for closure modelling. A major obstacle is the lack of agreement on a suitable measurement technique. Indirect measurements based on crack growth observations (often coupled with post-test fractography) are considered to be reliable but labour intensive. An *in situ* measurement method is undoubtedly desirable. Of the range of techniques which have been applied, ones based on different physical principles simply yield different results. The reasons for such differences have become largely understood to be due to particular failings in some of the techniques. Recently, researchers have tended to focus on mechanical compliance techniques to measure closure since they are relatively easy and cost effective to adopt and, according to some researchers, successful. However, subtle (and theoretically insignificant) differences between essentially identical mechanical compliance techniques can have a profound effect on measured closure levels. In addition, such techniques can be highly subjective with respect to identifying the precise location of the non-linearity point on a compliance curve.

Although the objective of a closure measurement is to identify ΔK_{eff}, none of the techniques used over the past 25 years makes any attempt to actually measure the stress intensity factor experienced by the crack tip throughout fatigue cycling. All techniques previously employed (direct and indirect) simply infer the crack tip driving force. A technique capable of an independent stress intensity factor measurement, without the *a priori* knowledge of crack length or applied load, would yield a direct measure of K_{max}, K_{cl} and therefore ΔK_{eff}.

Chapter 4: THE OPTICAL METHOD OF CAUSTICS

4.1 INTRODUCTION

This chapter of the thesis introduces the optical phenomenon of a *caustic* and the application of a novel technique utilising caustics to solve engineering problems within the framework of Linear Elastic Fracture Mechanics. A qualitative description of how a caustic is produced, both in general and at stress concentrations, is followed by a quantitative analysis showing how information can be obtained from a caustic.

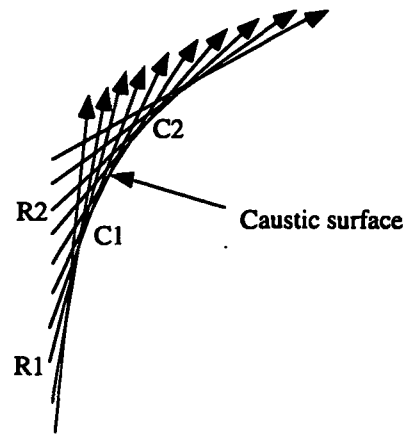

Figure 4.1: General principle of a caustic

A caustic is a geometrical optics term given to the envelope of a family of rays where, within this family, neighbouring rays cross at grazing incidence as illustrated in Figure 4.1. The name originates from the diminutive form of the Greek word for "burning iron" (Stavroudis 1972).

A caustic forms a 3-dimensional surface and can be produced in a multitude of natural and manufactured situations. As an example, a simple lens which exhibits spherical aberration would result in a caustic surface as illustrated in Figure 4.2. However, caustics are not widely observed in such artificial conditions. This is because in conventional optics a caustic is the result of aberrations in an optical component or system and is consequently avoided by design. The avoidance of a caustic results in a good point focus.

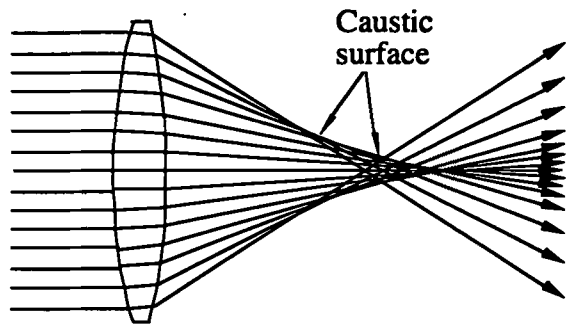

Figure 4.2: Caustic produced by a lens (exaggerated)

Nature does not apply such stipulations in reflecting or refracting surfaces (other than in the eye). The refraction of light through water droplets producing a rainbow is a classic example of a caustic. Many other examples can be found in nature in circumstances where there is no special symmetry such as the reflection of light from the surface of a rippling pond. By considering a caustic and a point focus it is easily seen that to achieve a sharp focus is the exception rather than the rule.

Regardless of the method of formation, there are two important general characteristics of caustics relevant to this present study. Firstly, in the region of the caustic there is an abrupt change in light intensity. According to the laws of geometrical optics the light intensity increases to infinity at the caustic surface and then falls to zero immediately outside the caustic. Of course, in practice, diffraction and interference occur according to wave theory and this modifies the intensity distribution around a caustic (Figure 4.3). This was

studied early in the last century when George Airy (1838) studied the diffraction effects and shows that there is an element of ambiguity to the precise location of the geometrical caustic surface (that is the position of the singularity according to geometrical optics). Nevertheless, a caustic provides a good, high contrast optical *edge* and it is this fact that is utilised in the use of an optical caustic as a measurement tool.

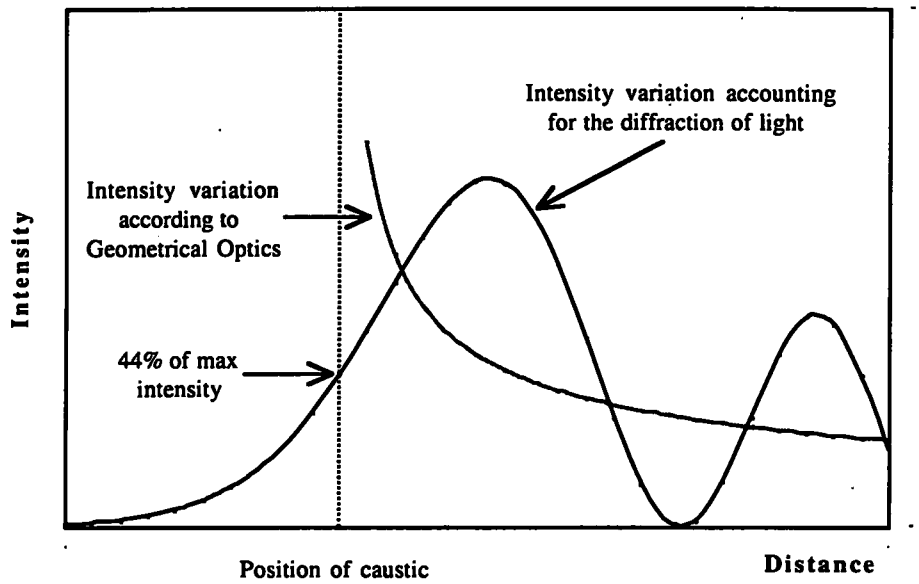

Figure 4.3 : The intensity of light in the vicinity of a caustic according to the laws of geometrical optics, interference and diffraction (after Airy 1838).

Secondly, any given point on the caustic surface is formed by a single ray. By definition, no ray can pass through the caustic but must constitute the caustic at some position on its surface. It can be seen in Figure 4.1 that the caustic at C1 is produced from the ray at R1. Similarly, the caustic at C2 is produced from R2.

It is interesting to note that despite being a common natural phenomenon and studied for over 150 years caustics have been considered as misfits within conventional optical theories and have only very recently found a home within the new branch of mathematics known as *catastrophe theory*. The resulting *catastrophe optics* provides a platform for the analysis of a whole range of caustic categories of which the type being described in this

thesis falls within the most elementary group of *fold* catastrophes. For a full account of catastrophe optics see Berry and Upstill (1980).

4.2 CAUSTICS IN FRACTURE MECHANICS - 'THE METHOD OF CAUSTICS'

4.2.1 Introduction

The 'optical method of caustics' is a relatively new experimental technique which has been developed for application to stress-strain analysis in the presence of stress concentrations. Being an optical technique it brings with it obvious benefits of being non-contact and non-destructive. However, whereas most optical measurement techniques are based on interference effects the method of caustics is based entirely on the principles of geometrical optics (except for the secondary consideration of diffraction effects around the caustic surface described in Section 4.1). This, in turn, provides an added advantage of being conceptually straightforward and requiring relatively simple apparatus with which to obtain measurements.

The technique was first developed in 1964 by Manogg (1964), a student of Schardin in Freiburg, who applied it to the study of stationary and dynamic cracks in PMMA (polymethyl-methacrylate). Around this time the method, which was usually referred to as the 'shadow spot method', was exclusively applied to transparent materials in a transmission mode. During the latter half of the 1960s the method went into complete oblivion until Theocaris and his co-workers in Athens resurrected and made substantial contributions to the technique by developing the 'method of reflected caustics', therefore extending its scope to opaque materials. These developments led to renewed interest in Freiburg where Kalthoff and his co-workers made further developments, perhaps most notably in the field of dynamic fracture.

Over the past two decades the technique has steadily gathered momentum around the world being applied to a plethora of materials and loading configurations (see Section 4.2.7). However, despite the fact that several institutions would, today, consider the

technique to be well established it is still not commonplace. Its application has been limited to pure research having not yet been accepted as an engineering tool.

4.2.2 Generation of Caustics by Stress Concentrations

The method of caustics is sensitive to stress gradients which can arise as a result of, for instance, notches or holes in a stressed plate (or even just a localised point load). By far the most widely studied stress concentration, however, is that caused by a through crack in a plate loaded in tension and/or shear. It will become clear throughout this and the following chapter that the method does not lend itself to non-planar configurations such as round bars or to plates loaded in bending.

This thesis is dedicated to the study of through-cracked plate specimens of an opaque engineering material (aluminium alloy) where the method is necessarily applied in its reflection mode.

Now, when a plate is subjected to a tensile stress its thickness reduces due to Poisson's effects. If there is a stress distribution the thickness change will be non-uniform, that is, there will be a surface deformation. For the case of a through crack in a parallel-sided plate subjected to a tensile stress, the stress concentration at the crack tip produces a surface deformation as shown schematically in Figure 4.4.

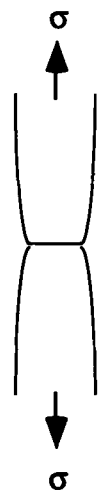

Figure 4.4 : Surface deformation in a cracked plate subjected to a tensile stress (shown in cross-section at the tip of the crack)

Now, the stress field around the crack tip causes one of those ubiquitous types of surface deformation described in Section 4.1 which is capable of producing a caustic. So if the specimen is mirrored and illuminated a caustic surface is produced as shown in Figure 4.5.

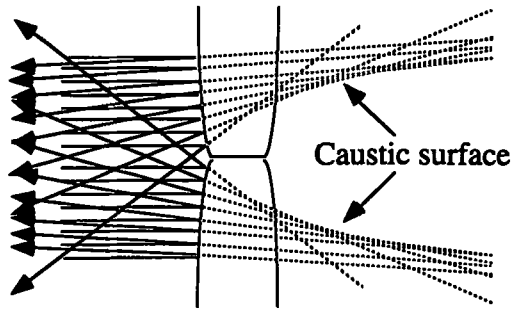

Figure 4.5 : Schematic of the formation of a reflected caustic in a stressed, cracked plate

It is necessary at this point to introduce the concept of a *virtual* caustic. That is, the condition where the virtual extension of the rays behind the specimen meets the criteria of a caustic surface. As it can be seen in Figure 4.5 the convex nature of the surface deformation produces a virtual caustic which can subsequently be viewed as a real image by placing a lens in front of the specimen such that the object plane of the lens is some distance behind the specimen.

The caustic surface produced in this way forms a long 'tube', the diameter of which continually increases with increasing distance from the specimen surface. Since the Poisson contraction varies directly with the magnitude of the stress field it follows that the diameter of the caustic will also be a function of the applied stress field. Since, in Linear Elastic Fracture Mechanics, the stress field is characterised by the stress intensity factor, K, the caustic diameter can be used as a non-contact, non-destructive means of measuring K.

Before elucidating on a more rigorous, quantitative analysis it is worth revisiting a point mentioned earlier. If the caustic diameter is used to measure a stress intensity factor then it is clearly necessary to specify the plane behind the specimen from which the diameter is taken. Now, as stated in Section 4.1, the caustic at a given plane is produced by a single ray (or more specifically in this case a single annulus of rays) from a *single radius* from the crack tip. It can be seen from Figure 4.5 that a caustic plane chosen close to the specimen surface

is generated from rays a small radius from the crack tip. Essentially, this means that it is possible to select the radius from the crack tip from where the stress gradient is being measured. The relevance of this fact will become clear later in this chapter.

4.2.3 Theoretical Background

This section of the thesis provides a quantitative description of how the caustic diameter relates to the stress intensity factor for an opaque plate. The analysis is taken from that provided in the literature, principally by Theocaris (1981), Beinert and Kalthoff (1981) and Kalthoff (1987) but is limited to the reflection mode as used in this thesis.

Consider a curved surface as shown in Figure 4.6. This is schematic of a crack tip deformation but could, in principle, be of any form. For convenience consider the deformation to be constant in the x-direction of a cartesian co-ordinate system, Oxyz. The surface deformation is therefore of the form:

$$z = f(y) \qquad (4.1)$$

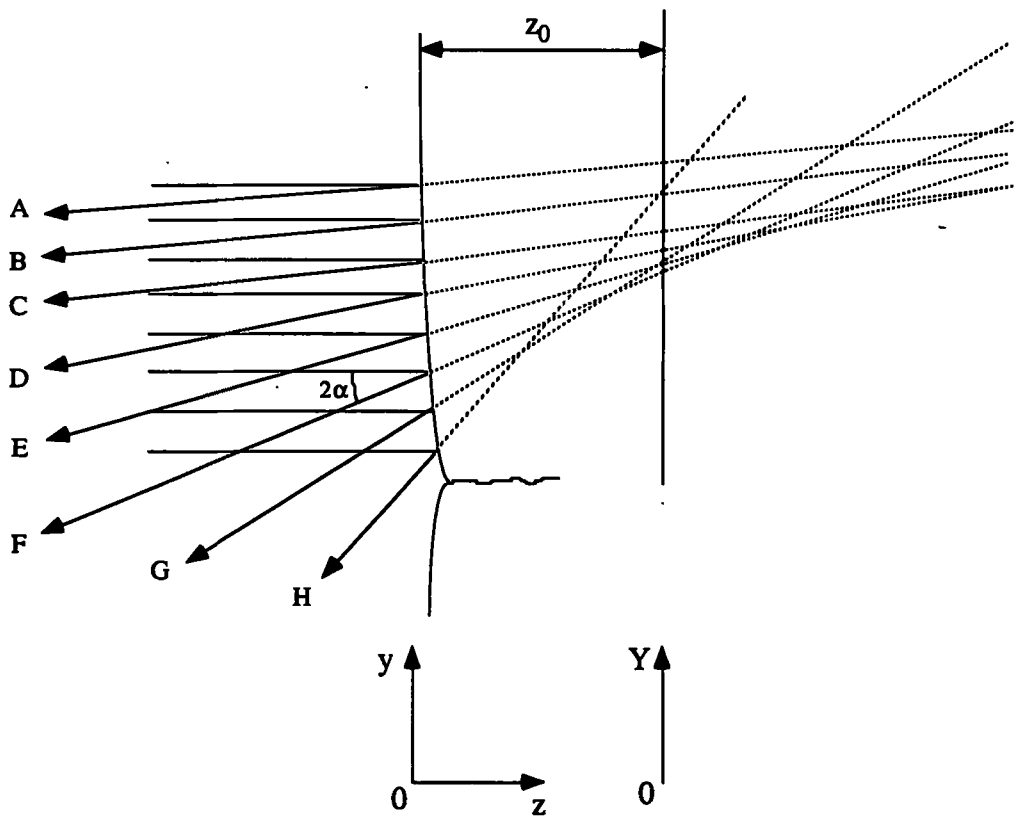

Figure 4.6 : Formation of a caustic on a reference plane

Consider now a reference plane a distance z_0 from the surface with a co-ordinate system, 0XY. All virtual extensions of rays (A-H) will cross the reference plane at some point. However, there is always a minimum value to Y on the plane where the rays cross. For the reference plane shown ray F, after being deflected through an angle 2α by a surface gradient α, provides this minimum and consequently constitutes the caustic for that z_0.

The point (Y) on the reference plane where a virtual ray extension from (y) on the surface meets the plane is given by equation (4.4) simply derived as follows:

$$\tan 2\alpha = \frac{Y-y}{z_0-z} \tag{4.2}$$

From equation (4.1)

$$\tan 2\alpha = \frac{Y-y}{z_0-f(y)} \tag{4.3}$$

therefore

$$Y = y + [z_0 - f(y)]\tan 2\alpha \tag{4.4}$$

Note that equation (4.4) applies to all rays not only to the caustic ray, F. It is clear from Figure 4.6 that

$$\tan\alpha = -f'(y) \tag{4.5}$$

Therefore

$$Y = y - [z_0 - f(y)]\left(\frac{2f'(y)}{1+f'^2(y)}\right) \tag{4.6}$$

Now, if $f(y) \ll z_0$ and the surface deformation gradient, $f'(y)$, is small then equation (4.6) can be simplified to

$$Y = y - 2z_0 f'(y) \tag{4.7}$$

Since, in general the surface deformation is 2-dimensional, that is:

$$z = f(x,y) \tag{4.8}$$

a more general form of equation (4.7) would be:

$$X = x - 2z_0 \frac{\partial f(x,y)}{\partial x}, \qquad Y = y - 2z_0 \frac{\partial f(x,y)}{\partial y} \tag{4.9}$$

or in vector notation

$$(X,Y) = (x,y) - 2z_0 \text{ grad } f(x,y) \tag{4.10}$$

Now, consider the incident beam from the point of view of a wavefront. That is, the wavefront is given by

$$z = c \tag{4.11}$$

where c is a constant. Using the assumption made earlier that the surface gradient, $f'(x,y)$, is small then the surface deformation will cause a change in path length, Δs, in the reflected wave. This change is given by

$$\Delta s = -2f(x,y) \tag{4.12}$$

Consequently equation (4.10) becomes

$$(X,Y) = (x,y) + z_0 \text{ grad } \Delta s \tag{4.13}$$

The preceding analysis applies to any caustic forming surface. The following analysis identifies Δs and consequently X and Y for a crack in a parallel plate under mode I loading. Under such conditions the path length change can be expressed as

$$\Delta s = -d\varepsilon_z \tag{4.14}$$

where d is the specimen thickness and ε_z is the strain component normal to the plane of the specimen (ie the Poisson contraction). According to Hooke's law

$$\varepsilon_z = -\frac{\nu}{E}(\sigma_x + \sigma_y) \qquad \text{for plane stress} \tag{4.15}$$

where ν is the Poisson ratio

E is the Young's modulus of the material

σ_x and σ_y are normal stresses related to the cartesian co-ordinate system.

Equation (4.15) applies to regions around the crack tip where plane stress conditions predominate. In reflected caustics there is no plane strain equivalent of equation (4.15) since ε_z would then be zero. From equations (4.14) and (4.15)

$$\Delta s = \frac{d\nu}{E}(\sigma_x + \sigma_y) \qquad \text{for plane stress} \tag{4.16}$$

From equation (4.13) and Figure 4.7 it follows that

$$\mathbf{r'} = \mathbf{r} + z_0 \, \mathbf{grad} \, \Delta s \tag{4.17}$$

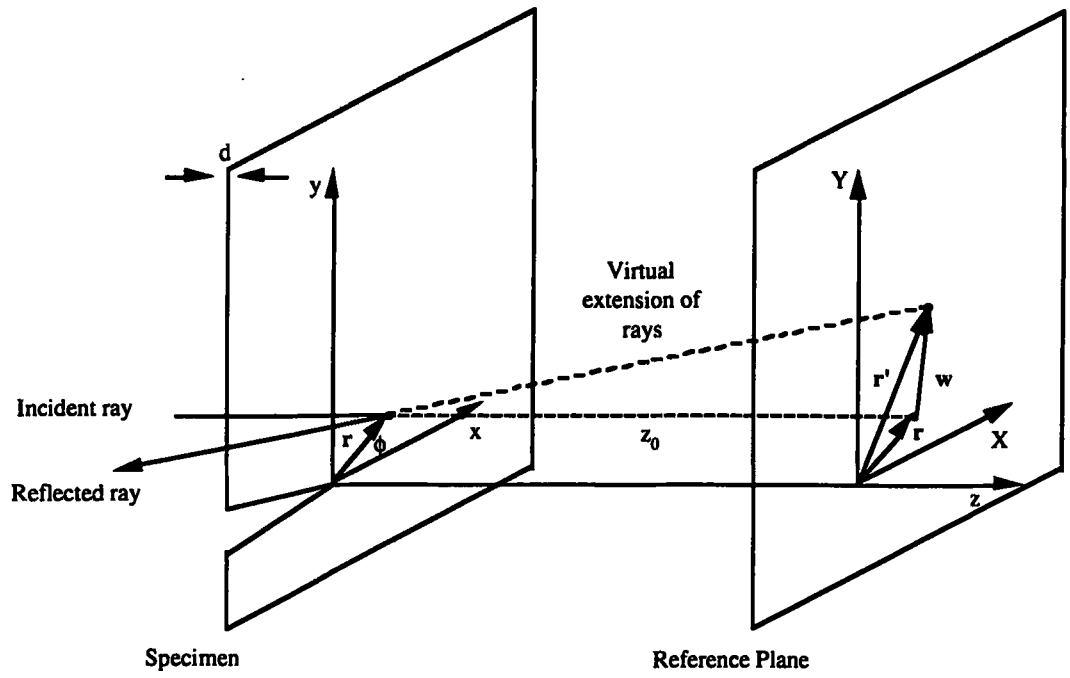

Figure 4.7 : Crack tip caustic ray diagram

therefore

$$\mathbf{r}' = \mathbf{r} + \frac{z_0 d\nu}{E} \mathbf{grad}\,(\sigma_x + \sigma_y) \tag{4.18}$$

For a crack under mode I loading in linear elastic materials the stress distribution in the vicinity of the crack is given by Sneddon (1946) and Williams (1957):

$$\sigma_x = \frac{K_I}{\sqrt{2\pi r}} \cos\frac{\phi}{2}\left(1 - \sin\frac{\phi}{2}\sin\frac{3\phi}{2}\right) + a_2$$

$$\sigma_y = \frac{K_I}{\sqrt{2\pi r}} \cos\frac{\phi}{2}\left(1 + \sin\frac{\phi}{2}\sin\frac{3\phi}{2}\right) \tag{4.19}$$

where K_I is the mode I stress intensity factor

r and ϕ are polar co-ordinates with the crack tip as the origin

a_2 is a constant

Hence, equations (4.16) and (4.19) define Δs in the vicinity of a crack tip under mode I loading. Substituting equation (4.19) into (4.18) defines the ray deflection which, in terms of the X and Y components of **r** is given by:

$$X = r\cos\phi - \frac{K_I z_0 dv}{\sqrt{2\pi E}} r^{-3/2}\cos\frac{3\phi}{2}$$
$$Y = r\sin\phi - \frac{K_I z_0 dv}{\sqrt{2\pi E}} r^{-3/2}\sin\frac{3\phi}{2} \qquad (4.20)$$

Thus, equation (4.20) describes the positions on the reference plane where all the virtual ray extensions meet the reference plane. However, for a given reference plane position only one ray constitutes the caustic. This ray extension meets the plane at minimum (or maximum) X for a given Y, and vice versa. This condition is satisfied if the determinant of the Jacobian of (4.20) vanishes, thus

$$J = \frac{\partial(X,Y)}{\partial(r,\phi)} = \begin{vmatrix} \frac{\partial X}{\partial r} & \frac{\partial X}{\partial \phi} \\ \frac{\partial Y}{\partial r} & \frac{\partial Y}{\partial \phi} \end{vmatrix} = 0 \qquad (4.21)$$

therefore

$$\frac{\partial X}{\partial r}\frac{\partial Y}{\partial \phi} - \frac{\partial X}{\partial \phi}\frac{\partial Y}{\partial r} = 0 \qquad (4.22)$$

Indeed it is necessary for the condition (4.21) to be met for a caustic to form at all. The above operation leads to:

$$r = \left(\frac{3K_I z_0 dv}{2\sqrt{2\pi E}}\right)^{2/5} \equiv r_0 \qquad (4.23)$$

Equation (4.23) indicates that the radius from the crack tip of the incident ray which forms a caustic at reference plane distance z_0 is a function of the specimen (ie material constants and thickness) and the stress intensity factor only. Being independent of ϕ this radius, which is termed the *initial curve*, is denoted as r_0. Substituting equation (4.23) into (4.20) gives the ray positions on the reference plane as a function of r_0:

$$X = r_0\left(\cos\phi + \frac{2}{3}\cos\frac{3\phi}{2}\right)$$
$$Y = r_0\left(\sin\phi + \frac{2}{3}\sin\frac{3\phi}{2}\right) \qquad (4.24)$$

That is, equation (4.24) defines the cross-section of the caustic surface at the reference plane distance z_0 (defined by r_0). This cross-section, usually referred to as the caustic curve,

forms a generalised epicycloid and is illustrated in Figure 4.8. The transverse diameter, D, of the caustic may be calculated from $2Y_{max}$ in equation (4.24) which gives

$$D = 3.17\, r_0 \tag{4.25}$$

Now, from (4.25) and (4.23) it is possible to calculate the stress intensity factor from the measurable quantity, D:

$$K_I = \left(\frac{2\sqrt{2\pi}\, E}{3(3.17)^{5/2}\, z_0 dv} \right) D^{5/2} \tag{4.26}$$

that is

$$K_I = \frac{ED^{5/2}}{10.71\, z_0 dv} \tag{4.27}$$

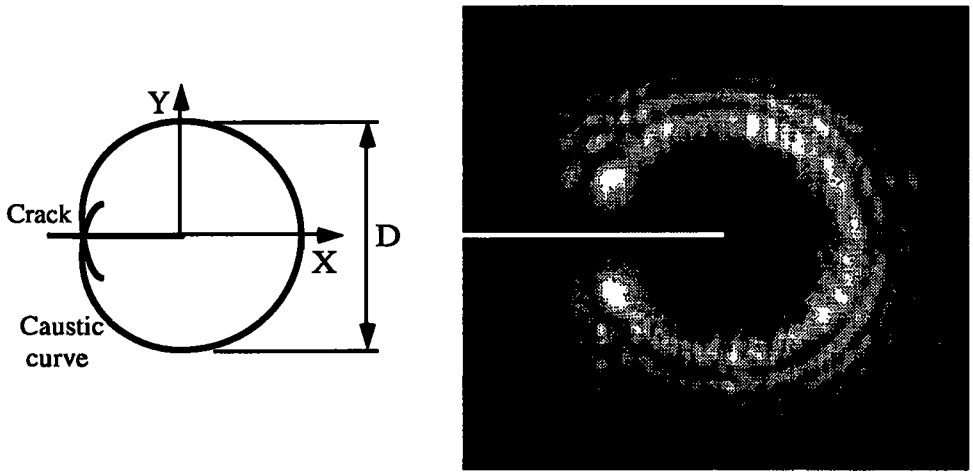

Figure 4.8 : Reflected caustic curve for a crack under mode I loading

4.2.4 Non-Collimated Beam Caustics

Section 4.2.3 described the method of caustics with the application of a collimated incident beam; that is, a beam which has a plane wavefront so that all rays (ignoring the effects of diffraction) are parallel to the optical axis. This is not, however, a prerequisite of the caustic technique. A caustic can be produced with a divergent or convergent beam but a scaling factor is required to obtain any quantifiable information such as a stress intensity factor. The concept of a non-collimated beam caustic is discussed in the literature (see, for example, Theocaris (1981), Beinert and Kalthoff (1981) and Kalthoff (1987)) and the appropriate scaling factor is quoted although not derived. These three references, however, appear to be

contradictory and cross referencing between them is confusing. Beinert and Kalthoff (1981) and Kalthoff (1987) explain the non-collimated beam arrangement from the point of view of transmission mode caustics and quote different scaling factor equations for divergent and convergent beams. Furthermore, the equations quoted are different between the two references, despite being writen by the same author, although this may be due to an inconsistent sign convention between the papers. Theocaris (1981) on the other hand describes a reflected convergent beam arrangement. However, although in reflection mode, his explanation shows a real rather than virtual reference plane and he quotes yet another scaling factor equation.

The following analysis shows the formation of non-collimated reflected beam caustics and derives a scaling factor which is applicable to the work of this thesis. The analysis also clarifies the sign convention adopted for both divergent and convergent beams.

Consider a cross-section through a collimated beam caustic in the (y,z) plane as shown in Figure 4.9. The caustic shown is therefore the locus of maximum transverse diameter, D, for the $y > 0$ half of the caustic.

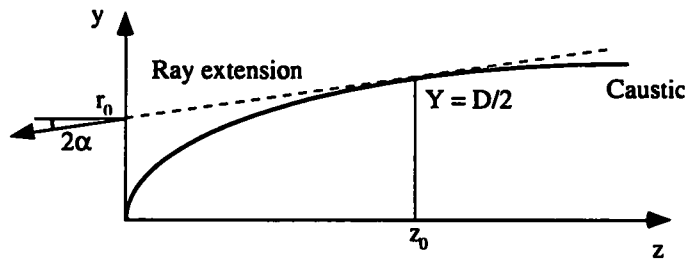

Figure 4.9 : Schematic of the ray which forms the caustic

Using the assumptions of Section 4.2.3 that the surface deformation, f(y), is small with respect to z_0 and that the surface gradient, f´(y), is also small, then the reflected ray deflection, 2α, is given by

$$2\alpha = \frac{D/2 - r_0}{z_0} \qquad (4.28)$$

Note that equation (4.28) is essentially the same as equation (4.2). Therefore from (4.25)

$$2\alpha = \frac{\frac{3.17}{2} r_0 - r_0}{z_0} = \frac{0.585 r_0}{z_0} \qquad (4.29)$$

Substituting z_0 from equation (4.27) gives

$$2\alpha = 0.585 \left(\frac{3dvK_I}{2\sqrt{2\pi}\, E} \right) r_0^{-3/2} \qquad (4.30)$$

Therefore, the surface gradient is given by

$$\alpha = 0.293 \left(\frac{3dvK_I}{2\sqrt{2\pi}\, E} \right) r^{-3/2} \qquad (4.31)$$

where the subscript is dropped from r since α is the surface gradient at all r. Therefore

$$\alpha = -f'(y) = 0.175 \left(\frac{dvK_I}{E} \right) y^{-3/2} \qquad (4.32)$$

Consider, now, a ray converging to a point a distance z_1 behind the specimen surface making an angle θ to the nominal surface normal. It will be reflected through an angle Δ which is greater than θ due to the surface gradient.

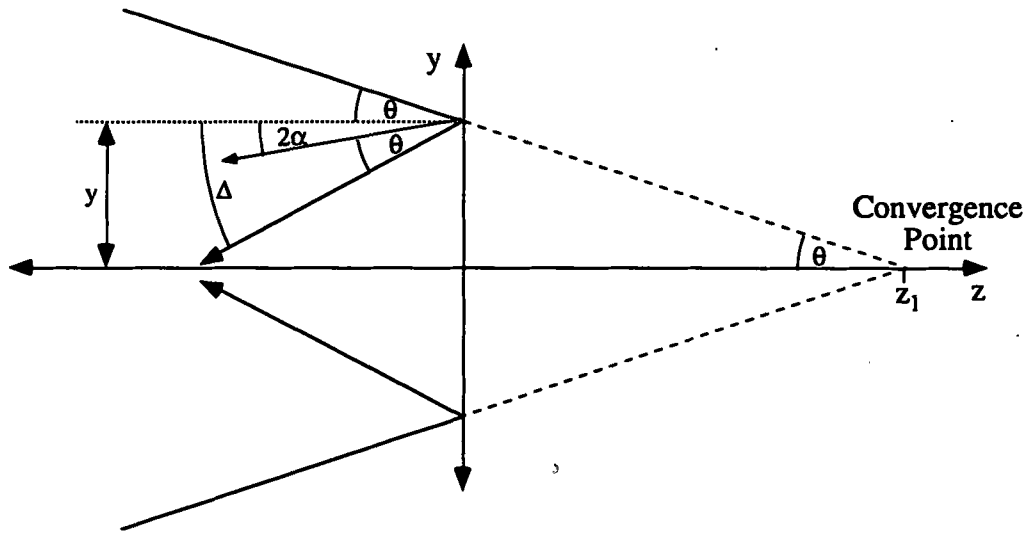

Figure 4.10 : Deflection of a converging beam

Now, assuming $z_1 \gg y$ then

$$\tan\theta = \theta = \frac{y}{z_1} \qquad (4.33)$$

also

$$\Delta = 2\alpha + \theta \qquad (4.34)$$

therefore, from equation (4.32)

$$\Delta = 0.35\left(\frac{dvK_I}{E}\right)y^{-3/2} + \frac{y}{z_1} \qquad (4.35)$$

Equation (4.35) is therefore the gradient of a reflected ray incident at any position y on the specimen surface after initially converging towards a point z_1 behind the specimen. By designating the incident position on the specimen as y_0 the general equation of a reflected ray is given by:

$$y = \left(0.35\left(\frac{dvK_I}{E}\right)y_0^{-3/2} + \frac{y_0}{z_1}\right)z + y_0 \qquad (4.36)$$

As previously stated the caustic ray has a minimum y at a given z and y_0. Therefore

$$\frac{dy}{dy_0} = 0 \text{ at } y_0 = r_0 \text{ (and so } z = z_0)$$

$$\frac{dy}{dy_0} = -\frac{3}{2}\left(0.35\left(\frac{dvK_I}{E}\right)z_0\, r_0^{-5/2}\right) + \frac{z_0}{z_1} + 1 = 0 \qquad (4.37)$$

therefore

$$r_0 = \left[0.525\left(\frac{dvK_I}{E}\right)\frac{z_0 z_1}{z_1+z_0}\right]^{2/5} \qquad (4.38)$$

Now, substituting equation (4.38) into the general ray equation (4.36) and limiting the rays to the caustic rays, ie setting y_0 as the initial curve radius r_0, which means z then becomes z_0 and y becomes D/2 the resulting equation can be re-arranged to show

$$K_I = \left(\frac{ED^{5/2}}{10.71 z_0 dv}\right)\left(\frac{z_1}{z_1+z_0}\right)^{3/2} \qquad (4.39)$$

from which it follows that

$$r_0 = \frac{D}{3.17}\left(\frac{z_1}{z_1+z_0}\right) \qquad (4.40)$$

Equations (4.39) and (4.40), therefore, are the general equations for calculating a stress intensity factor and initial curve radius for any z_1 up to infinity and show that the non-collimated beam scaling factor is given by

$$m = \frac{z_1}{z_1+z_0} \qquad (4.41)$$

A similar analysis to that above yields the same result for a divergent beam. Of course, for a divergent beam z_1 has a negative value since the incident beam is diverging from a point at a negative z. By comparing equation (4.41) with the equations quoted by Theocaris (1981), Beinert and Kalthoff (1981) and Kalthoff (1987) it can be seen that these equations do, in

fact, yield the same scaling factor provided the sign convention and definitions of z_1 and z_0 are adhered to.

Rather than referring to collimated, divergent and convergent beams as discrete types of illumination (as is common in the literature) it is more appropriate to consider these as the same but that it is necessary to specify the position of the beam focus with respect to the specimen surface. That is, the focus can be located at infinity (collimated beam), at a negative z (divergent beam) or a positive z (convergent beam). Of course, at a positive z the focus is virtual.

Before concluding this section of the thesis it is worth investigating the formation of caustics at a range of z_1 distances since comparison between them reveals some interesting phenomena. This is best done illustratively with the aid of equation (4.36). This equation describes the ray reflected from the surface of a given specimen (E, v and d) at a given loading (K_I) after impinging at a distance, y_0, from the crack tip from an incident beam with a focus at z_1. By calculating a family of rays at a range of y_0 it is possible to model the reflection of a complete incident beam and therefore observe the resultant caustic. Further to this, it is possible to model the reflected rays passing through an imaging lens of focal length, f, positioned a distance, b, from the specimen surface and so observe the real image of the caustic. Caustic imaging is explained in detail in Section 4.2.6.

Figures 4.11 a-d show such ray traces for a range of z_1 distances. In Figure 4.11a, where $z_1 = \infty$, the caustic diameter increases as $z^{2/5}$. In Figure 4.11b, where z_1 is finite and negative, it can be seen that a maximum z_0 limit exists beyond which there is no caustic. This limit occurs at $z_0 = -z_1$ where the caustic diameter is zero and m (equation (4.41)) becomes infinity. In Figure 4.11c, where z_1 is finite and positive, the caustic diameter increases with z but more rapidly than with a collimated beam. Figure 4.11d shows the same convergent beam caustic as Figure 4.11c but without an imaging lens. This is the same representation as Theocaris has shown (Theocaris 1981) and demonstrates that a convergent beam can produce a real caustic in reflection. However, a virtual caustic is also produced and a close examination of Figure 4.11d reveals that the real caustic (negative z_0) is formed from rays at a large radius, r_0, with the virtual caustic (positive z_0) formed from small radii. Consequently, there exists an initial curve radius which is the boundary between

the real and virtual caustics. Neighbouring rays around this initial curve are parallel and so its caustic is situated at an infinite z_0 and has an infinite diameter. A caustic at an infinite z_0 may appear to be of no consequence. However, the inclusion of an imaging lens (Figure 4.11c) shows that a real image of this caustic can be presented on a screen. The lens produces a continuous real image of both real and virtual caustics. This extraordinary phenomenon seems not to have been previously noticed in 30 years' caustic research. Its

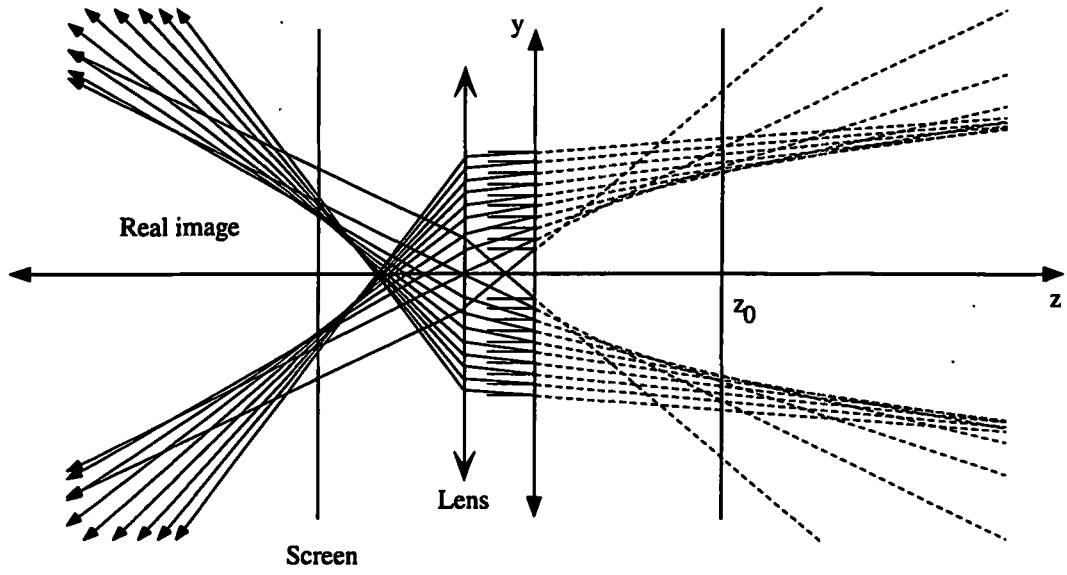

Figure 4.11a : The virtual caustic and the corresponding real image from a collimated incident beam

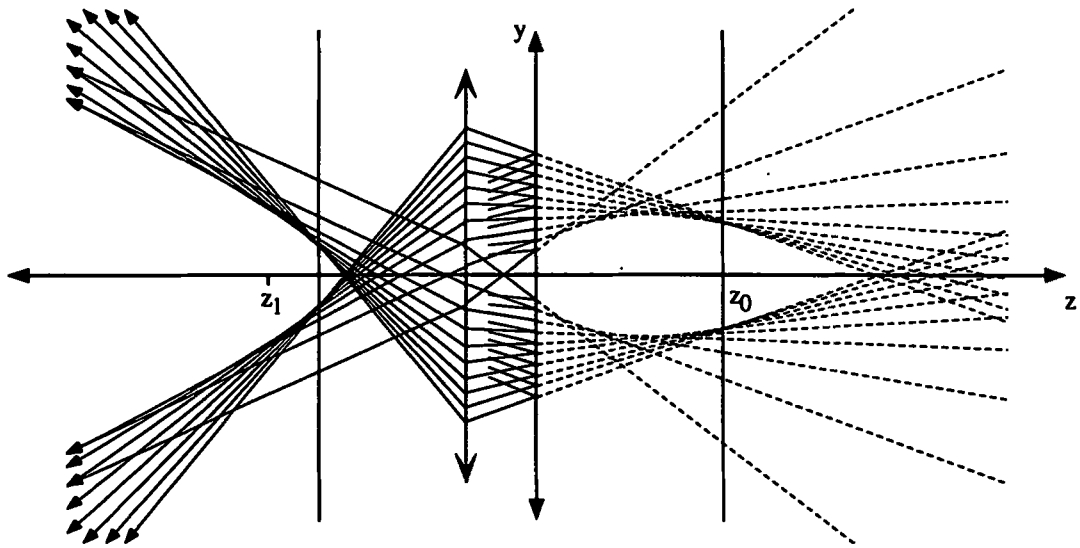

Figure 4.11b : The caustic produced from a divergent beam

physical significance will be discussed in Chapter 5.

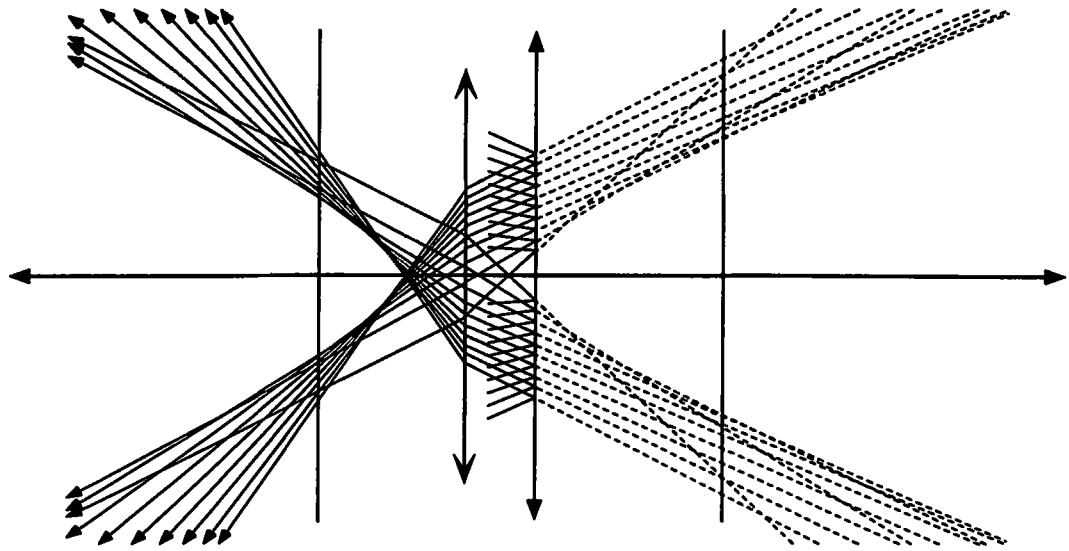

Figure 4.11c : The caustic produced from a convergent beam

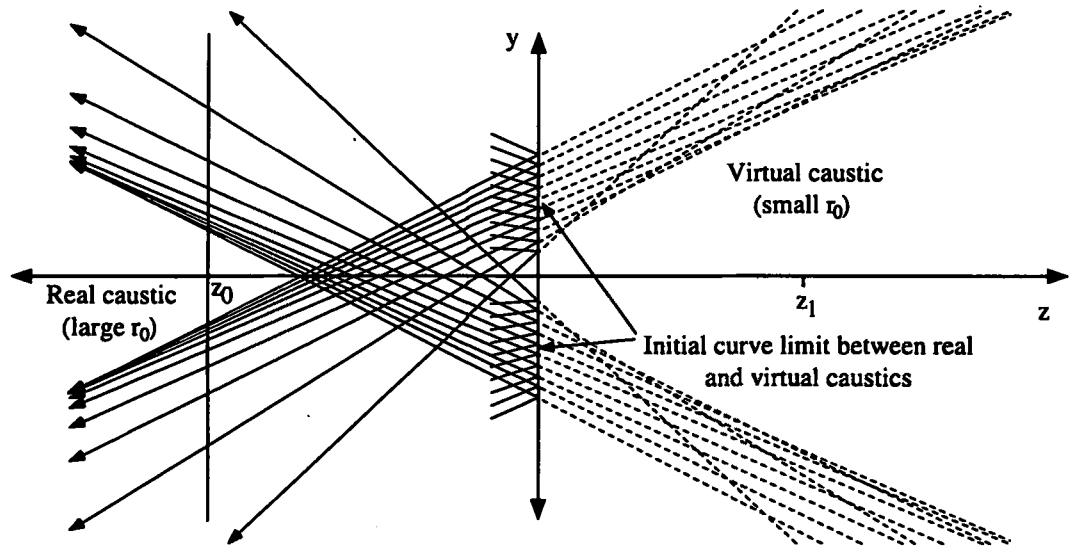

Figure 4.11d : Real and virtual caustics produced from a convergent beam without an imaging lens

4.2.5 Limitations of Stress Intensity Factor Measurements

In deriving the caustic formula (equation (4.27)) several assumptions are made:

both the surface deformation, f(x,y), and the surface gradient, f´(x,y), are small,

the specimen is in a plane stress state, and

the measurements are made within a K-dominant zone

For all conceivable engineering applications of caustics the surface deformation will be small with respect to the reference plane distance, z_0, and the surface gradient will be small with respect to unity. Consequently, the first assumption will be easily met.

Several researchers (Rosakis and Ravi-Chandar, 1986; Nigam and Shukla, 1987; Rosakis *et al*, 1990; Ma, 1990; Meletis *et al*, 1991; Smith and Freund, 1991) have analysed the limitations of the plane stress interpretation both experimentally and numerically and identified that plane stress conditions prevail at distances from the crack tip greater than half the plate thickness. Meletis *et al* (1991) provide the most specific results stating that this ratio actually varies between 0.7 and 0.37 for plate thicknesses from 3 to 12.5mm respectively. Regions closer to the crack tip exhibit a 3-dimensional stress state and yield smaller surface deformations than the elastic $1/\sqrt{r}$ singular field predicts (according to equations (4.15) and (4.19)). Caustics generated from initial curves within this triaxial stress state region will, therefore, have a reduced diameter and will consequently yield erroneous stress intensity factor measurements. The implications of this criterion cannot be underestimated. Achieving caustic measurements typically several millimetres from the crack tip where surface deformations are minute (particularly at low stress intensity factors) is a demanding requirement as will be demonstrated in the following chapters.

Violation of the assumption that the surface deformation is described to a good approximation by the inverse square root singularity field (equation (4.19)) can occur as a result of two factors. Firstly, close to the crack tip plastic zone there is a well known stress relaxation (described in Section 2.3) which causes a deviation from the $1/\sqrt{r}$ field. Zehnder and Rosakis (1986) have identified that the extent of this plasticity effect on caustic measurements will be small provided the initial curve radius from which the data are collected is greater than one and a half times the plane stress plastic zone size according to equation (2.6).

$$r_y = \frac{1}{2\pi}\left(\frac{K_I}{\sigma_{ys}}\right)^2 \qquad \text{(eqn. 2.6)}$$

where σ_{ys} is the yield strength of the material. In practice this criterion is unlikely to present a problem. Linear Elastic Fracture Mechanics is reliant on the small scale yielding criterion and most engineering materials of interest exhibit a sufficiently high yield strength to ensure

that measurements taken close enough to the plastic zone to violate this assumption will have already violated the plane stress assumption.

Far from the crack tip the stress field can also no longer be approximated by equation (4.19) since higher order terms in the series expansion begin to take effect. Theocaris & Petrou (1987) have numerically analysed this problem for a centre-cracked plate of infinite dimensions and crack length 2a and identified that the stress field can only be accurately described by the $1/\sqrt{r}$ term of the expansion for distances from the crack tip of up to 0.13a. This finding is re-iterated by Ma (1990) who identified (also by numerical analysis on a centre-cracked plate of infinite dimensions) that singular field dominance can be assumed for distances from the crack tip up to one-tenth of the crack length. Of course, since infinite plates were assumed in these analyses there is no edge effect limit defined using the more commonly quoted a/W ratio.

The initial curves chosen for caustic measurement, therefore, cannot be too small

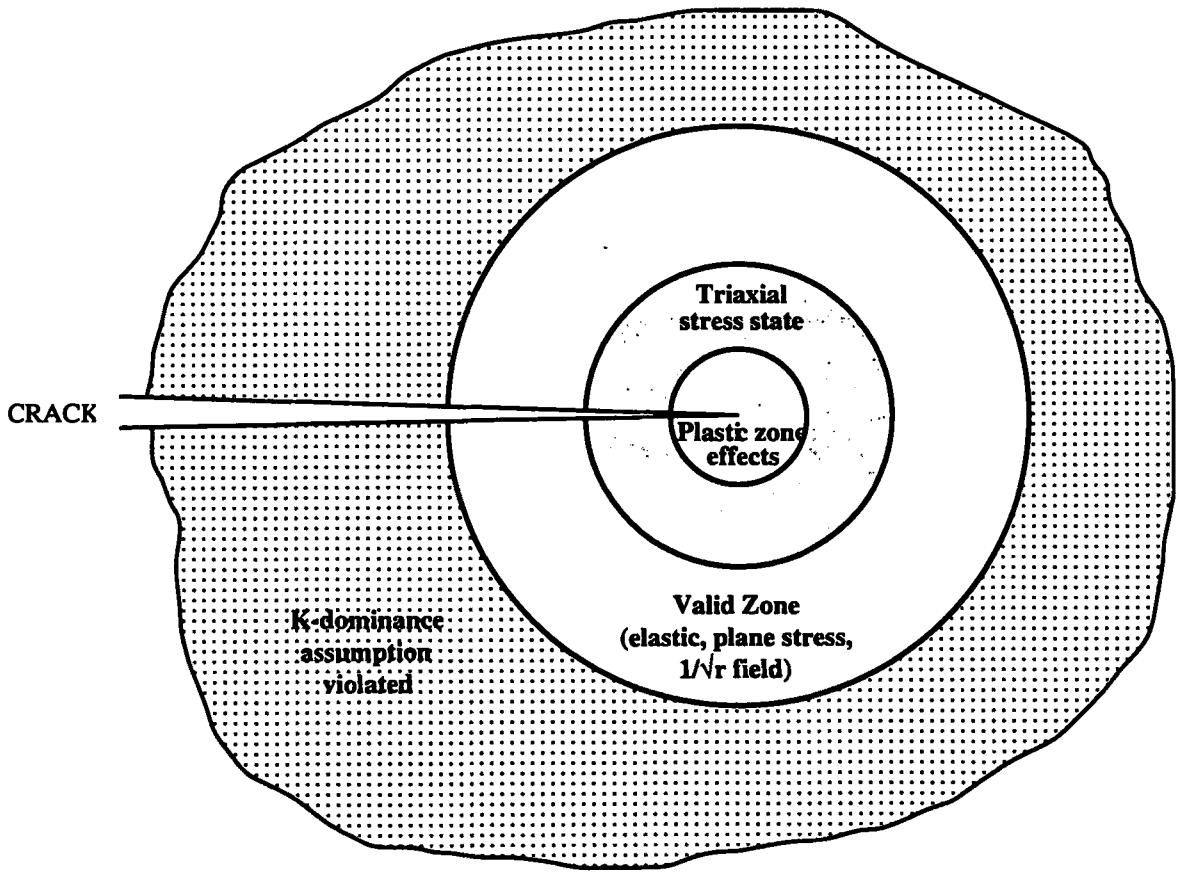

Figure 4.12 : Limits of r_0 which can be used for caustic measurements

because of the restrictions of the stress state and plasticity effect and cannot be too large because of the singular field dominance assumption. These limitations are summarised in equation (4.42) and in Figure 4.12 and show that the technique lends itself to thin, long-cracked specimens.

$$\sim\frac{1}{10}\text{ crack length (a)} > r_0 > \begin{cases}\frac{1}{2}\text{ specimen thickness (d)}\\ 1\frac{1}{2}\text{ plastic zone size } (r_y)\end{cases} \qquad (4.42)$$

4.2.6 Experimental Techniques

In this section of the thesis the basic experimental set-up shall be described together with the means of identifying the virtual caustic diameter and reference plane distance from the real image on the screen. The actual set-up used in this work is described in detail in Chapter 5.

One of the advantages of the method of caustics is the relative ease with which measurements can be taken. Basically, a light source, a lens and a means of viewing the caustic are all that are required for both transmitted and reflected caustics.

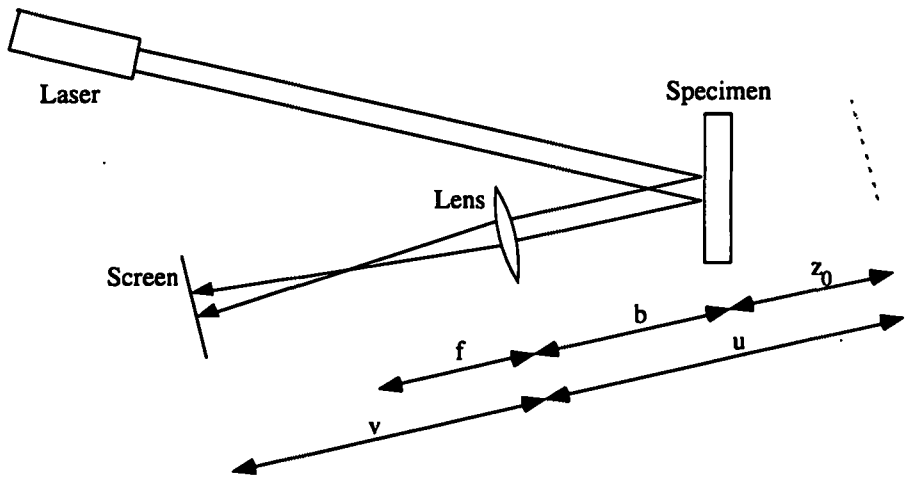

Figure 4.13 : Commonly used experimental set-up for reflected caustics (plan view)

Figure 4.13 shows the basis of the experimental arrangement used by virtually every researcher using reflected caustics. A light source, usually but not exclusively a laser (see for example Meyn (1992) and Konsta-Gdoutos and Gdoutos (1992)), is used to illuminate a plane specimen at a small angle of incidence. The reflected beam is passed through a positive lens and onto a screen where the real caustic image can be observed. Remarkably,

most researchers record the image by subsequently photographing the screen (see, for example, Theocaris, 1970, Theocaris and Philippidis; 1987; Rosakis *et al*, 1988; Zehnder and Rosakis, 1990; Shimizu and Takahashi, 1990; Meletis *et al*, 1991; Lee and Hahn, 1991) when it is clearly preferable to replace the screen with a camera body thus making the camera film itself the screen. In recent years a range of electro-optic sensors has been utilised as image detectors (see for example Rossmanith and Knasmillner (1991)) which have facilitated the measurement of caustic intensities. As described in Section 4.1, identification of the caustic intensity profile alleviates the ambiguity in the precise location of the geometrical caustic. Kamath and Kim (1986) have stated that the caustic diameter should be measured from points approximately half way between the inner edge and the peak intensity of the caustic ring.

To produce a finite z_1 a lens is used to focus the laser as shown in Figure 4.14.

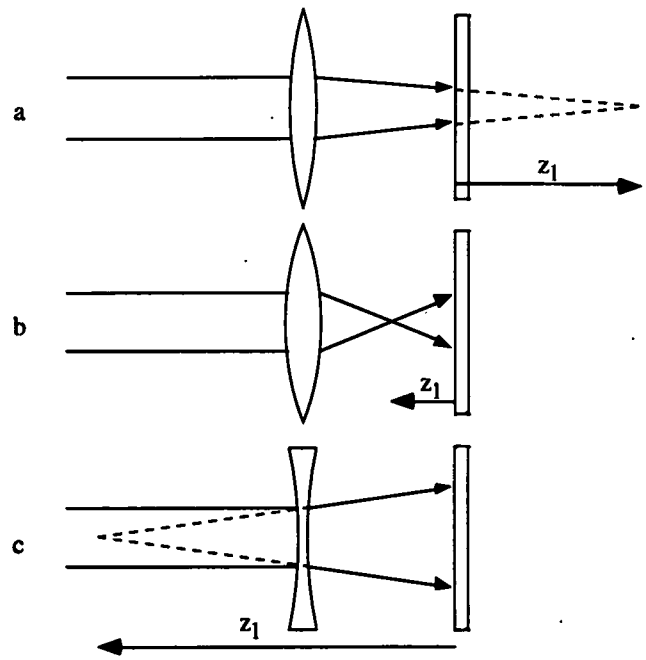

Figure 4.14 : Producing a non-collimated beam

Figure 4.14a shows a positive lens converging the beam to produce a virtual focus at a positive z_1. If the focus is before the specimen the beam then becomes divergent as in Figure 4.14b. An alternative means of producing a divergent beam, particularly for a long z_1, is with a negative lens as shown in Figure 4.14c.

The virtual caustic diameter, D, is calculated from image of the caustic, of diameter D′, and the magnification, M, of the imaging lens. The lens magnification can be determined by comparing the dimensions of a calibrated scale placed at the reference plane or actually on the specimen surface with its image on the screen (Kalthoff, 1987). The reference plane, however, is not readily accessible, being behind the specimen, and a scale placed on the specimen will appear out of focus. The magnification can more easily be calculated with the knowledge of the focal length of the lens, f, and the lens-screen separation, v, using the famous Gaussian lens equation:

$$\frac{1}{f} = \frac{1}{v} + \frac{1}{u} \tag{4.43}$$

and given that

$$M = \frac{v}{u} \tag{4.44}$$

which gives

$$D = \frac{f}{v-f} D' \tag{4.45}$$

where: f is the focal length of the lens

v is the distance between the lens and the screen

u is the distance between the reference plane and the lens

M is the magnification of the lens

Equation (4.43) can also be used to locate the reference plane which is being imaged. Equation (4.43) can be rearranged to:

$$u = \frac{fv}{v-f} \tag{4.46}$$

where

$$u = z_0 + b \tag{4.47}$$

and b is the specimen to lens distance. Therefore,

$$z_0 = \frac{fv}{v-f} - b \tag{4.48}$$

Thus, stress intensity factors can be determined for a given specimen by the measurement of the specimen to lens distance, b, lens to screen distance, v, and the caustic diameter, D′, using equations (4.27), (4.45) and (4.48).

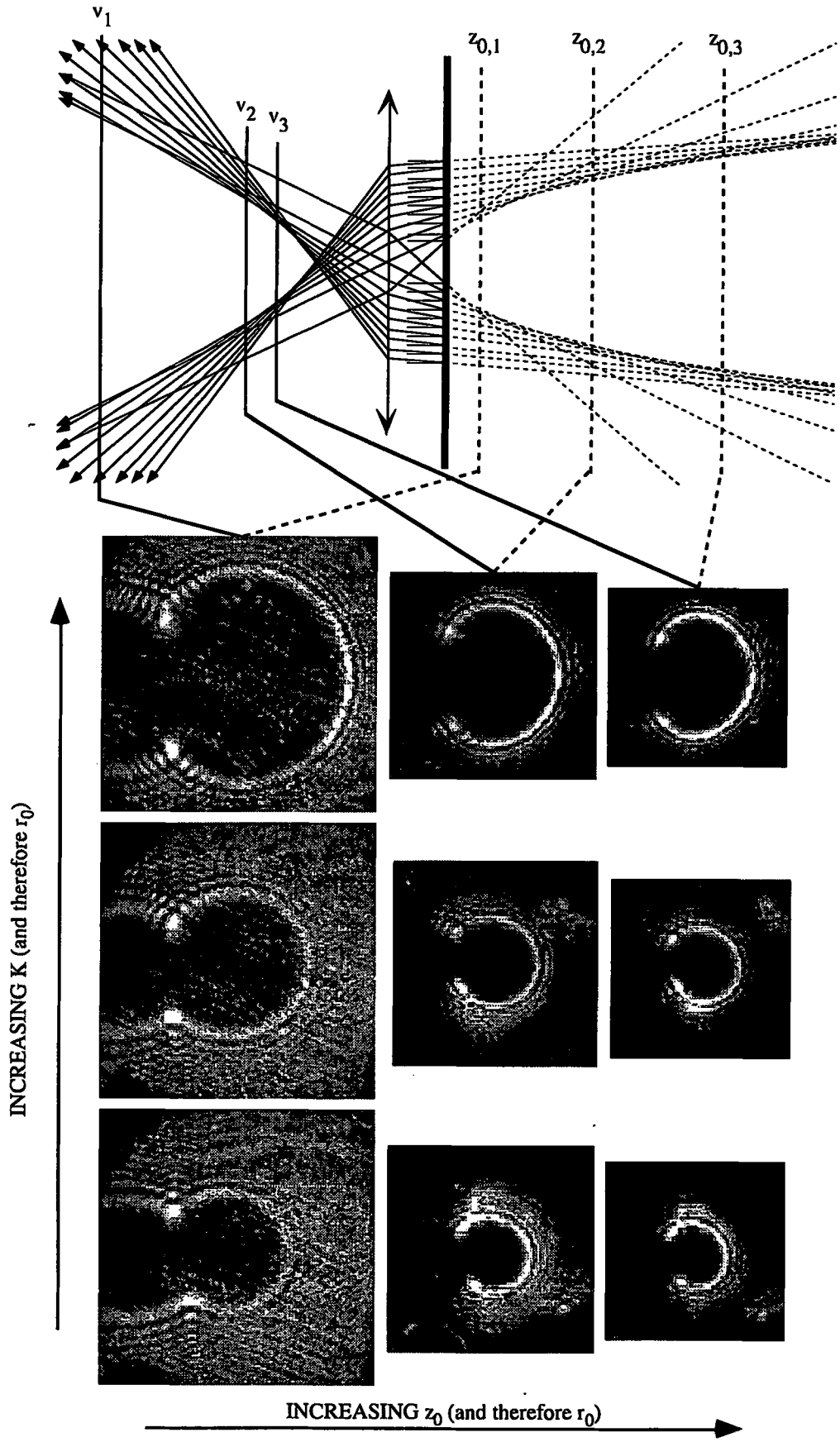

Figure 4.15 : Caustic images from a range of screen positions

In order to select the required initial curve radius such that it lies within the boundaries described in Section 4.2.5 the experimental arrangement is manipulated by adjustment of the lens to screen distance, v, to vary the reference plane distance, z_0, (equation (4.48)) which in turn changes the r_0 (equation (4.23)). If a range of stress intensity factors is measured it is usual for the lens to screen distance to require adjustment to keep the initial curve radius within the valid zone boundaries. To illustrate this, consider a typical compact tension specimen, where d=6mm, a=30mm and W=50mm, which is used to measure a stress intensity factor range from, say, 1-11 MPa$\sqrt{m}$. The minimum initial curve permitted for this specimen is 3mm (i.e. d/2). The maximum initial curve is 3.9mm (i.e. 0.13a). Now, equation (4.23) shows the initial curve radius to be proportional to $K_I^{2/5}$.

$$r_0 = \left(\frac{3K_I z_0 dv}{2\sqrt{2\pi}\, E}\right)^{2/5} \qquad \text{(eqn. 4.23)}$$

If the initial curve is set at the minimum 3mm when K=1 MPa$\sqrt{m}$ then the initial curve radius will reach the maximum 3.9mm at a stress intensity factor of 1.92 MPa$\sqrt{m}$. In order to measure up to 11 MPa$\sqrt{m}$ the caustic reference plane distance, z_0, needs to be incrementally adjusted for each K measured by adjustment of the lens to screen distance, v.

Figure 4.15 illustrates caustic images from three screen positions (and their corresponding z_0 positions). As the screen approaches the lens focus the diameter of the caustic image reduces (although the diameter of the virtual caustic increases) and both z_0 and r_0 increase. Also shown is the effect of the applied stress intensity factor on the caustic diameters for the three screen positions. For a given stress intensity factor a screen position can be chosen to select an initial curve within the required range. However, as Figure 4.15 demonstrates, to take measurements at large initial curves, particularly at low K, requires the measurement of small caustic diameters.

4.2.7 Applications of Caustics to Fracture Problems

Over the past 30 years the technique has been applied to a wide range of fracture problems. Whilst there has been some pioneering theoretical work ahead of the practical application (principally by Theocaris (1977, 1988, 1989a,b,c, 1991a,b)) most research has, understandably, focused on situations where alternative stress intensity factor measurements

and calculations are difficult or impossible (see, for example, the work of Sukere (1987) who measured stress intensity factors in rotating discs).

Mode I crack problems, being commonplace in engineering, have been awarded a substantial share of caustic effort. The technique has, however, been widely applied to a range of mixed mode loading conditions (Kalthoff, 1982, 1987; Nishioka *et al*, 1990a,b; Theocaris and Lazopoulos, 1991; Zhang and Ravi-Chandar, 1991; Hinderliter *et al*, 1991). Here the application of a shear component to the load causes the caustic to form a spiral curve (compare with Figure 4.8) with the size and eccentricity of the spiral revealing the stress intensity factor and mode mixity respectively.

The method of caustics has undoubtedly found a niche, however, in the field of dynamic fracture. Coupled with high speed photographic equipment, an optical technique is ideal for the measurement of dynamic stress intensity factors under impact conditions. Manogg's original work (Manogg, 1964) included dynamic fracture of PMMA using Schardin's multiflash source, and Kalthoff and his co-workers (Kalthoff *et al*, 1979, 1982; Beinert and Kalthoff, 1981) continued a similar line of work in a range of materials during the 1970s and 80s. As the caustics technique became more widespread during the 1980s its value in the study of dynamic fracture became recognised by various researchers (Rosakis *et al*, 1981, 1988, 1990; Vasudevan and Knauss, 1988; Nishioka *et al*, 1990a,b; Papadopoulos, 1990; Shigeru and Tadashi, 1991; Smith and Freund, 1991).

Environmental effects in fracture have also been analysed using caustics. Hermann and Holroyd (1985, 1986) investigated stress corrosion cracking (SCC) in aluminium alloy observing the change in caustic diameter in a range of environments. Gdoutos and Aifantis (1986) studied environmental cracking under mixed mode conditions, Abo-El-Ezz *et al* (1986) investigated methanol-induced crazing in PMMA and Meyn *et al* (1989) have investigated hydrogen assisted cracking in 4340 steel.

Although the caustic technique was developed for LEFM conditions, manipulation of the optical arrangement can facilitate measurements within the plastic zone to study plasticity effects. Rosakis *et al* (1988) applied caustics to elastic-plastic fracture mechanics to

investigate the J-integral under dynamic conditions and Theocaris (1991c) has been able to determine plastic stress intensity factors under similar elastic-plastic conditions.

Recently, the method has been applied to more complex situations such as interface cracks (Herrmann and Noe, 1992, 1993; Ahmad *et al*, 1994) between dissimilar materials. Such conditions have important engineering implications in areas such as the study of defective adhesive bonds. Here, caustics have the advantage of measuring the actual crack tip condition which is complex to calculate analytically or experimentally measure by other means.

Surprisingly, very little caustic work has been done to investigate fatigue phenomena, especially since the stress intensity factor is widely applied to fatigue. The first application seems to have been in 1991 when Hermann (1991) used caustics to investigate plasticity-induced closure in aluminium alloy compact tension specimens. This work was limited in scope, however, in that variations in closure as a result of variable amplitude loading or a change in stress ratio were not studied. In 1992 Leftheris and Papazian (1992) investigated compression fatigue. This study is peculiar, however, in that a Poisson expansion is observed at the crack tip as a result of a compression. The point of this work is that, according to Leftheris and Papazian, the compression caustic is generated from an initial curve which corresponds to the edge of the compressive plastic zone. The caustic was therefore used to predict the arrested crack length which corresponds to the edge of the compressive overload plastic zone. A series of tests measuring stress intensity factors throughout various fatigue cycles in a range of materials have been performed by Güngör *et al* (1992). Whilst these tests indicated some reduction in ΔK it was not possible to quantify ΔK_{eff}.

Of all the research conducted using the method of caustics the majority has utilised low elastic modulus materials such as PMMA, and usually in a transmitted caustics arrangement. When the method has been applied to the investigation of the properties of opaque materials, where it has been necessary to utilise reflected caustics, most of the work has centred on dynamic fracture. Now, by referring to equations (4.23) and (4.27) it can be seen that these two conditions are convenient for this technique. The use of a material with a low modulus of elasticity means that a large initial curve radius is more readily achieved (equation (4.23))

and the resulting caustic will have a large diameter (equation (4.27)). Impact tests are obviously performed at high stress intensity factor and again, even in stiff materials such as steel, yield a large initial curve and caustic diameter (see Figure 4.15). This has implications regarding the main limitation described in Section 4.2.5, that is, achieving an initial curve of at least half the specimen thickness. The use of a higher modulus material at a lower K requires a larger z_0 which, in turn, produces a smaller caustic image.

Measurements of low stress intensity factors in, say, aluminium alloy or steel have been conspicuous by their absence in the open literature. This is aptly demonstrated by the work of Rosakis and Ravi-Chandar (1986) who investigated the required initial curve radius to thickness ratio (r_0/d) for correct K measurement in PMMA and steel. The r_0/d presented for PMMA ranged from 0 to 2, whereas for steel the largest ratio presented was 0.6. Regarding this limit they state, "In the reflection arrangement, increasing r/h [r_0/d] above 0.6 proved increasingly difficult due to limitations in the experimental arrangement". Unfortunately, they failed to clarify both the precise experimental problem and the maximum stress intensity factor applied.

Other researchers seem to have encountered the same problem as Rosakis and Ravi-Chandar. Meletis *et al* (1991) conducted a similar set of tests analysing the required initial curve radius using 2090 aluminium alloy presenting results with r_0/d values limited to 0.65 at a stress intensity factor of 8.34MPa$\sqrt{m}$ in a 5.5mm thick specimen. Ogasawara *et al* (1992) reported that they could not achieve initial curves of d/2 in silicon nitride ceramic.

Initial results from this project echoed the above findings. Measurements at suitably large initial curves were fraught with imaging problems and experimental errors leading to excessive scatter in the results. In order to apply the method of caustics to engineering materials over a range of stress intensity factors it is clear that some refinement of the technique is required.

Chapter 5: OPTIMISATION OF THE REFLECTED CAUSTIC TECHNIQUE

5.1 INTRODUCTION

Chapter 4 detailed the theory underpinning the method of caustics and outlined the basic principles behind the practical application of the technique. In this chapter the method is scrutinised from an experimental point of view. A number of critical factors are highlighted which have a strong bearing on the accuracy of the method and a novel modification of the technique is described which produces a remarkable increase in its precision.

Despite the increasing popularity of the technique little attention has been given to experimental considerations. Theocaris and Razem (1981) have published an error analysis paper which assesses the effects of errors in, for instance, screen position and specimen thickness. Rossmanith (1983) has analysed the effects of an irregular specimen thickness on caustic measurements. Meyn (1992) has produced a number of practical recommendations regarding the photography of caustics and a few researchers (for instance, Rossmanith and Knassmillner (1991) and Sukere (1986)) have discussed their use of electro-optic detectors to measure caustic images.

The experimental considerations behind generating caustic measurements can be divided into two categories:

i) producing the virtual caustic - this includes the optical source to produce the incident beam, and the specimen

ii) imaging the caustic - this includes the imaging lens and the detector system

5.2 PRODUCTION OF THE VIRTUAL CAUSTIC

5.2.1 Properties Of The Incident Beam

5.2.1.1 General

The incident beam used for caustic measurements is required to be spatially and (preferably) temporally coherent. Spatial coherence means that the beam is generated from a point source and despite the fact that some researchers (for instance, Konsta-Gdoutos and Gdoutos (1992)) neglect this requirement a simple geometrical argument as described by Meyn (1992) demonstrates its significance. Temporal coherence is provided by a monochromatic source and, although is not essential, facilitates the use of non-achromatised lenses to manipulate the incident beam and image the caustic.

Such a coherent source lends itself to spatial filtering. This is commonly done by focusing the incident beam on a pinhole to remove high spatial frequencies present in the beam. The result of this filtering is to eliminate scattered light from the beam and so improve its imaging qualities. Spatial filtering is described in many optical texts, for instance, Klein (1970).

The diameter of the incident beam is merely required to be greater than the initial curve diameter which is unlikely to exceed 30mm for most applications. A helium-neon laser, with a suitably expanded beam, provides a readily available and cost effective source to meet these requirements.

5.2.1.2 Beam Configuration

The type of incident beam used in caustic measurements, that is, the location of the beam focus, z_1, was described in Section 4.2.4 which showed that dramatically different caustics

can be produced with different configurations. Simple comparisons between them, however, do not reveal an obviously advantageous beam type. The following analysis assesses the configurations from the point of view of experimental errors.

Recalling equations (4.39), (4.45) and (4.48):

$$K_I = \left(\frac{ED^{5/2}}{10.71 z_0 dv}\right) . m^{3/2} \qquad \text{(eq. 4.39)}$$

where:

$$m = \frac{z_1}{z_1+z_0}$$

$$D = \frac{f}{v-f} D' \qquad \text{(eq. 4.45)}$$

$$z_0 = \frac{fv}{v-f} - b \qquad \text{(eq. 4.48)}$$

Now, substituting equations (4.45) and (4.48) into equation (4.39), standard error analysis shows the relative error in stress intensity factor measurement is given by:δ

$$\left(\frac{\delta K_I}{K_I}\right)^2 = \left[\frac{\left(\frac{fv}{v-f}\right)^2\left(\left(\frac{\delta v}{v}\right)^2 + \left(\frac{\delta v}{v-f}\right)^2\right) + (\delta b)^2}{z_0^2}\right] + \left(\frac{\delta d}{d}\right)^2 + \frac{5}{2}\left[\left(\frac{\delta D'}{D'}\right)^2 + \left(\frac{\delta v}{v-f}\right)^2\right]$$

$$+ \frac{3}{2}\left[\left(\frac{\delta z_1}{z_1}\right)^2 + \frac{(\delta z_1)^2 + \left(\frac{fv}{v-f}\right)^2\left(\left(\frac{\delta v}{v}\right)^2 + \left(\frac{\delta v}{v-f}\right)^2\right) + (\delta b)^2}{(z_1+z_0)^2}\right] \qquad (5.1)$$

where the errors are limited to the measurable quantities of z_0, z_1, D', v, d and b (that is, errors in the material modulus, Poisson's ratio and the lens focal length are assumed to be negligible; they are, of course, irrelevant for the purpose of comparing beam configurations).

The next section of the analysis will quantify the measurement parameters (z_0, D' and v) for given specimen (E, v and d), loading (K) and optical arrangement (f, b and z_1). It is necessary to maintain a fixed initial curve radius between beam configurations and so

comparisons shall be made for caustics taken from initial curve radii equal to d/2. Recalling equation (4.40)

$$r_0 = \frac{D}{3.17}\left(\frac{z_1}{z_1+z_0}\right) \qquad \text{(eq. 4.40)}$$

and rearranging to

$$D = 3.17\left(\frac{z_1+z_0}{z_1}\right)\cdot\left(\frac{d}{2}\right) \qquad (5.2)$$

Equation (5.2) can be substituted into equation (4.39) to produce:

$$K_I = \left(\frac{(3.17)^{5/2}\, E\, d^{3/2}}{2^{5/2}\,(10.71)\,v}\right)\cdot\left(\frac{z_1+z_0}{z_1 z_0}\right) \qquad (5.3)$$

which rearranges to:

$$\frac{1}{z_0} = \frac{K_I\, v\,(10.71)(2)^{5/2}}{(3.17)^{5/2}\, E\, d^{3/2}} - \frac{1}{z_1} \qquad (5.4)$$

Therefore, for a given specimen, loading and z_1, equation (5.4) defines the required z_0 to achieve an initial curve radius of half the specimen thickness. Notice that for a collimated beam the $1/z_1$ term vanishes.

Equation (4.48) can be rearranged to determine the required lens-screen distance, v:

$$v = \frac{f\,(z_0+b)}{z_0+b-f} \qquad (5.5)$$

By substituting equation (5.5) into equation (4.45) it follows that the measured caustic diameter, D′, can be given by:

$$D' = \frac{fD}{z_0+b-f} \qquad (5.6)$$

Equation (5.2) can be substituted into equation (5.6) to give:

$$D' = 3.17\left(\frac{z_1+z_0}{z_1}\right)\cdot\left(\frac{d}{2}\right)\cdot\left(\frac{f}{z_0+b-f}\right) \qquad (5.7)$$

Therefore, equations (5.4), (5.5) and (5.7) define the variables which, when input into equation (5.1), determine the experimental error in stress intensity factor measurement for any z_1.

Figures 5.1 and 5.2 show the relative error in K measurement as a function of z_1 for a range of stress intensity factors and lens focal lengths respectively. For completeness a wide

range of z_1 distances is modelled despite the fact that some will be impractical to use in the laboratory. The parameters and errors used in the calculation are:

δd=20μm (d=5mm) δb=5mm (b=0.5m)

δv=3mm δz_1=3mm + 0.1% of z_1

$\delta D'$=20μm

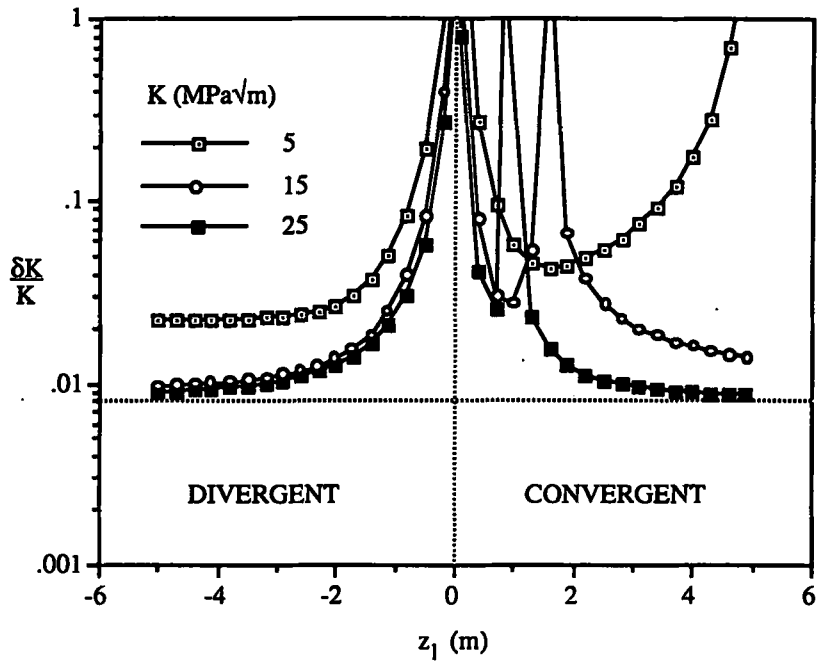

Figure 5.1 : Experimental errors as a function of z_1 for a range of stress intensity factors (lens focal length = 1m)

As Figures 5.1 and 5.2 show, the measurement errors tend to infinity as z_1 tends to zero. A second singularity is seen with a convergent beam at a z_1 value which is a function of the stress intensity factor. This point corresponds to the screen being positioned at a distance from the lens equal to the lens focal length (that is v = f in the Gaussian lens equation (4.43)). This means the lens is being used at infinite conjugate; it will produce an image from an infinite object distance. A screen placed at this position will, therefore, display a caustic from an infinite z_0 as mentioned in Section 4.2.4. It can be seen from equations (4.45) and (4.48) that the calculated virtual caustic diameter, D, and reference plane distance, z_0, are highly sensitive to the screen position in this region which leads to erroneous stress intensity factor measurements.

Figure 5.1 concludes that, for a given imaging lens, experimental errors vary inversely as the z_1 and stress intensity factor. Furthermore a divergent beam with a z_1 of less than about 1m and all convergent beams should be avoided. Whilst experimental errors remain relatively constant for z_1 values above around 2m, the impracticality of measuring very long z_1 distances indicates that a collimated incident beam should be used.

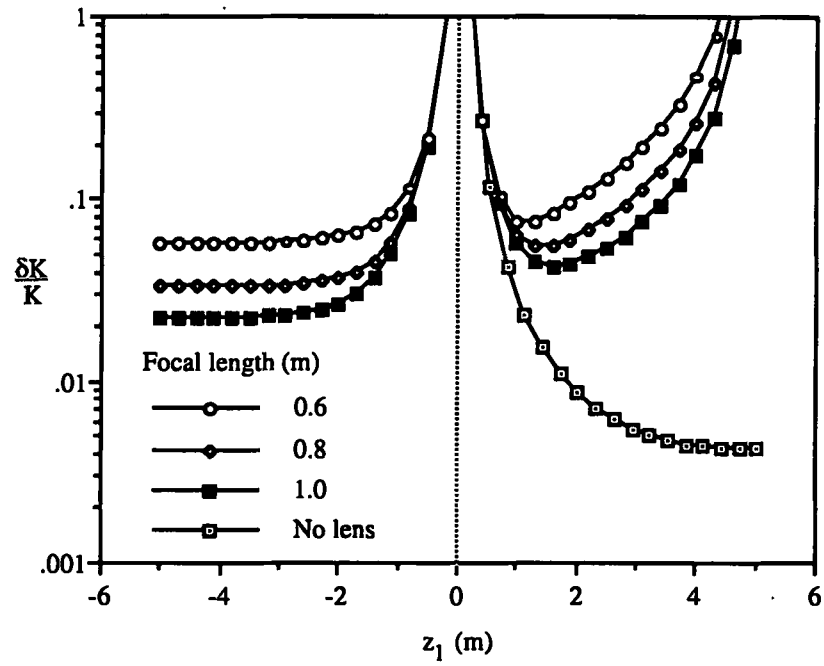

Figure 5.2 : Experimental errors as a function of z_1 for a range of lens focal lengths

(K=5MPa$\sqrt{m}$)

Figure 5.2 shows the error in K measurement as a function of the focal length of the imaging lens and demonstrates that experimental errors vary inversely as the focal length of the imaging lens. Figure 5.2 also indicates that using a long z_1 convergent beam without an imaging lens (modelled as an infinite focal length imaging lens) would minimise errors. However, the focal length of the convergent beam lens must exceed the z_1 required (see Figure 4.14a) and so this is impractical for z_1 distances much greater than 1m since lenses of very long focal length are not freely available. Furthermore, as Figure 4.11d demonstrates, the specimen to screen distance (z_0 in this configuration) must exceed z_1 and it is generally desirable for this to not extend to several metres.

The conclusion from Figures 5.1 and 5.2 is that the optimum experimental arrangement for measuring K using caustics is a collimated incident beam coupled with a long focal length imaging lens.

5.2.1.3 Incident Beam Quality

A collimated beam can also be described as a beam of light with a plane wavefront. A divergent or convergent beam is similarly described as having a spherical wavefront. Each configuration, however, will inevitably exhibit wavefront errors resulting from errors in the optics used to produce the incident beam.* In conventional imaging systems a wavefront error results in an image degradation. This section analyses the effects of an incident beam wavefront error on caustic measurements.

Consider a nominally plane wavefront but with a radius, r, and an error, ε. For simplicity, assume the error is spherical, that is, the beam is slightly diverging as shown in Figure 5.3.

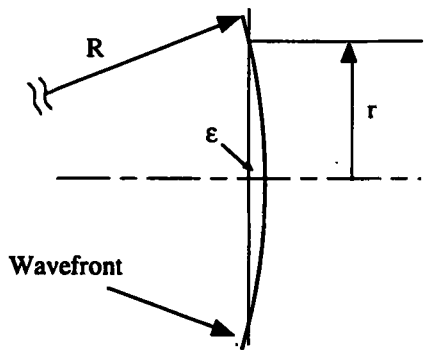

Figure 5.3 : A simplified wavefront error on a collimated beam

There is one important distinguishing feature between caustic imaging and conventional imaging. Normally an image is formed by bringing a family of rays to a common focus. In the analysis of caustics, however, it is necessary to consider only the annulus of rays which produces the caustic at the particular z_0 position to which the screen corresponds since all

---

* *A divergent beam can be produced by focusing a beam onto a small pinhole (of several micrometres diameter). The pinhole then acts as a point source of a spherical wavefront which requires no further optics and so has essentially no wavefront error. Since, in this arrangement, the pinhole position determines the z_1, this property of a divergent beam would only be relevant at small z_1 distances.*

other rays merely produce the illumination outside the caustic. Now, by definition, a ray is normal to a wavefront and so in the above example all rays diverge from a point a distance R behind the wavefront. (For a general wavefront error the divergence or convergence point will be a function of the rays considered). From the theorem of intersecting chords, the divergence point is given by:

$$R = \frac{r^2}{2\varepsilon} \tag{5.8}$$

In equation (5.8) R corresponds to z_1 and r is the radius of the incident beam and so the non-collimated beam scaling factor of equation (4.39) can be given as:

$$m^{3/2} = \left(\frac{-r^2/2\varepsilon}{-r^2/2\varepsilon + z_0} \right)^{3/2} \tag{5.9}$$

Therefore, an incident beam wavefront error has the effect of modifying the size of the caustic rather than influencing its image quality. If the incident beam is assumed to be collimated then equation (5.9) determines an error factor in the K measurement.

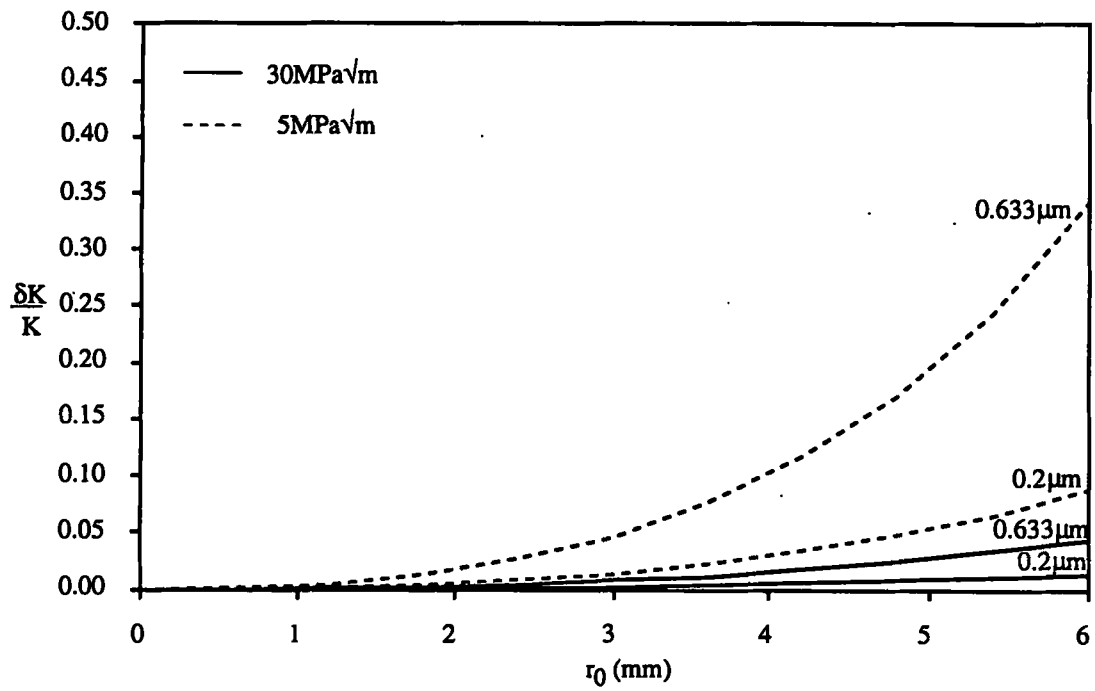

Figure 5.4 : Experimental errors resulting from an incident beam spherical wavefront error

Figure 5.4 displays the error in stress intensity factor as a function of initial curve radius for the case of a 25mm diameter incident beam with wavefront errors of 0.2μm and 0.633μm* on a 6mm thick aluminium alloy specimen loaded to stress intensity factors of 5MPa$\sqrt{m}$ and 30MPa$\sqrt{m}$. Figure 5.4 indicates that the sensitivity to wavefront error increases rapidly with initial curve radius and varies inversely as the stress intensity factor. Of course, as mentioned in Section 4.2.5, the initial curve radius is required to be greater than d/2 (ie 3mm in this case) for a stress intensity factor measurement to be in the plane stress region of the specimen. A modest wavefront error of one wavelength can introduce substantial errors in the measurement of low stress intensity factors. Measurements at K_I values approaching the fracture toughness, however, will not be greatly affected.

The above analysis assumes the wavefront error is spherical. In fact, the form of the error for a typical laser beam expander will approximate to that shown in Figure 5.5. In this case the rays close to the beam axis will be converging whereas at the edge of the beam they will be diverging. Although the above analysis is a simplified account of a typical error the effect is essentially the same and the analysis gives an indication of the sensitivity of this type of error. A high quality (multi-element), commercially available beam expander is likely to have a wavefront error of better than 0.2μm over an aperture of at least 25mm. An expander assembled from singlet lenses of similar f/number will be considerably worse.

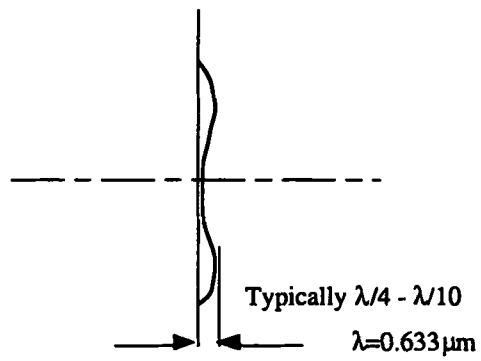

Figure 5.5 : Typical wavefront error in a commercially available laser beam expander

* *0.633μm is equivalent to one wavelength of a helium-neon laser.*

Although the utilisation of a high quality beam expander should alleviate the problem described in the above analysis, it is nevertheless imperative that the expander is suitably focused to produce an accurately collimated beam; focus adjustments are normally provided, the whole range of which may produce a barely discernible change to the beam divergence. A small optical testing device known as a 'shear plate interferometer' is commonly used to measure very small beam di/convergences and is recommended to accurately collimate the incident beam.

5.2.2 Optical Properties of the Specimen

The method of caustics is based on the physical principle that a stress concentration induces an out of plane surface displacement field. As mentioned previously, the measurement region (the initial curve) may be several millimetres from the crack tip where the effects of a Poisson contraction are relatively small, particularly at low stress intensities. It is imperative, therefore, that the surface of the unloaded specimen is nominally flat and that this flatness is maintained upon the application of a load. This section examines the required specimen surface flatness and the effect of form error on caustic measurements. This analysis is not applicable to caustics in transmission where sensitivity to form error is greatly reduced.

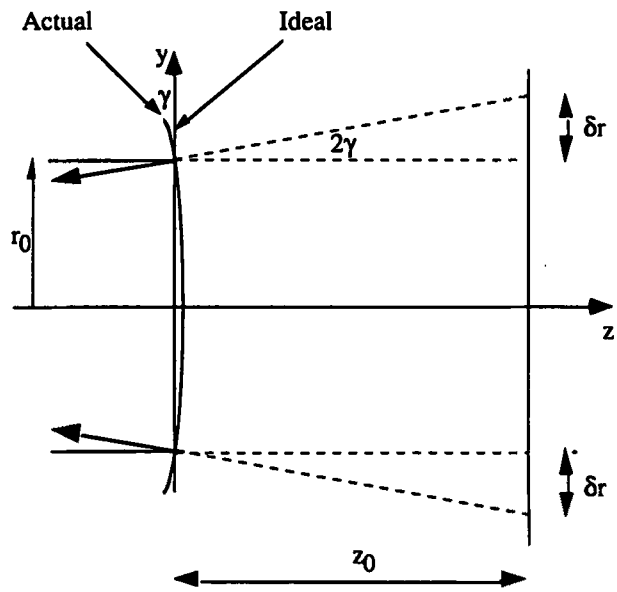

Figure 5.6 : Modelling the caustic effects of a specimen surface form error

Consider a specimen whose surface departs from an ideal plane with a form error as shown in Figure 5.6 such that

$$z = g(y) \qquad (\text{or } z = g(r_0)) \qquad (5.10)$$

where, of course, y is equivalent to r_0 in the y-direction when a caustic ray is considered. Although, in practice, a form error will be a function of both x and y it is assumed for convenience that there is no form error in the x-direction. If this surface makes an angle, γ, with the x,y-plane, then

$$g'(y) = -\tan\gamma \qquad (5.11)$$

This will cause an incident ray to be deviated by 2γ such that its virtual ray position a distance z_0 behind the surface is deviated by δr. Now, assuming g(y) and g'(y) are small then

$$\delta r = 2z_0\gamma \qquad (5.12)$$

Now, consider Figure 5.6 to be describing a cracked specimen prior to loading. Upon loading, the surface will deform in the characteristic way to produce a caustic but the existing form error will still deviate the rays by an extra 2γ over and above that deviation caused by the K-field. This will have the effect of changing the size of the caustic produced a distance z_0 behind the surface by $2\delta r$. Equation (5.12) shows that for a given form error the actual change in the caustic diameter is proportional to z_0. Referring again to equations (4.39) and (4.40):

$$K_I = \left(\frac{ED^{5/2}}{10.71 z_0 dv}\right) . m^{3/2} \qquad (\text{eq. 4.39})$$

$$r_0 = \frac{D}{3.17} m \qquad (\text{eq. 4.40})$$

Note that, to maintain a generalisation, the non-collimated beam scaling factor, m, is included. Substituting equation (4.40) into (4.39) gives:

$$K_I = \left(\frac{ED^{5/2}}{10.71 z_0 dv}\right) . \left(\frac{3.17 r_0}{D}\right)^{3/2} \qquad (5.13)$$

which rearranges to

$$D = \left(\frac{10.71\ K_I\ z_0 dv}{E}\right).\ (3.17 r_0)^{-3/2} \qquad (5.14)$$

Dividing equation (5.12) by (5.14) produces

$$\frac{\delta r}{D} = 2\gamma\left(\frac{E}{10.71\ K_I\ dv}\right).\ (3.17 r_0)^{3/2} \qquad (5.15)$$

therefore

$$\frac{\delta D}{D} = \frac{2\delta r}{D} = 4\gamma\left(\frac{E}{10.71\ K_I\ dv}\right).\ (3.17 r_0)^{3/2} \qquad (5.16)$$

Equation (5.16) describes the relative change in caustic diameter as a result of a form error on the specimen surface. It shows that for a given γ the fractional change in the caustic transverse diameter is proportional to $r_0^{3/2}$ and that since both m and z_0 are absent from equation (5.16) this effect is independent of beam configuration.

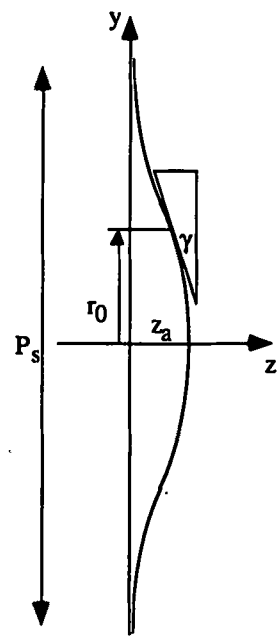

Figure 5.7 : Sinusoidal surface form error

Now, consider a surface form error which is sinusoidal (and for simplicity centred on the crack) as in Figure 5.7. There is no particular reason why the surface should be sinusoidal but it is assumed that the random action of a surface preparation method such as polishing is more likely to approximate to this form than, say, a spherical form. Regardless of the validity of this assumption, the following analysis will give an indication of the sensitivity of

a surface form error on stress intensity factor measurements. The surface topography can therefore be assumed to be given by

$$z = \frac{z_a}{2} + \frac{z_a}{2}\cos\left(\frac{2\pi r_0}{P_s}\right) \tag{5.17}$$

where z_a is the depth of the surface sag and P_s is the period of the sine wave. The surface gradient is therefore given by:

$$g'(r_0) = \frac{dz}{dr_0} = -\frac{\pi z_a}{P_s}\sin\left(\frac{2\pi r_0}{P_s}\right) = -\gamma \tag{5.18}$$

therefore:

$$\gamma = \frac{\pi z_a}{P_s}\sin\left(\frac{2\pi r_0}{P_s}\right) \tag{5.19}$$

Substituting equation (5.19) into (5.16) produces:

$$\frac{\delta D}{D} = \frac{4\pi z_a}{P_s}\left(\frac{E}{10.71\ K_I\, dv}\right).(3.17 r_0)^{3/2}.\sin\left(\frac{2\pi r_0}{P_s}\right) \tag{5.20}$$

Equation (5.20) gives the relative change in caustic diameter as a result of a surface sag of z_a which approximates to a sinusoidal form over a period, P_s. The error in K calculated from this is amplified since D is raised to the power of 5/2 in equation (4.39) and is therefore given by:

$$\frac{\delta K}{K} = \frac{10\pi z_a}{P_s}\left(\frac{E}{10.71\ K_I\, dv}\right).(3.17 r_0)^{3/2}.\sin\left(\frac{2\pi r_0}{P_s}\right) \tag{5.21}$$

Equation (5.21) further demonstrates the strong dependence of the initial curve radius and stress intensity factor on experimental errors. Figure 5.8 shows equation (5.21) graphically as $\delta K/K$ as a function of r_0 for a 6mm thick aluminium alloy specimen with form errors of 0.2μm and 0.633μm over a period of 50mm loaded to 5MPa$\sqrt{m}$ and 30MPa$\sqrt{m}$. In order to maintain errors to less than 10% Figure 5.8 indicates that, unless very high stress intensity factors are measured, the specimen needs to be manufactured to a flatness of within a small fraction of a micrometre over a 50mm range. Surprisingly, Theocaris and Razem (1981) stated that specimen used in caustic experiments need no special surface preparation.

Achieving such a demanding accuracy necessitates the use of optical manufacturing technology. Non-ferrous metallic mirrors (and some non-metallic components) are usually

manufactured to a high specification by the method of single point diamond machining. This technique can routinely achieve sub-micrometre flatness over relatively large areas, say, 150mm diameter. Some materials, steel for instance, cannot be diamond machined and so the recommended method of surface preparation for these is the 'coating adhesion' technique as described by Zhilkin *et al* (1990) and also by Ahmad and Edwards (1994). In this technique a metallic coating is first deposited onto a flat glass substrate and then bonded to the specimen. Once cured the substrate can be removed leaving the coating adhered to the specimen with a thin layer of epoxy. The epoxy acts to accommodate the mismatch between the specimen and the flat glass substrate.

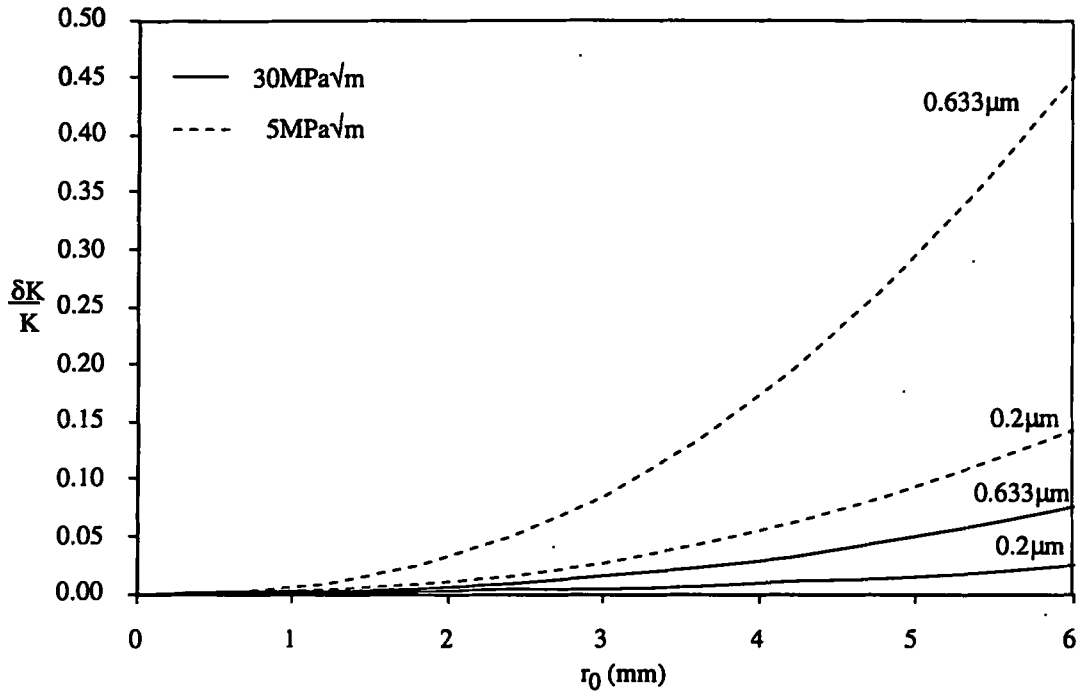

Figure 5.8 : Experimental errors resulting from a sinusoidal surface form error

5.2.3 Split Beam Caustics

The use of an accurately flat specimen, however, does not guarantee the elimination of surface form error. Upon specimen loading any misalignment between the loading clevises will introduce a slight bend into the nominally flat specimen producing an identical effect to that described above. In this case the error will be limited to the loading (y) direction. Figure 5.9 shows caustics produced from misaligned loading fixtures. Figure 5.9a describes the caustic from a surface deformed in a convex manner showing an reduced

caustic (the deformation opposing the Poisson contraction). The caustic in Figure 5.9b is produced from a concave surface. During the early phases of this research it was not anticipated that pure tension loading would induce any bending in the specimen. Consequently, misalignment induced distortion was found to be a major problem in achieving reliable caustic measurements.

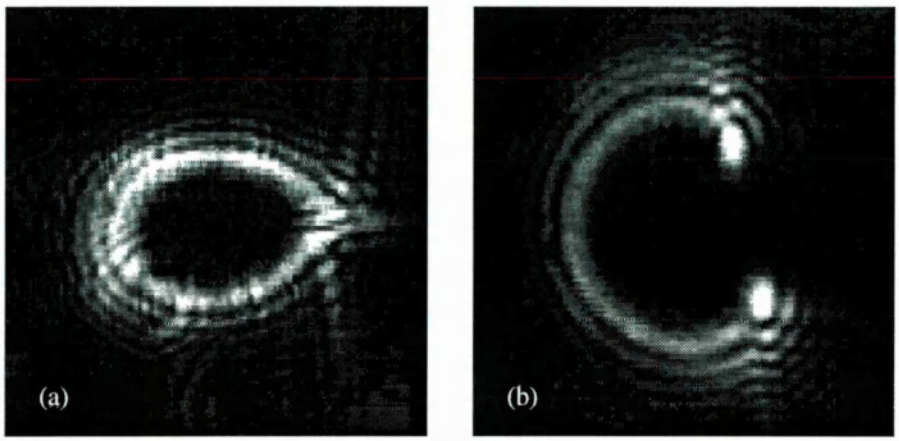

Figure 5.9 : The effect of load induced distortion on caustic images

In order to overcome this problem the misalignment needs to be measured. To determine the specimen form error an interferometer of the Twyman-Green type can be built around the apparatus utilising the existing laser as described by Wallhead *et al* (1994).

Once the misalignment is identified it can be minimised by a fine adjustment of the angle between the clevis pins in the loading mechanism. A technique was developed for this research whereby the pins are mounted in eccentric adjusters within the clevises (see Figure 5.10). By rotating an adjuster the clevis pin precesses a cone about the nominal pin axis. If the two adjusters are contra-rotated to the same extent the result is to produce a net lateral tilt to the whole specimen and an equal and opposite vertical tilt to each pin (see Figure 5.11). This allows the specimen to be manually deformed in a cylindrical manner. An adjuster eccentricity of a fraction of a millimetre was found to provide sufficient adjustment to deform the specimen surface between Figures 5.9a and 5.9b.

This adjustment technique together with the *in situ* interferometry enables the specimen distortion to be minimised. However, all adjustments must be made at relatively low applied loads where the friction between the adjuster and the clevis can be overcome. Upon

changing the load some element of distortion can be reintroduced into the specimen. This residual distortion is observed to be a variable function of the applied load and as such cannot be eliminated.

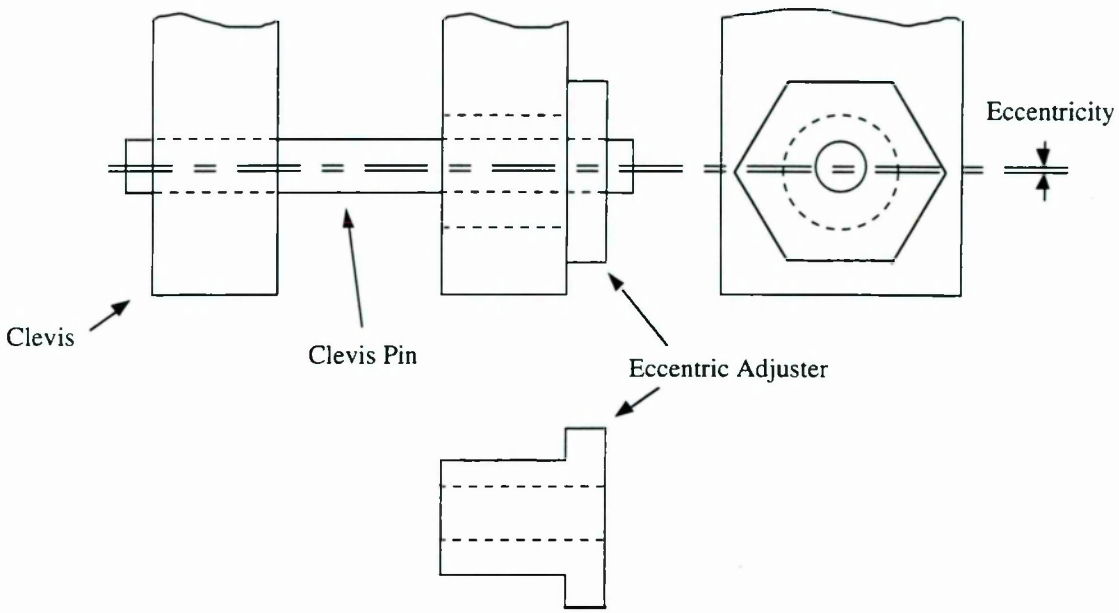

Figure 5.10 : Eccentric method of fine adjustment of loading clevises

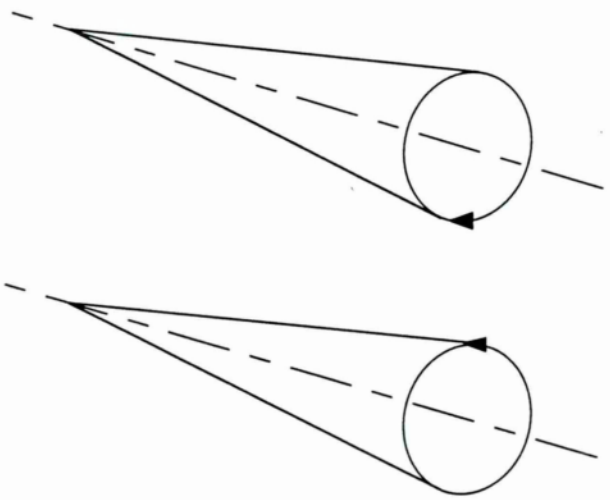

Figure 5.11 : Contrarotating eccentric adjusters

Despite some success with this technique a different philosophy has subsequently been adopted in this research. Rather than to eliminate all of the distortion, the aim has been to identify the extent of bending and to then compensate for it. In achieving this objective a

novel modification of the reflected caustic technique has been developed. This modification, termed "Split Beam Caustics", has been used in all of the experiments described in Chapter 6.

The total transverse diameter of the caustic is produced from both the localised Poisson contraction and the overall specimen distortion. Now, the Poisson contraction is identical on both sides of the specimen whereas the distortion on one side will be equal and opposite to that on the other. If both sides of the specimen are simultaneously measured the two caustic diameters should facilitate discrimination between the Poisson contraction and the specimen distortion.

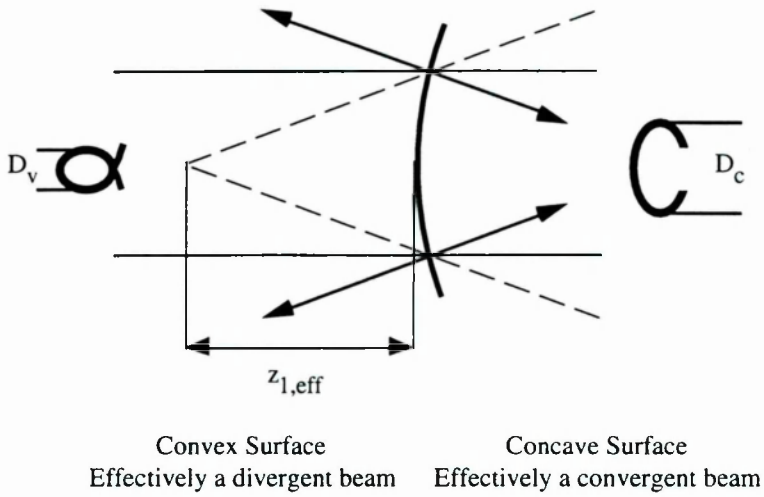

Figure 5.12 : Distorted specimen ray trace

Consider a specimen loaded in tension with the inevitable misalignment induced distortion as in Figure 5.12. The beam on the concave side of the specimen reflects as if the incident beam were convergent. On the convex side the reflected beam appears to be divergent. Both beams have the same effective focus, a point at a distance $z_{1(eff)}$ from the specimen. (In fact $z_{1(eff)}$ should be measured from each surface. However, $z_{1(eff)} \gg d$ and so this difference can be ignored). Figure 5.12 also shows the compression and elongation of the caustic on the convex and concave side of the specimen respectively.

If the specimen is assumed to distort in a manner approximating to a cylindrical cross-section then the caustics can be analysed as if incident with a non-collimated beam. Referring, again, to equation (4.39):

$$K_I = \left(\frac{ED^{5/2}}{10.71 z_0 dv}\right) \cdot \left(\frac{z_1}{z_1+z_0}\right)^{3/2} \qquad \text{(eq. 4.39)}$$

This rearranges to

$$\frac{10.71\ K_I\ dv}{E} = \frac{D^{5/2}}{z_0} \cdot \left(\frac{z_1}{z_1+z_0}\right)^{3/2} \qquad (5.22)$$

For a given specimen (ie. for a fixed d, E and ν) distorted under loading to a stress intensity factor (K_I) to give an effective z_1 ($z_{1(eff)}$):

$$\frac{10.71\ K_I\ dv}{E} = \frac{D_v^{5/2}}{z_0} \cdot \left(\frac{z_{1(eff)}}{z_{1(eff)}-z_0}\right)^{3/2} = \frac{D_c^{5/2}}{z_0} \cdot \left(\frac{z_{1(eff)}}{z_{1(eff)}+z_0}\right)^{3/2} \qquad (5.23)$$

For a measurement on the convex surface — For a measurement on the concave surface

where: D_v is the virtual caustic diameter as measured from the convex surface of the specimen

D_c is the virtual caustic diameter as measured from the concave surface of the specimen

Therefore

$$\frac{D_v^5}{(z_{1(eff)}-z_0)^3} = \frac{D_c^5}{(z_{1(eff)}+z_0)^3} \qquad (5.24)$$

from which it follows that

$$z_{1(eff)} = \left(\frac{D_c^{5/3} + D_v^{5/3}}{D_c^{5/3} - D_v^{5/3}}\right) z_0 \qquad (5.25)$$

Now, by substituting equation (5.25) into either form of equation (5.23) it can be shown that

$$K_I = \frac{E}{10.71 z_0 dv} \cdot \left(\frac{D_c^{5/3}+D_v^{5/3}}{2}\right)^{3/2} \qquad (5.26)$$

By comparing equation (5.26) with equation (4.27) it can be seen that the collimated beam caustic equation is modified such that the one caustic diameter is replaced by a weighted average of the caustics from each surface.

To simultaneously produce caustics from either side of the specimen requires an experimental arrangement radically different from that used by other caustic researchers

which was shown in Figure 4.13. The arrangement used in this work is shown in Figures 5.13 and 5.14. The incident laser beam is split by a 50/50 beamsplitter. The beams are then directed by a series of fold mirrors to either side of the specimen from where they retroreflect back to the beamsplitter. Here they recombine, pass through the imaging lens to form two images on the screen or optical detector. A small tilt should be introduced to one of the fold mirrors to separate the images.

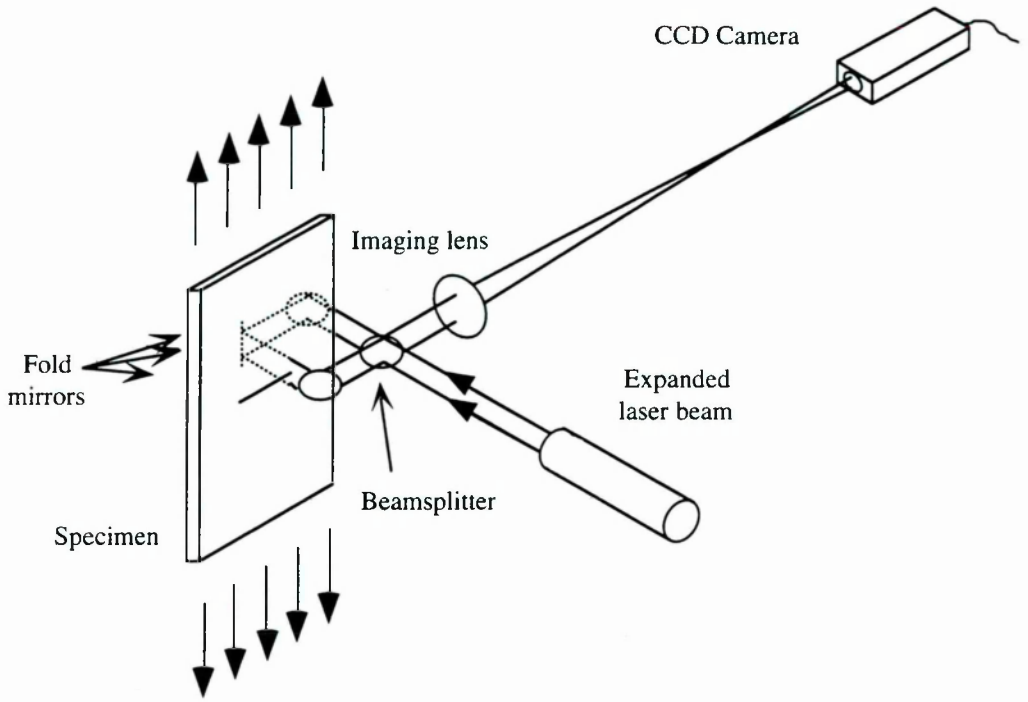

Figure 5.13 : Split beam caustics set-up

When adopting this technique several important criteria must be considered. Firstly, to compensate for surface distortion it is imperative that the specimen form error on each surface is no greater than the load induced distortion (though the specimen need not be parallel). Secondly, the incident beam should be accurately collimated, that is, z_1 should be much higher than $z_{1(eff)}$. These two criteria ensure that $z_{1(eff)}$ is the same on either side of the specimen. Thirdly, it can be seen from Figure 5.13 that the distance, b, between the imaging lens and each surface is different. This δb gives rise to a difference in z_0 in equation (4.48). However, as equation (4.48) shows, an error δb in b results in an error δb in z_0 , therefore provided $z_0 \gg \delta b$ this effect can be ignored.

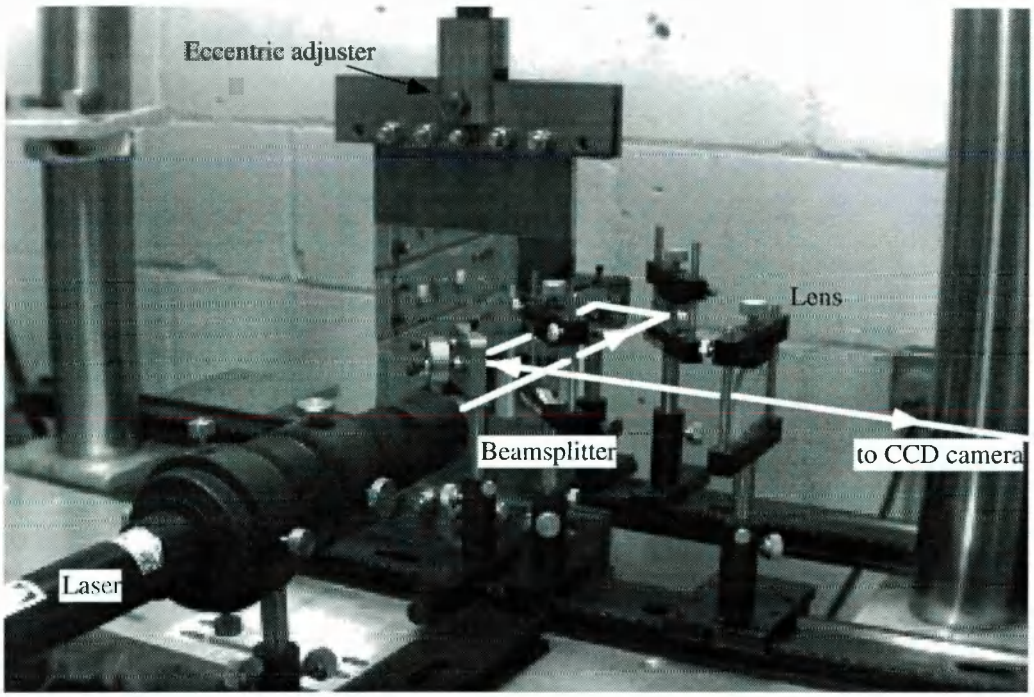

Figure 5.14 : Experimental set-up

One final point is that Figure 5.12 is not entirely representative of a real split beam ray trace. The caustics from each surface of a bent specimen (from the same z_0) are, in fact, generated from different initial curves, the difference being a function of the difference between D_c and D_v. Provided both caustics are generated from a region of the specimen which meets the limitations described in Section 4.2.5 equation (5.26) is reliable. This will be the case if the caustic diameters, and therefore initial curves, are similar. It is therefore necessary that the procedure of clevis pin adjustment is utilised to produce similar caustic diameters and that equation (5.26) is used to compensate for residual errors.

Figure 5.15 presents split beam caustic results for a 6mm thick aluminium alloy specimen loaded to a stress intensity factor of 4.3MPa$\sqrt{m}$. The Figure shows the ratio of the stress intensity factor measured using caustics to those calculated from far field variables against the normalised initial curve radius (r_0/d). The curves from the individual surface measurements, which are calculated without accounting for specimen bending, indicate errors increasing rapidly with r_0 and reach almost 50%. The curve calculated using equation (5.26), however, shows excellent agreement with theory for r_0/d ratios between 0.5 and 1.0 (which correspond to z_0 distances of between 10m and 30m respectively).

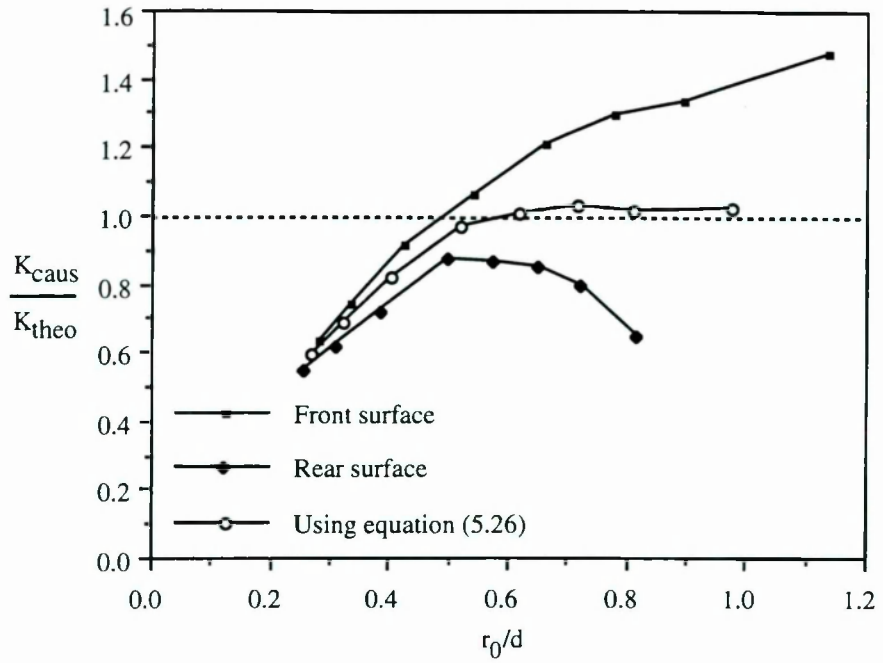

Figure 5.15 : Results using the split beam caustic technique (d=6mm, K=4.3MPa$\sqrt{m}$)

To appreciate this technique's sensitivity to errors consider the extent of the bending which introduced the errors in Figure 5.15. The $z_{1(eff)}$ calculated for these measurements was approximately 100m. That is, over an initial curve radius of 6mm the specimen approximates a cylinder with a radius of curvature of 200m and so a diameter of 400m. Using the theorem of intersecting chords to calculate the sagittal height (h) of a surface of diameter (ϕ) over radius (r):

$$(\phi - h)h = r^2 \qquad (5.27)$$

Given that ϕ=400m and r=6mm

$$h \approx 0.1\mu m \qquad (5.28)$$

Therefore, a surface sag of only 0.1μm over a 12mm area can produce up to 50% error in stress intensity factor measurement if a single surface measurement is made. This level of sensitivity to surface distortion is of the same order of magnitude as that described in Section 5.2.2 for surface form error resulting from specimen manufacturing.

5.3 IMAGING THE CAUSTIC

Given that an accurate virtual caustic is produced, what remains is to ensure that information is not lost when producing an image of the caustic on a screen. This section details the requirements of the imaging lens and describes a suitable means of recording the caustic.

5.3.1 The Imaging Lens

It was stated in Section 5.2.1.2 that the imaging lens should have as long a focal length as is practically possible. This results in a large image magnification between the virtual and real caustics and so minimises the uncertainty in the diameter measurement. It would be understandable to assume that the only additional requirement would be for the lens to produce a high resolution caustic image implying the need for a large aperture, perhaps multi-element, lens. This assumption seems to have been made by Meyn (1992) who, in analysing the caustic technique, recommends the use of a high resolution imaging lens with a minimum depth of field. The depth of field requirement stems from the desire to avoid a finite depth of the caustic surface (ie. a range of z_0 distances) being imaged onto the same screen position resulting in a blurred caustic image.

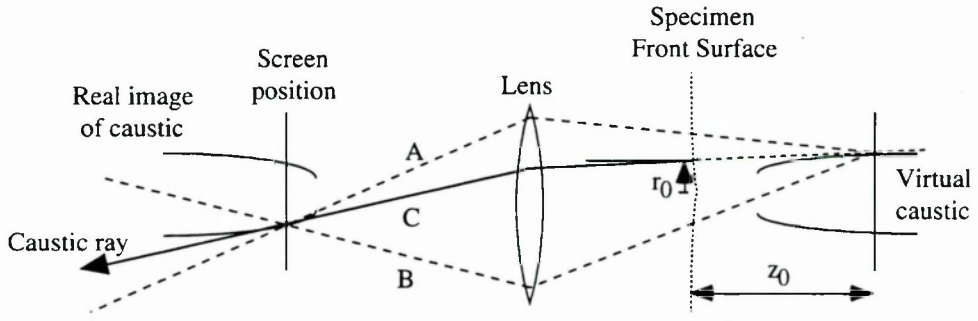

Figure 5.16 : Comparison of caustic imaging and conventional imaging

In fact, this assumption is incorrect (Wallhead and Edwards, 1993). As stated previously when imaging a caustic some conventional optical analyses do not apply. In conventional imaging a lens collects a solid angle of rays from a point on an object and focuses them to a spot of finite size dependent upon the lens resolution. It is this principle which gives rise to a depth of field. Since only the ray tangential to the caustic surface produces the caustic image this effect is not observed.

This is explained in Figure 5.16 which shows the caustic imaging. If the virtual caustic were a solid object then the lens would collect a solid angle of rays (with A and B being the extreme rays) and focus them to produce an image of the object at the screen position. Movement of the screen would bring the image in and out of focus and there would be a depth of field. However, only the tangential ray (ray C) emanates from that position on the caustic at that particular z_0. Ray C passes through the lens and becomes tangential to the real image of the caustic at the position where it is intercepted by the screen. The lens, in fact, can be considered to be merely deviating a ray by a certain angle rather than providing a focusing action *per se*. Figure 5.17 shows that at a different z_0 (say z_{02}) the caustic ray would propagate in a different direction passing through the lens at a different position and would be deviated by a different angle. This ray would be tangential to the real caustic surface at screen position 2 and would intercept a screen in position 1 outside the caustic diameter. In fact, rays from all other z_0 distances intercept the screen outside the caustic. Consequently, these rays do not blur the caustic, nor do they introduce any ambiguity into the caustic measurement. An alternative way of considering this is that movement of the screen between positions 1 and 2 continually selects the rays which intercept the screen immediately outside the shadow spot and that the caustic image can never actually be 'out of focus'. Furthermore, stopping down the aperture which, according to Meyn, would increase the depth of field and blur the caustic will actually only prevent the illumination outside the caustic from reaching the screen. Not until the lens is stopped down as far as ray C will it have the catastrophic effect of obliterating the caustic from that z_0 altogether.

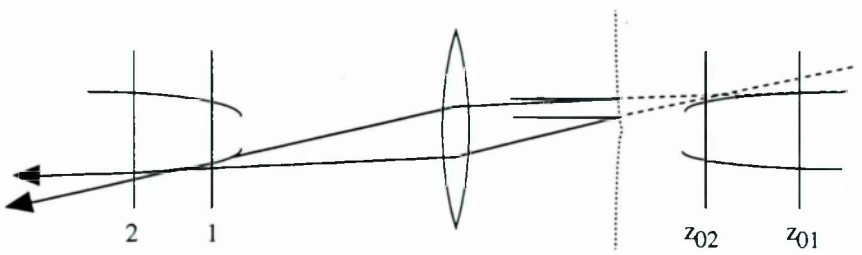

Figure 5.17 : Caustic rays from different z_0 distances

It should be noted that despite describing the lens as a means of deviating individual rays rather than focusing a group of rays, the fact that ray C of Figure 5.16 is equivalent to one of

a cone of rays (between A and B) in conventional imaging means that the Gaussian lens equation (4.43) can still be applied to the caustic ray to calculate the z_0 and the caustic magnification.

The resolution requirements of the lens, from the point of view of caustics, can be analysed using similar considerations as those for depth of field. In conventional imaging the resolving power of a lens is a function of its aperture due to both diffraction effects and aberrations. The unusual diffraction effects around caustics have been thoroughly analysed by Kamath and Kim (1986) and appear to be independent of any lens aperture contributions. The following analysis shows that the presence of aberrations in caustic experiments has a completely different effect to conventional imaging.

Limiting the analysis to monochromatic light and very low field angles (as is the case with caustic measurements) restricts imaging errors to only spherical aberration. Figure 5.18 schematically shows the effects of spherical aberration on the imaging ability of a singlet lens. This aberration causes marginal rays to be brought to a closer focus than axial rays, the result being an increase in the focus spot size and therefore a blurring of the image. A larger aperture at the same focal length (ie a higher relative aperture or lower f-number) increases this effect and so reduces the resolution of the lens.

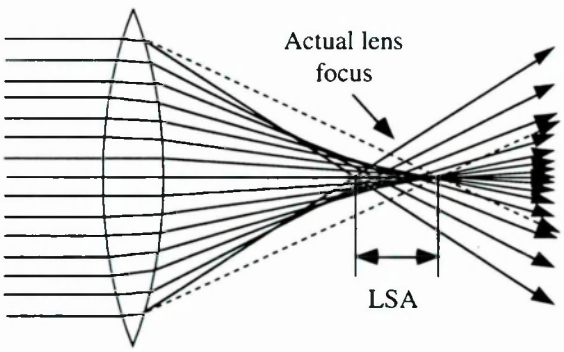

Figure 5.18 : Spherical aberration

For caustic imaging, however, where annuli of rays are selected, spherical aberration does not result in a degradation of the image but causes the focal length of the lens to be a function of the rays considered. That is, rays from a large initial curve are deviated through a greater angle than if the lens were free of spherical aberration (the dashed rays in Figure 5.18) and

this results in an increased caustic diameter from that initial curve. Figure 5.18 shows this focus shift which is known as longitudinal spherical aberration (LSA). LSA is proportional to the square of the aperture (Longhurst 1966) and, by simple geometry, is proportional to the focal length at the same f-number. As an example, an f/5 bi-convex lens with a 100mm focal length operating at unity conjugate ratio (magnification of 1) will have a longitudinal spherical aberration of approximately 1.7mm. Therefore, with caustic measurements from an initial curve radius of 10mm the focal length should be assumed to be 98.3mm (a 1.7% shift). Using a lens with a focal length of 500mm under the same conditions will reduce the LSA to a negligible 0.34mm (a 0.068% shift). A long focal length lens has the properties of producing a high caustic magnification and a low spherical aberration. Therefore, a simple, long focal length singlet lens provides an ideal means of imaging the virtual caustic.

5.3.2 Detection of the Caustic

It has been common practice to record the caustic image on photographic film. As described in Chapter 4, it is well known that there is ambiguity in the location of a caustic edge due to diffraction effects. This was first realised in the early 19th century by Airy (1838) and has been recently studied with respect to crack tip caustics by Kamath and Kim (1986). They recommend that the diameter should be measured from a caustic intensity profile plot across the caustic diameter and that the caustic edge according to geometrical optics occurs at approximately half the maximum intensity point in the diffracted caustic. From a photograph this point can only be estimated and is further complicated by the non-linearity of the film and by the risk of over- or underexposure.

More recently several researchers (see, for example, Rossmanith and Knassmillner (1991)) have adopted electro-optic detectors to measure the caustic intensity profile. Such detectors are available in a variety of forms; single detectors which can be used to scan the caustic, linear detector arrays and 2-dimensional arrays commonly used in CCD cameras. The experiments described in Chapter 6 utilise a CCD camera with computer interface

incorporating image processing software*. An example of an intensity plot across a caustic transverse diameter using this system is shown in Figure 5.19.

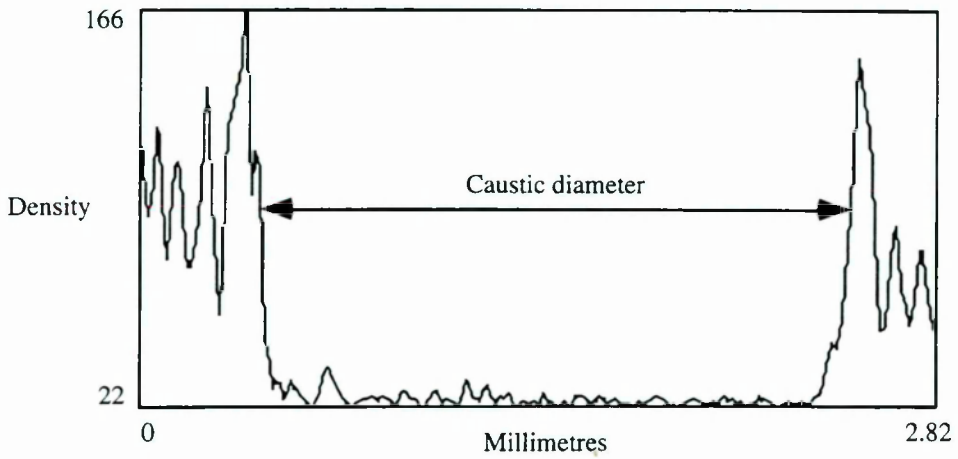

Figure 5.19 : Caustic intensity plot generated from image processing of caustic captured using a CCD camera

5.4 CONCLUSIONS

The optical method of caustics provides a convenient way of experimentally determining stress intensity factors in flat plates containing through-thickness cracks. However, caustic measurements are highly sensitive to experimental errors. Errors vary inversely as the stress intensity factor and also increase dramatically with initial curve radius. This is exacerbated by the fact that this radius needs to be greater than half the specimen thickness. By modelling each section of the caustic forming process the following conclusions are drawn.

i) The specimen should be illuminated with an accurately collimated laser beam produced from a high quality expander. The collimation can be best set using a shear plate interferometer.

---

* *Analysis performed on a Macintosh IIsi computer using the public domain NIH Image program (written by Wayne Rasband at the U.S. National Institutes of Health and available from the Internet by anonymous ftp from zippy.nimh.nih.gov or on floppy disc from NTIS, 5285 Port Royal Rd., Springfield, VA 22161, part number PB93-504868).*

ii) The specimen form error should not exceed a small fraction of a micrometre per 50mm diameter specimen area. The most practical way of achieving this on most metallic specimens is to use high precision single point diamond machining.

iii) The loading train must be accurately aligned to minimise specimen distortion upon loading. The Split Beam Caustic set-up should be utilised to eliminate the effects of any residual load induced distortion.

iv) A simple singlet lens is sufficient to image the caustic. A lens of long focal length is recommended for high magnification and low spherical aberration.

v) An electro-optic detector, such as a CCD camera, is recommended to record the caustic so that the effects of diffraction at the caustic edge can be accounted for in the diameter measurement.

Chapter 6: THE APPLICATION OF REFLECTED CAUSTICS TO FATIGUE CRACK GROWTH

6.1 INTRODUCTION

Chapters 4 and 5 demonstrated that the method of caustics provides an effective means of remotely and non-destructively measuring stress intensity factors. However, analytical solutions of stress intensity factors are widely tabulated (see, for example, Sih, 1973; Rooke and Cartwright, 1976). Only in circumstances where

a) no analytical solution exists

b) one or more of the analytical parameters (eg crack length or applied load) cannot be determined

c) the analytical solution cannot be applied

will the technique find widespread application.

In fatigue crack growth where crack closure is prevalent, the premature contact between the crack surfaces provides a force which will perturb the crack tip stress field. Only when the crack is fully open will the stress intensity factor be calculable with the analytical solution; as was illustrated in Chapter 3, at the minimum load of the fatigue cycle the crack tip actually experiences a higher stress intensity factor, K_{cl}, as a result of the load borne by

the crack surfaces. A partially or fully closed crack therefore falls within category c) above where the analytical solution is known to be invalid. The method of caustics therefore has an application in the study of the variations in the crack tip stress field during fatigue crack growth so as to ascertain ΔK_{eff}. By comparing the stress intensity factor measured using caustics, K_{caus}, with the analytically determined theoretical stress intensity factor, K_{theo}, over the range of the fatigue cycle it should be possible to determine the extent of the crack tip shielding due to closure.

Experiments conducted at constant amplitude loading which produces a fixed level of crack closure can be compared with controlled variable amplitude loading (eg single tensile overload) which will shift the closure level and accordingly change the crack growth rate, da/dN.

6.2 EXPERIMENTS

To investigate the application of the method of caustics to the measurement of crack closure a series of experiments has been conducted under a range of loading conditions using the caustic set-up described in Chapter 5.

6.2.1 Specimen Material and Configuration

The material used in these experiments was 2024-T3 aluminium alloy configured into centre-cracked panel specimens (300mm × 160mm in plane dimensions by 6-7mm thickness) (see Figure 6.1). The material properties of this alloy are given in Table 6.1.

Table 6.1: 2024-T3 Aluminium Alloy Material Properties

Young's Modulus (E)	69 GPa
Poisson's ratio (ν)	0.34
Yield Strength (σ_y)	363 MPa
Ultimate Tensile Strength (σ_{UTS})	476 MPa

This material is widely used in the aerospace industry and is known to exhibit substantial crack closure. Consequently it has been the subject of much research. Being configured

into a centre-cracked panel specimen, it conforms to a common engineering problem of a crack growing from a fastener hole (for instance, in an aircraft wing skin). In addition, it provides a suitable comparison for the original experimental closure work by Elber (1971), and the analytical and numerical work of Newman (1981, 1984). Both of these researchers considered 2024-T3 aluminium alloy centre-cracked panel specimens.

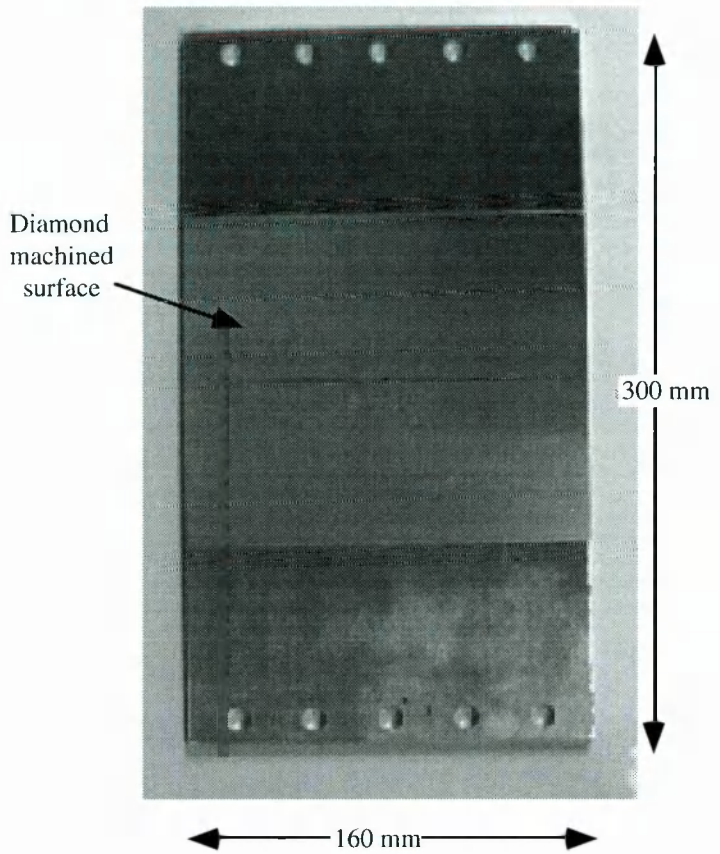

Figure 6.1 : Example of a centre-cracked panel specimen used in the experiments

Several analytical solutions exist for this specimen configuration (Ewalds and Wanhill, 1986). The one adopted by the American Society for Testing and Materials (ASTM) (equation 6.1) is given by Feddersen (1967).

$$K = \sqrt{\sec\left(\frac{\pi a}{W}\right)}\,\sigma\sqrt{\pi a} \qquad (6.1)$$

where a is the half crack length; W is the total plate width and σ is the far field applied stress. Equation (6.1) is valid for $2a/W<0.95$ and is accurate to 0.3% for $2a/W<0.7$.

The specimens were prepared by electro-discharge machining a narrow notch (approximately 80μm root radius) to a length of typically 60mm (30mm half crack length).

Both surfaces were prepared by single point diamond machining to a flatness of typically 0.1μm per 25mm diameter so that the specimens exhibited a mirror finish.

6.2.2 Stress Intensity Factor Measurement

Before covering the detail of the range of experiments it is first necessary to elaborate on the precise process of the calculation of K from the caustic measurements. Figure 4.12 illustrated that a caustic can be measured, and stress intensity factor calculated, from a range of radii from the crack tip where an elastic, plane stress, $1/\sqrt{r}$ K-field dominates. Since the initial curve radius is not known prior to the measurements, the first step of the K calculation is to determine the limits of the valid zone. As described in Chapter 4, the initial curve radius is a function of the lens to screen distance, v. Therefore, by recording a caustic at several camera positions the stress intensity factor will be measured at a range of initial curves which are determined from equation (4.25) ($D=3.17r_0$). By plotting the measured stress intensity factors, K_{caus}, against the initial curve radii the measurements which were made within the valid zone can then be identified. Figure 6.2 shows a plot of K_{caus} against r_0 for a 2024-T3 centre cracked panel specimen with an applied stress intensity factor of 11.1 MPa$\sqrt{m}$ (shown on the Figure). Points are shown for eight different camera positions

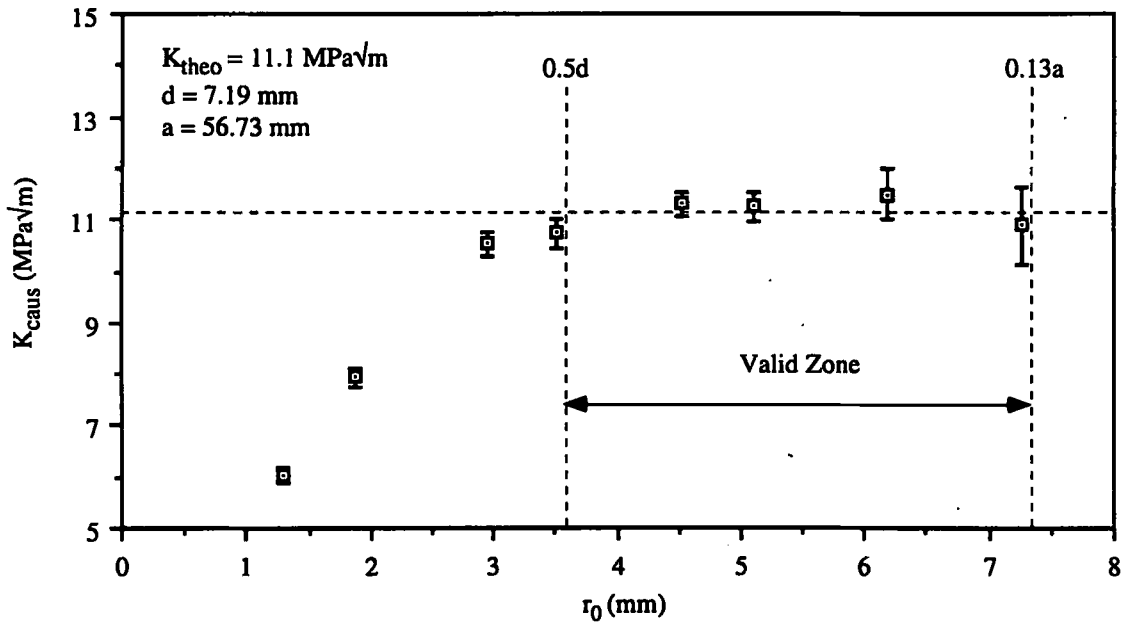

Figure 6.2 : Measured stress intensity factor versus initial curve radius (K=11MPa$\sqrt{m}$, d=7.19mm, a=56.73mm)

corresponding to z_0 distances from approximately 0.5 m to 15 m which result in initial curve radii from 1.3 mm to 7.3 mm respectively. The dimensions of this specimen (ie. thickness and crack length) facilitated a large valid zone within which the measured stress intensity factor agrees well with theory. In general, when K_{theo} is not known, K_{caus} is determined by the two stage process of first producing a curve analagous to Figure 6.2 and then taking the mean of the values within the valid zone. Note that, as described in Chapter 4, if a different K is measured a different range of lens to screen distances would correspond to valid zone measurements. To measure a range of stress intensity factors the lens to screen distances must be repeatedly adjusted as the applied load to the specimen is incrementally adjusted throughout the range.

It should be noted that caustic data are widely observed to follow the curve of Figure 6.2 (see, for instance, Rosakis and Ravi-Chandar, 1986; Meletis *et al*, 1991). That is, the existence of a plateau region indicates that that portion of the specimen is within a plane stress field which varies as $1/\sqrt{r}$. If such a flat region is not present then the crack tip stress field must be of some other form.

Close to the crack tip, where the stress state is known to be triaxial (although still varying as $1/\sqrt{r}$), the out of plane stress, σ_z, provides a constraint which opposes the Poisson contraction. This suppressed surface deformation therefore results in a reduced caustic diameter and so a smaller measured K. Again, if the form of the caustic data differs from that in Figure 6.2 in the triaxial stress region then the stress field must differ from a $1/\sqrt{r}$ stress field.

The general form of Figure 6.2 occurs for all specimen thicknesses. That is, there is a plane stress region at a distance of greater than d/2 from the crack tip even in specimens which are nominally referred to as *plane strain* specimens.

Error bars, calculated from equation (5.1), are included in Figure 6.2* to indicate that errors increase with initial curve radius. Notice that measurement uncertainty approaches

---

* *Note that the four smaller initial curve values were taken with a 500mm focal length lens; the four larger values were taken with a 1000mm focal length lens. This accounts for the abrupt change in the error bar dimensions between the 3.5mm and 4.5mm initial curve points.*

10% as the r_0 value approaches d (7.19mm). This is found to be a practical limit to caustic measurements since larger initial curves yield caustics of rapidly diminishing size. This limit compares favourably with that found by Rosakis and Ravi-Chandar (1986) and Meletis *et al* (1991) described in Section 4.2.7 (0.6d and 0.65d respectively).

One final point regarding Figure 6.2 is that, using the data in Table 6.1 and equation (2.4), the plane stress (surface) plastic zone extends approximately 0.15mm forward of the crack tip for 11.1 MPa$\sqrt{m}$ applied loading. Therefore, virtually all data points in Figure 6.2 are in excess of an order of magnitude from the plastic zone.

6.2.3 Measurements over a Fatigue Cycle

Stress intensity factor measurements over a fatigue cycle have been conducted on an electro-discharge machined (EDM) notch and a fatigue crack, and are shown in Figure 6.3. The Figure shows three curves; the loading and unloading halves of the first cycle of the EDM notch and the unloading half cycle of the fatigue crack. In each case the fatigue cycle had a ΔK of 10 MPa$\sqrt{m}$ and stress ratio, R, of 0.1. In order to record caustic images the fatigue machine was halted and manually adjusted over the fatigue cycle. Each point in Figure 6.3 was produced from the mean of a series of points within the valid zone of a curve analagous to Figure 6.2. Measurements which were found to be outside this zone were discarded*. The procedure to produce Figure 6.2 was therefore repeated 30 times to produce the three curves in Figure 6.3.

Despite the electro-disharge machined notch having a finite root radius (which is large compared to that of a crack) the crack tip stress field given by equation (2.1) is still applicable since the root radius « a (Tada *et al*, 1973). Consequently, the EDM notch can be assumed to behave as a crack of an equivalent length, that is, its stress field can be described by a stress intensity factor, and the monotonic and cyclic plastic zones ahead of the notch can be approximated by equations (2.7) and (2.10) respectively. Furthermore, an EDM notch has the characteristics of an ideal crack; the lack of a crack wake behind the notch tip

---

* *Discarded measurements were from initial curves <0.5d. No measurements exceeded 0.13a.*

precludes any crack closure effect. The only difference, therefore, between an EDM notch and a real fatigue crack is the effect of the crack wake.

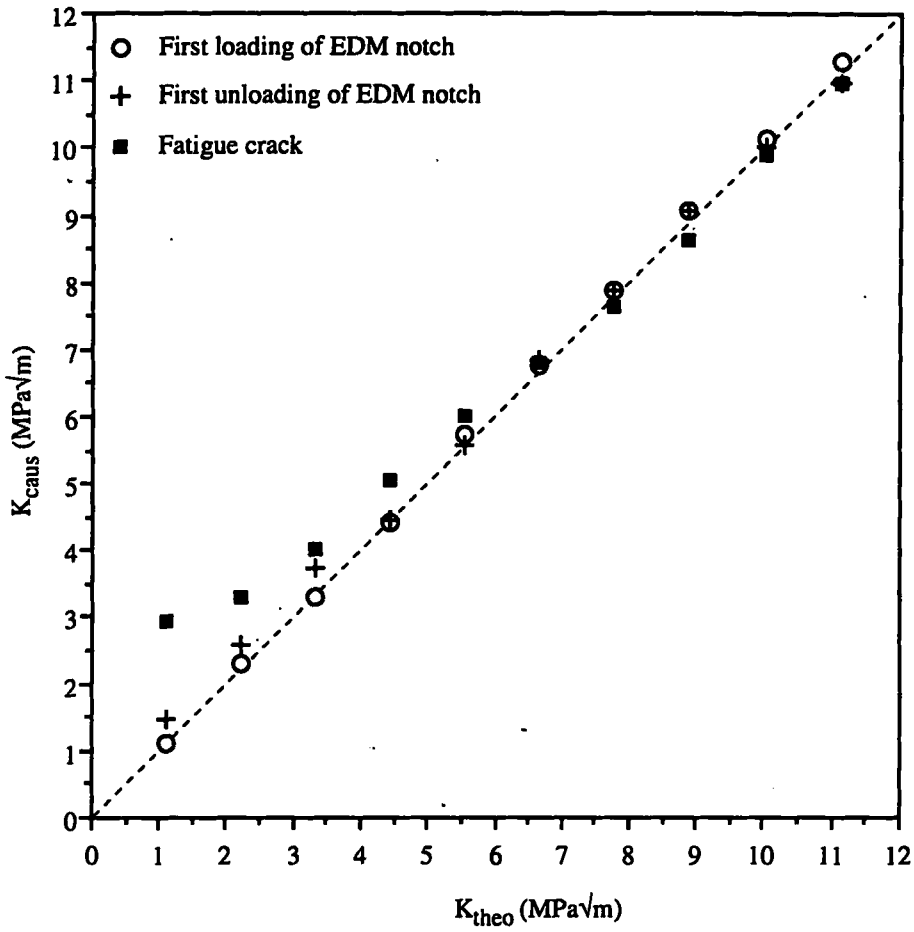

Figure 6.3 : K_{caus} versus K_{theo} for the fatigue cycles of an electro-discharge machined notch and a fatigue crack (ΔK=10MPa√m, R=0.1)

Figure 6.3 shows that the closure free notch measurements are in good agreement with theory over the full fatigue cycle. In addition, there is no apparent hysteresis in the caustic measurements. The fatigue crack, on the other hand, exhibits a marked departure from theory over part of the fatigue cycle. Only between K_{max} and approximately 7 MPa√m are the measurements are in good agreement with the analytical solution. It follows from this that between 7 and 11 MPa√m the crack is fully open. Below 7 MPa√m the deviation from theory must be caused by the crack experiencing an increasing amount of crack tip shielding due to premature contact of the crack surfaces. Notice that the curve indicates a gradual closure of the crack rather than an abrupt closure which would be expected to result in the schematic curve shown in Figure 6.4.

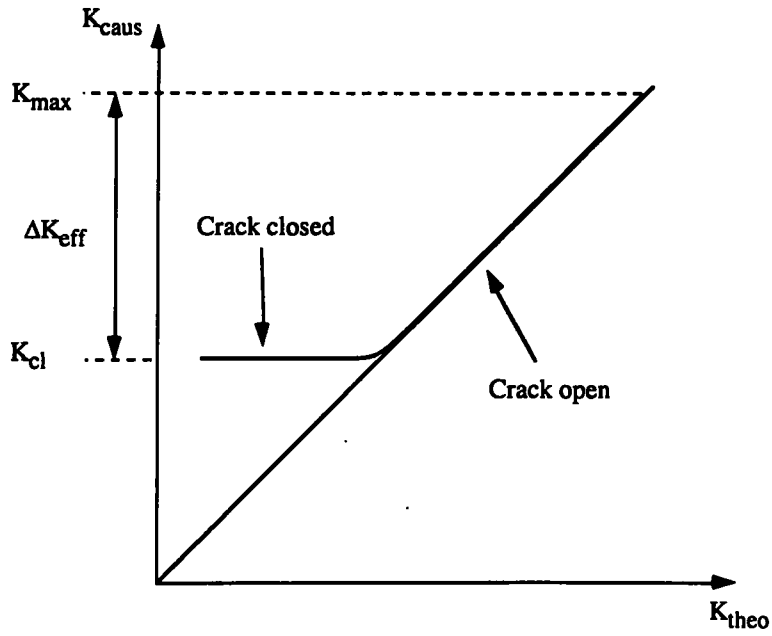

Figure 6.4 : Expected curve for an abrupt crack closure

Now, a distinction should be drawn between this technique and others (such as mechanical compliance) which produce similar curves. As described in Section 3.4.1 most researchers consider the first non-linearity point of a compliance curve to indicate crack closure. However, since the method of caustics measures the actual crack tip stress field the caustic at minimum load should indicate K_{cl} whereas first non-linearity point (7 MPa$\sqrt{m}$) should indicate the load at which the crack surfaces begin to come into contact. At K_{min} the crack surfaces are supplying a load which, together with the applied 1.1 MPa$\sqrt{m}$, gives the actual stress intensity factor experienced by the crack tip (approximately 3 MPa$\sqrt{m}$).

6.2.4 Crack Extension and Wake Removal

To investigate how the closure level varies as the crack extends from the EDM notch a specimen was tested six times during a crack growth of approximately 10mm with a constant amplitude loading of ΔK=10 MPa$\sqrt{m}$, R=0.1.

Figure 6.5 shows the caustic measurements over the six crack extensions. The K_{caus} measurements for the EDM notch follow the theoretical curve (dashed line) closely indicating no closure. For a fatigue crack with a wake length of 0.59 mm the caustic results show a small departure from theory around K_{min}. As the crack extends further closure is observed to increase as the crack generates up to 10 mm of wake.

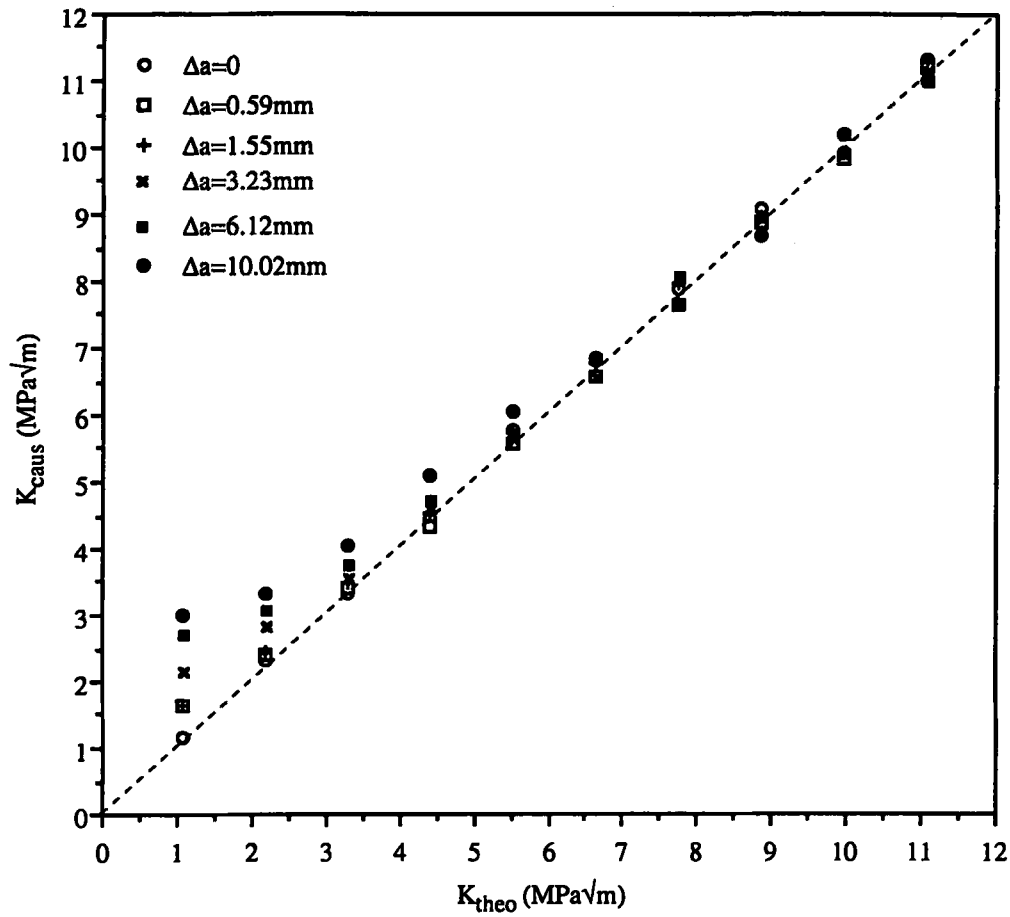

Figure 6.5 : Variation in measured closure with crack extension from an EDM notch

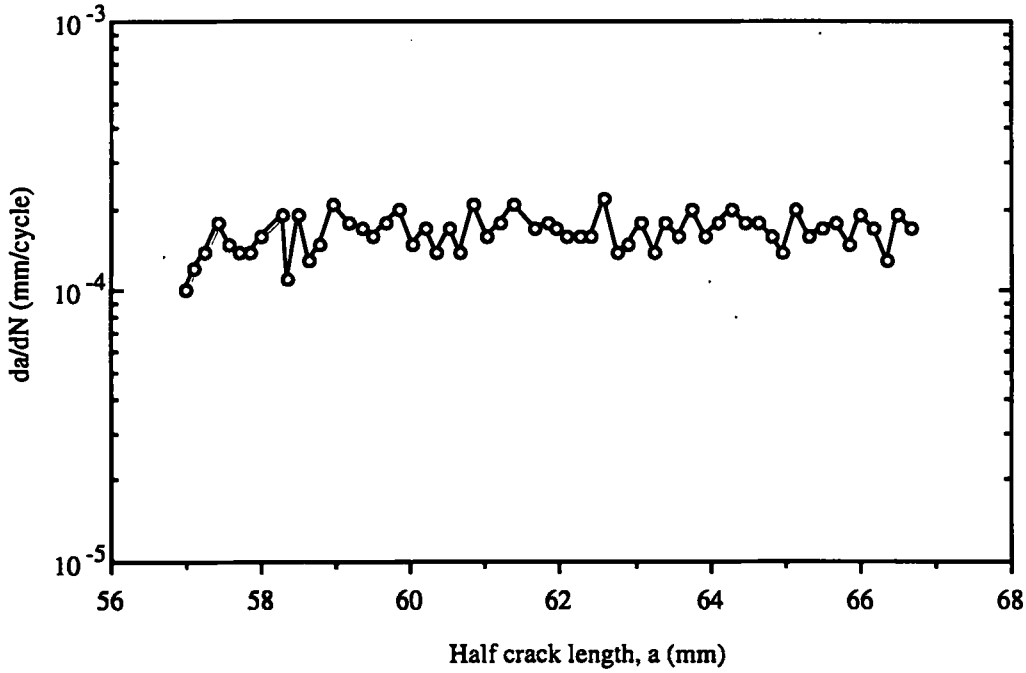

Figure 6.6 : Crack growth rate over 10mm of crack extension

Despite the change in the caustic measurements over the 10 mm of crack growth Figure 6.6 shows that growth rate is stable throughout this range which would indicate a constant ΔK_{eff}.

Once the fatigue crack had generated over 10 mm of wake a reverse experiment was conducted in which the wake was progressively removed with a fine jeweller's saw. From a length of 10.02 mm the wake was removed in three stages; firstly to 5.34 mm, secondly to 1.73 mm and, thirdly, to 0.14 mm from the tip. Caustic measurements were taken over the fatigue cycle at each wake removal stage; the results are presented in Figure 6.7. These results show the same trend as in Figure 6.5. That is, a longer crack wake appears to produce an increased level of crack closure.

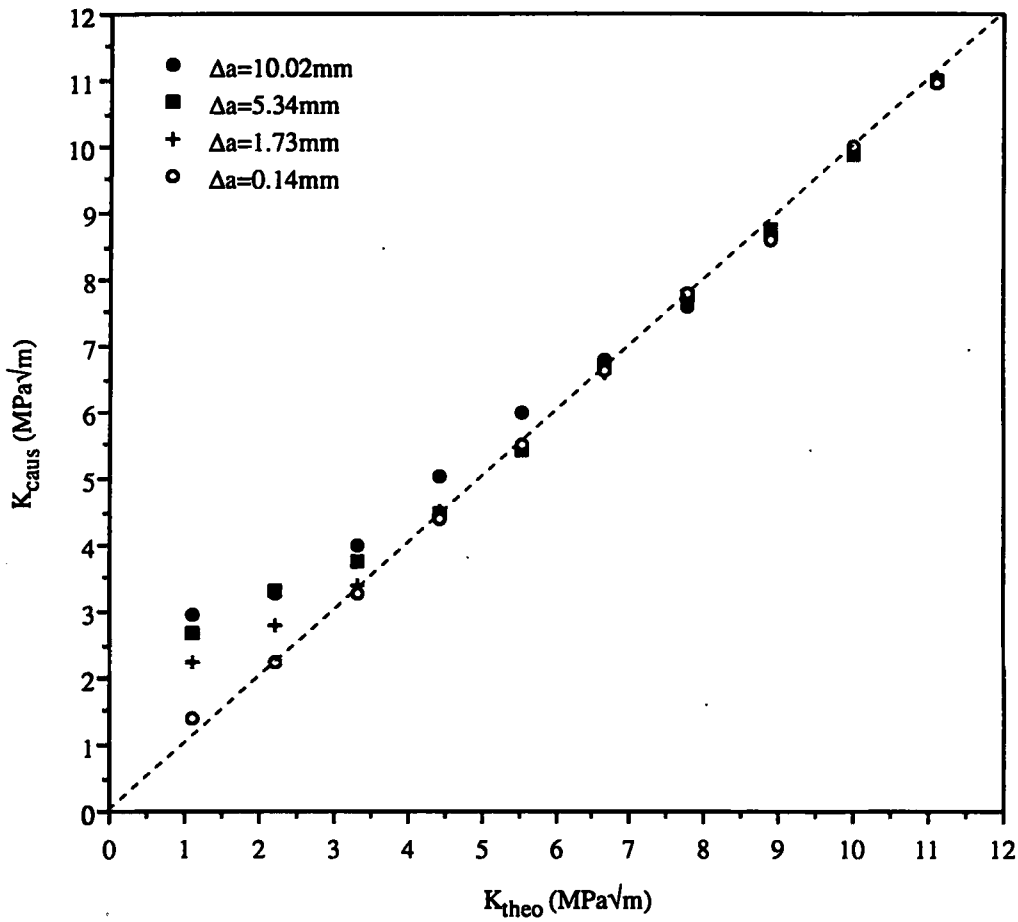

Figure 6.7 : Variation in measured closure with the crack wake progressively removed with a jeweller's saw

6.2.5 Measurements During a Compressive Underload

A crack grown at a ΔK of 10MPa$\sqrt{m}$ (R=0.1) was subjected to a compressive underload of an equal magnitude to the fatigue cycle maximum tensile load. Caustic measurements were taken from the maximum of the fatigue cycle to the load where the caustic became immeasurably small (which occurred when a compressive load equivalent to a stress intensity factor of 2 MPa$\sqrt{m}$ in tension was reached).

Figure 6.8 presents the results of this test showing that a caustic was still observed under compressive loading, that is, even under a remote compressive load a local tensile field was apparent ahead of the crack tip. Notice that below K_{min} of the fatigue cycle K_{caus} continues to fall but at a lower rate than K_{theo} indicating the crack is continuing to close but that the extent of crack tip shielding is increasing. It follows from this that although the crack surfaces may be in contact at some load above K_{min} the further reduction in load and subsequent compression causes an increase in reverse slip at the crack tip.

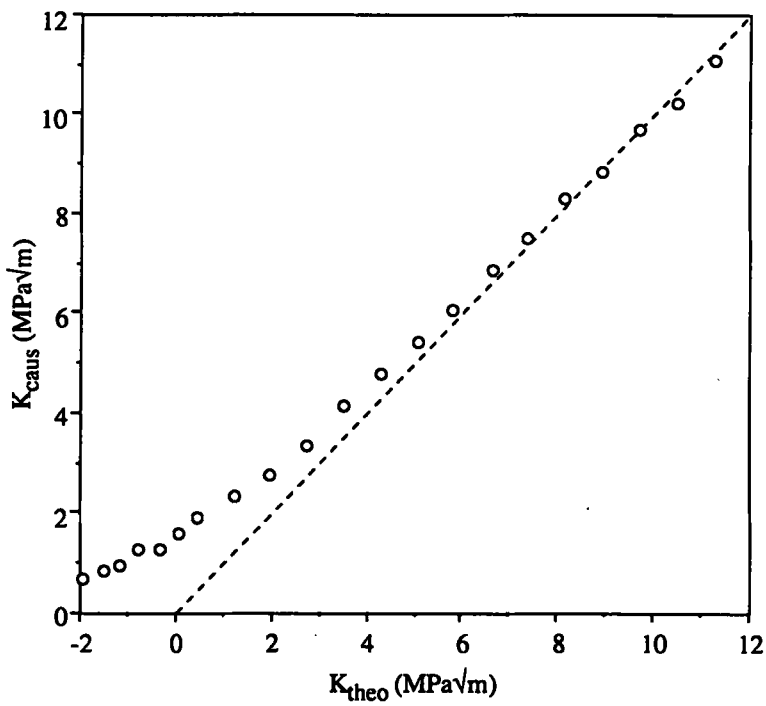

Figure 6.8 : Measured stress intensity factors from a crack subjected to a fatigue cycle followed by a compressive underload. (Note that a K_{theo} of "-2" MPa$\sqrt{m}$ has no physical significance but serves to illustrate a compressive load of equal magnitude to a load which would produce 2 MPa$\sqrt{m}$ in tension)

6.2.6 Measurements Following a Single Tensile Overload

The above observations of a difference between a fatigue crack and an EDM notch and that a tensile field exists ahead of the crack tip even under compression confirms that crack closure can be detected using caustics. To investigate this further a crack grown under the same conditions as previously (ΔK=10 MPa$\sqrt{m}$, R=0.1) was subjected to a 60% overload in order to induce an increase in plasticity induced closure and consequent crack growth retardation. Caustic measurements were taken over the range of the fatigue cycles pre-overload, at two points within the retardation zone and also after the crack had returned to the pre-overload growth rate.

Figure 6.9 shows the plot of crack growth rate against crack length (measured with a travelling microscope) highlighting the familiar overload induced crack growth retardation. Also shown in the Figure are the points where the caustic measurements were taken.

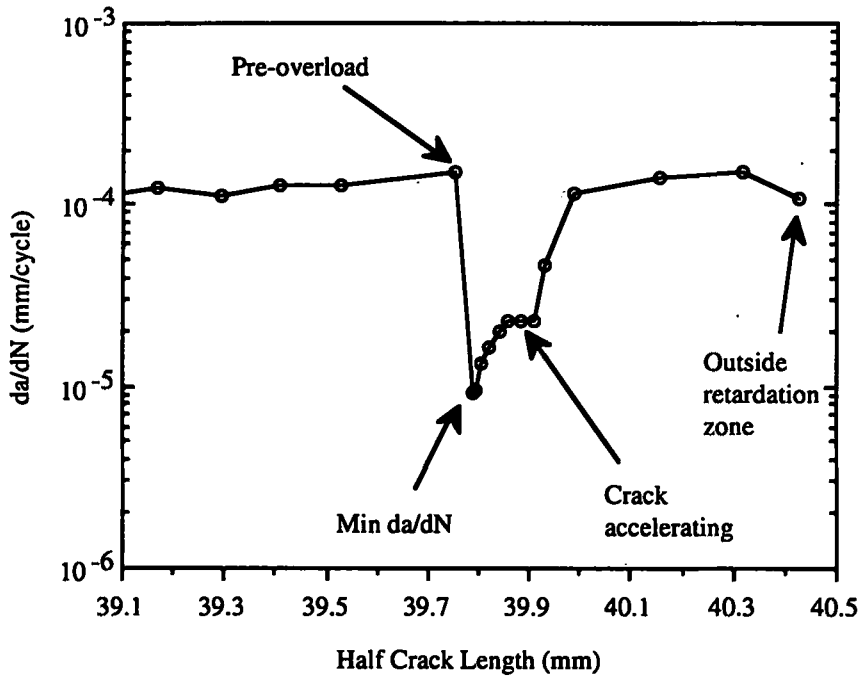

Figure 6.9 : Overload induced crack growth retardation

Figure 6.10 shows the four sets of caustic measurements over the same fatigue cycle. Remarkably, despite the dramatic retardation, the caustic results exhibit no discernible difference. Any transient change in crack closure caused by the overload did not

significantly affect the crack tip stress/strain distribution where the caustics were measured, several millimetres from the crack tip.

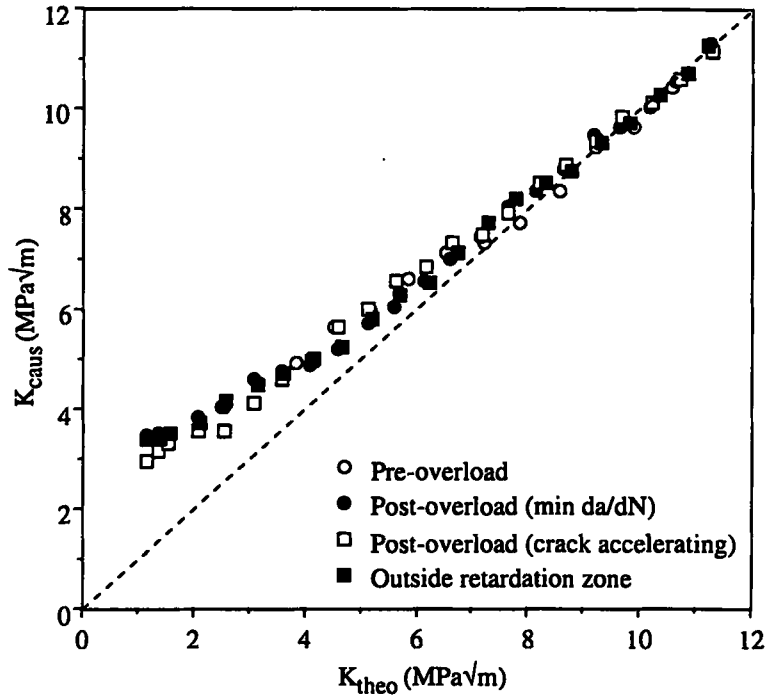

Figure 6.10 : Results of caustic measurements pre- and post-overload

6.2.7 Analysis over a Range of Initial Curves

As described earlier, each point in Figures 6.3, 6.5, 6.7, 6.8, and 6.10 was calculated from the mean of a series of (typically four) measurements within the valid zone of the specimen where the (plane) stress field is known to vary as $1/\sqrt{r}$. This means, the results are based on stress field measurements taken several millimetres from the crack tip. In order to investigate effects more local to the crack tip a series of experiments was conducted where measurements were taken over a range of initial curves which extended into the triaxial stress state region ($r_0<0.5d$) although still well outside the maximum plane stress plastic zone. Measurements taken within the triaxial region are presented as K_{caus} (or K_{caus}/K_{theo}) despite the fact that such caustic measurements are known to be invalid.

Figure 6.11 presents the results of measurements on a 6 mm thick specimen with an EDM notch over a fatigue cycle of $\Delta K=10$ MPa√m, $R=0.1$. K_{caus} normalised by K_{theo} is shown plotted against the r_0/d ratio at four stress intensity factors in the ΔK range. Note that

the results for all four stress intensity factors are similar. Since the form of these curves is similar to Figure 6.2 this indicates that in each case there is a K-field at the crack tip. That is, the stress field ahead of the crack varies as $1/\sqrt{r}$.

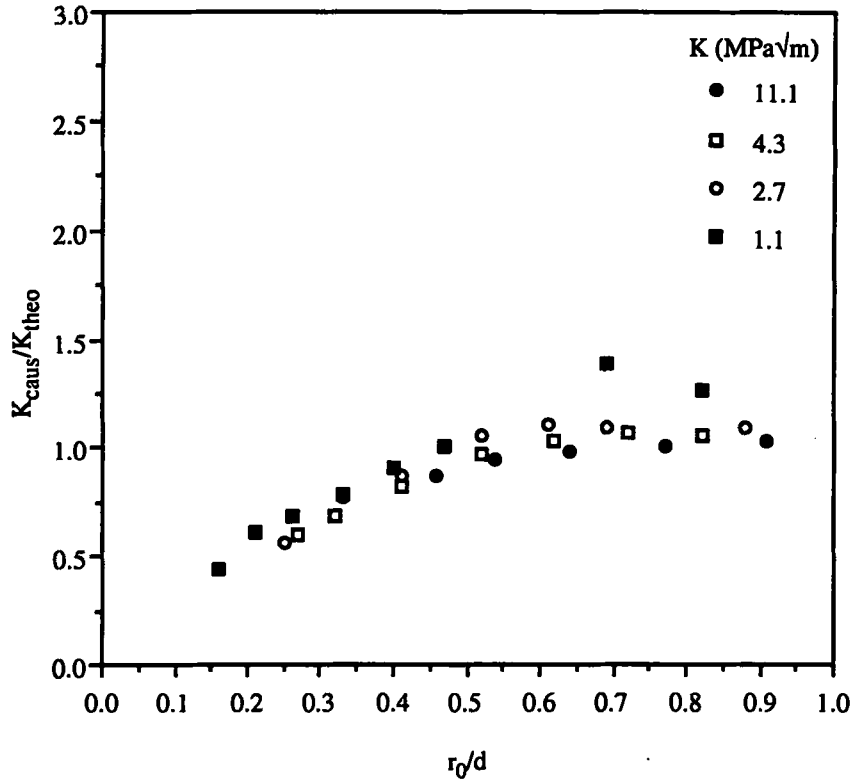

Figure 6.11 : Caustic results over a range of initial curves for an EDM notch (ΔK=10MPa$\sqrt{m}$, R=0.1)

After 3.3 mm of crack growth from the EDM notch the same series of measurements was repeated, the results of which are shown in Figure 6.12. Also shown in Figure 6.12 are the curves which are expected to be produced from such a test assuming that the crack closes for part of the fatigue cycle. It is assumed that the stress field ahead of the crack will remain a $1/\sqrt{r}$ K-field throughout the fatigue cycle. Hence, for these curves, the K_{caus}/K_{theo} ratio exhibits a plateau within the plane stress region ($r_0/d>0.5$) and falls within the triaxial stress state region ($r_0/d<0.5$) for each K. Since it is expected that the crack would close for part of the fatigue cycle, in these curves the K_{caus}/K_{theo} ratios increase as the applied load is reduced for all r_0/d.

At K_{max} (11.1 MPa$\sqrt{m}$) the measured curve follows the expected curve. This means that the stress field ahead of the crack varies as a $1/\sqrt{r}$ and is therefore a K-field. As the applied load is reduced the K_{caus}/K_{theo} ratios increase. However, the increase is more

pronounced at smaller initial curves where the measured and expected curves fail to agree, particularly at K_{min} (1.1 MPa$\sqrt{m}$).

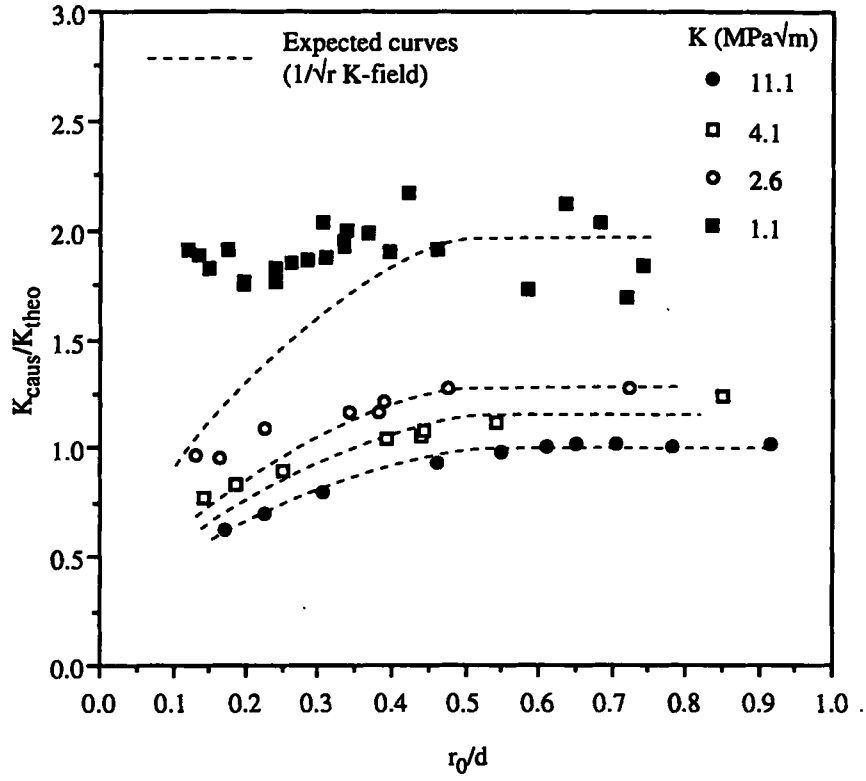

Figure 6.12 : Caustic results over a range of initial curves for a fatigue crack (ΔK=10MPa$\sqrt{m}$, R=0.1)

Consider the results for K=1.1 MPa$\sqrt{m}$. Measurements in the plane stress region ($r_0/d>0.5$) follow the expected curve (albeit with some scatter). Recall that in all previous experiments, measurements were only taken from this region. At smaller initial curves the measurements produce a higher K_{caus}/K_{theo} ratio compared to the expected curve. This trend is apparent at all stress intensity factors below K_{max} but is best illustrated at K_{min}. The fact that these measured points are higher than the expected curve indicates that the stress gradient at these small initial curves is higher than previously assumed (remember that caustics provide a measure of local stress gradients). This suggests that close to the crack tip under conditions of crack closure the stress field may not be a K-field.

To investigate this further the specimen was tested under an increased level of crack closure (i.e. such that the was closed for a higher proportion of the fatigue cycle). To do this the specimen was subjected to a high/low block loading sequence of ΔK=10 MPa$\sqrt{m}$ (R=0.6) for 10mm of crack growth followed by ΔK=10 MPa$\sqrt{m}$ (R=0.1). Under the first

block fatigue cycling (15-25 MPa√m) the crack was expected to close at approximately 16-MPa√m*. Therefore, under the subsequent low stress ratio cycling (1.1-11.1 MPa√m) the crack was expected to be closed for the whole cycle. Note that the crack arrested for 100,000 lower block cycles after which the test was ceased.

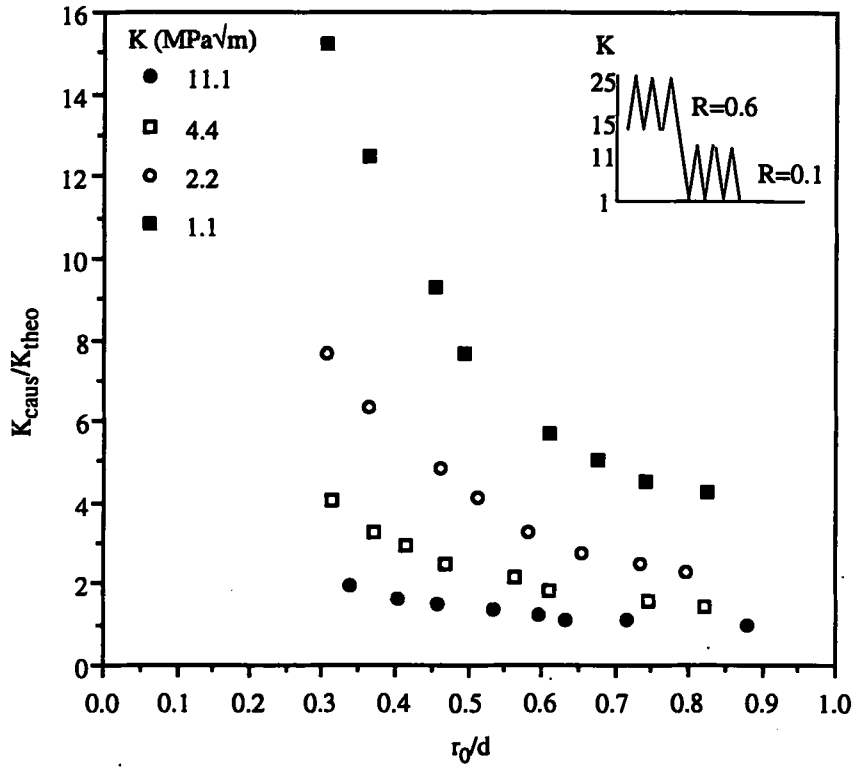

Figure 6.13 : Caustic results over a range of initial curves for a fatigue crack (ΔK=10MPa√m, R=0.1) following 10mm of crack growth at (ΔK=10MPa√m, R=0.6)

Figure 6.13 shows the results of caustic measurements at four applied stress intensity factors within the lower block (i.e. similar measurements to those in Figures 6.11 and 6.12). In this case, however, since the crack is expected to be closed for the whole lower block, it should experience the same stress intensity factor, K_{cl}, at all applied loads.

The difference between the results of this exaggerated closure test and Figures 6.11 and 6.12 is immediately apparent (notice the change in ordinate scale). Even at K_{max} the curve fails to exhibit the expected fall in K_{caus}/K_{theo} ratio for $r_0/d<0.5$. At K_{min} (1.1-MPa√m) the

---

* *Elber's equation (3.3) and Newman's equations (3.4-3.9) predict closure at 17.6 MPa√m and 16.0 MPa√m respectively.*

curve even fails to flatten within the plane stress region (r_0/d=0.5-0.9). The increased closure caused by this block loading sequence has caused an increased stress gradient (compared to a $1/\sqrt{r}$ K-field) to be observed as far as several millimetres from the crack tip. This suggests that under these exaggerated closure conditions the stress field ahead of the crack is not a K-field at any K.

It should be noted that these results are not influenced by the increased plastic zone size and its effect on caustic measurements. The plastic zone only extends 0.75 mm ahead of the crack tip under 25 MPa$\sqrt{m}$ loading (a distance which would correspond to an r_0/d ratio of 0.13 in Figure 6.13). Consequently, all caustic measurements are well outside the plastic zone criterion of Zehnder and Rosakis (1986) (see Section 4.2.5).

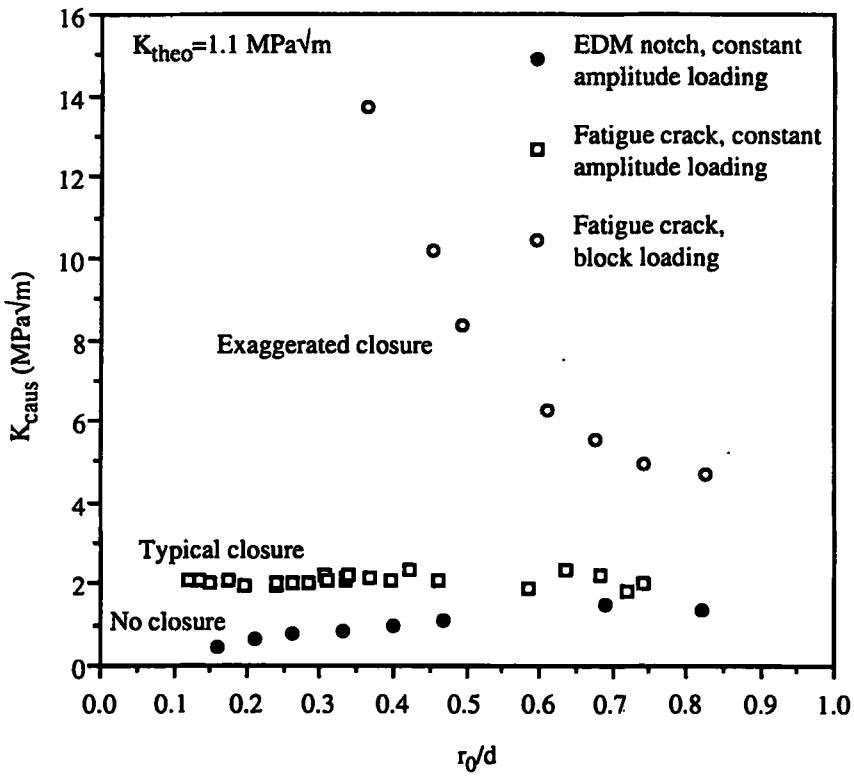

Figure 6.14 : Comparison of the K_{min} caustic results for the different loading conditions

In summary, Figure 6.14 shows a comparison of the K_{min} curves for the three loading conditions. These are no crack closure, 'typical' closure which might occur under service conditions, and exaggerated closure which would cause crack arrest. The ordinate, in this case, is K_{caus} since K_{theo} is a constant. The stress field ahead of the closure free crack varies as $1/\sqrt{r}$ and so can be expressed as a stress intensity factor. The field ahead of a

closed crack which has been subjected to typical service conditions *approximates* to a K-field within the plane stress zone ($r_0/d>0.5$) but exhibits an increased stress gradient close to the crack tip. Under exaggerated closure conditions the stress field ahead of the crack is markedly different from a K-field and so cannot be described as a stress intensity factor.

Chapter 7: DISCUSSION

7.1 INTRODUCTION

In this chapter the results of the experiments in Chapter 6 are discussed and interpreted in relation to other similar research. The discussion is presented in three sections. The first relates to the caustic measurements of 'true' stress intensity factors (ie. at large initial curves). The second encompasses the measurements over a range of initial curves, part of which is known to yield invalid stress intensity factors. The third section compares and contrasts , in detail, the results presented herein with a piece of closely related recent work.

7.2 STRESS INTENSITY FACTOR MEASUREMENTS AT LARGE INITIAL CURVES

By measuring caustics throughout a fatigue cycle for the case of both a narrow electro-discharge machined notch and a real fatigue crack (Figure 6.3) it has been possible to explicitly show that the method of caustics is responsive to material contact in the wake of a fatigue crack causing a perturbation of the crack tip stress field. This is concluded since the difference between the measured stress intensity factors for the EDM notch and the fatigue crack can only arise as a result of material contact in the wake of the fatigue crack as the load

is reduced. This is further emphasised with measurements during a compressive underload (Figure 6.8) which show that owing to a permanently stretched wake a tensile field exists ahead of a fatigue crack tip even under a far field compressive load.

The variation in the measured K_{caus} as the applied load is reduced from 11.1 MPa$\sqrt{m}$ in Figure 6.3 implies that the crack starts to close at around 7 MPa$\sqrt{m}$ and that the minimum stress intensity factor experienced by the crack tip is approximately 3 MPa$\sqrt{m}$ rather than the applied 1.1 MPa$\sqrt{m}$ (ie. ΔK_{eff} = 8.1 MPa$\sqrt{m}$). This is in contradiction with the generally considered view that the load at which the crack *starts* to close is the relevant closure load implying that the stress/strain state at the crack tip is maintained and that no further damage (no reverse slip) occurs below this load (Fleck, 1982). That is, crack closure is an abrupt event (from the point of view of the crack tip) in which case the stress intensity factor experienced by the crack tip would be expected to follow the schematic curve shown in Figure 6.4. It is possible that this opinion is drawn from experimental evidence based on compliance measurements; the first non-linearity point on a compliance plot, considered to represent the load at which the crack starts to close, appears to yield a realistic K_{cl} (ie. one which is in reasonable agreement with theoretical models and collapses da/dN data on a ΔK_{eff} plot).

Given that the caustic measurements point to K_{cl} being 3 MPa$\sqrt{m}$ then U_{caus} is given as

$$U_{caus} = \frac{\Delta K_{eff}}{\Delta K} = \frac{8.1}{10} = 0.81 \qquad (7.1)$$

This value can be compared to Elber's original experimental results (Elber, 1971) and the equations derived from Newman's model (Newman, 1984). Elber's empirical equation (3.3) indicates a U value of

$$U_{Elber} = 0.5 + 0.4R = 0.54 \qquad (7.2)$$

Newman's equations described in Section 3.5 point towards a U value of

$$U_{Newman} = 0.69 \qquad (7.3)$$

for a 2024-T3 aluminium alloy specimen with a constraint factor, α, of 1.8.

The caustic measurements therefore indicate considerably lower closure than both Elber found and Newman's model suggests.

By further investigating the difference in caustic measurements between an EDM notch and a fatigue crack, Figures 6.5 and 6.7 show that the level of crack closure varies directly as the length of the fatigue crack wake for wake lengths up to at least 10 mm. It is expected that closure should increase with wake length. However, to measure a progressive increase in crack closure over a 10 mm extension of a crack from an EDM notch is in profound contradiction with other experimental evidence. An increase in closure (and therefore a reduction in ΔK_{eff}) over this range would necessarily be accompanied by a reduction in crack growth rate. Figure 6.6, however, shows that over this 10 mm propagation the crack growth rate remained constant. In addition, Zaiken and Ritchie (1984) concluded that in 7150-T6 aluminium alloy compact tension specimens crack wake contact within 0.5 mm of the crack tip accounts for 40% of the effects of closure. The conclusion that closure is a very localised phenomenon occuring close to the crack tip is also supported by Zaiken and Ritchie's (1984) finding that a transient sub-threshold crack growth is observed if the crack wake is cut away close to the crack tip (ie. closure is removed).

There is clearly a major discrepancy between the caustic measurements and other observations. The caustic results can be physically interpreted by saying that crack wake contact as far as 10 mm from the crack tip perturbs the stress field around the crack tip (manifested by a change in the surface deformation) despite causing no change in the local crack tip stress/strain state.

This is an important observation which contradicts the implicit assumption of the stress intensity factor concept that the stress/strain condition at the crack tip is uniquely related to the stress field around the tip. *In other words, the measured effective stress intensity factor range does not govern the crack propagation rate.*

The caustic results following a single tensile overload produce the same conclusion in a converse manner. That is, a change in the crack tip condition following an overload, manifested as a dramatic change in crack growth rate, produces no discernible change in the measured effective stress intensity factor range. In this case, since the crack retardation covered a crack propagation of approximately 0.3 mm (see Figure 6.9), all closure mechanisms must occur in close proximity to the crack tip.

It is apparent from these observations that the crack closure being measured by the method of caustics is not that which is generally referred to by other researchers in the field. The phenomenon conventionally termed crack closure which affects fatigue crack growth rate is clearly a very local crack tip mechanism. The stress field measured a few millimetres from crack tip using caustics which one would intuitively expect to be a good measure of the K-field, however, is affected by a more remote crack closure. That is, premature crack wake contact as far as 10 mm from the crack tip. Observations under long term steady state loading conditions indicate that this remote closure is related to conventional crack tip closure. However, under transient loading conditions such as a single tensile overload remote closure measured by caustics is unaffected by local crack tip closure variations.

7.3 MEASUREMENTS OVER A RANGE OF INITIAL CURVES

By taking caustic measurements over a range of initial curves it has been possible to investigate how the crack tip stress field varies through a fatigue cycle. This investigation has led to some surprising results. Figure 6.11 shows that, in the absence of closure, caustic measurements over a fatigue cycle correspond to a stress field which varies as $1/\sqrt{r}$ (which is demonstrated by the similarity to the curve in Figure 6.2) and so for all loads the stress field can be characterised by a stress intensity factor. For a real fatigue crack grown under constant amplitude loading the stress field varies as $1/\sqrt{r}$ only around K_{max}, where the crack is fully open. As the crack closes the stress field deviates from this form but this is only detectable close to the crack tip (Figure 6.12) where the stress gradient* is observed to be higher than that expected for a K-field. Further from the crack tip where caustics are conventionally measured the stress field shows a good approximation to a $1/\sqrt{r}$ form.

When excessive closure is induced via a high/low block loading sequence the increase in the stress gradient is amplified and, although it still predominates close to the crack tip, it can also be observed as far as 6 mm away where the largest initial curve caustic was measured (Figure 6.13).

---

* *Recall fron Chapter 4 that the method of caustics is sensitive to stress gradients.*

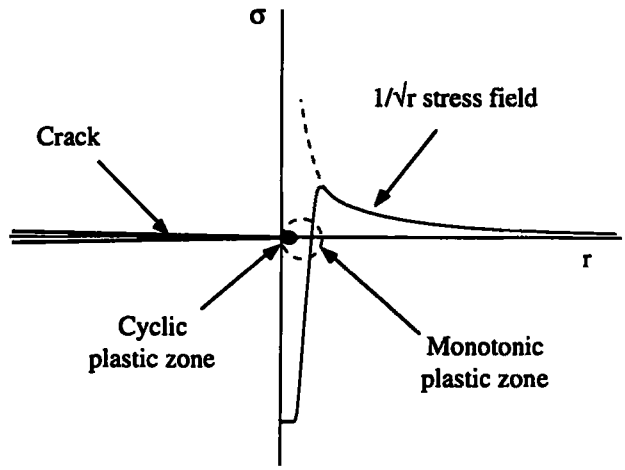

Figure 7.1 : Schematic of the stress field for a closure-free EDM notch at K_{min} (1.1MPa√m)

The K_{min} stress fields from the above observations are illustrated schematically in Figures 7.1-7.3. Unfortunately, the process of the optical mapping of the caustic described in Chapter 4 results in a multivalued, singular solution of the mapping equations (Kalthoff, 1987) and so is irreversible. It is therefore not possible to determine the actual stress field from the measured caustics.

For the case of the EDM notch (Figure 7.1) the stress field outside the monotonic plastic zone exhibits a good approximation to a 1/√r field, the only perturbing effect being the small region of compressive stress within the monotonic plastic zone.

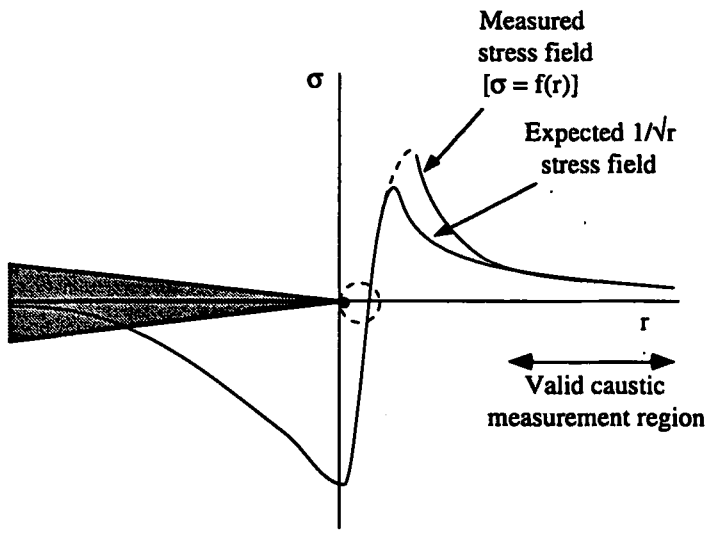

Figure 7.2 : Schematic of the measured and expected stress fields for a fatigue crack (grown under constant amplitude loading) at K_{min} (1.1 MPa√m)

For a fatigue crack at K_{min} (Figure 7.2) the large region of compression in the crack wake causes a tensile field ahead of the crack which ceases to approximate to a $1/\sqrt{r}$ field close to the crack tip.

When the magnitude of the wake compression increases, as shown in Figure 7.3 for the case of high/low block loading, the resulting tensile field ahead of the crack bears little relation to a $1/\sqrt{r}$ K-field. This field, which cannot be described in terms of a stress intensity factor, can be expressed as

$$\sigma = f\left(\frac{1}{r^n}\right) \qquad \text{where } n>0.5 \qquad (7.4)$$

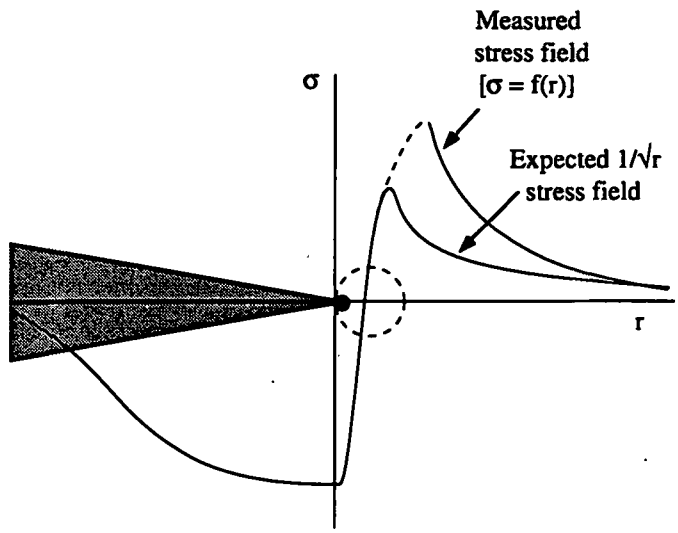

Figure 7.3 : Schematic of the measured and expected stress fields for a fatigue crack (grown under a high/low block loading sequence) at K_{min} (1.1MPa$\sqrt{m}$)

These observations, together with those in Section 7.2, question the use of the stress intensity factor concept in fatigue applications. Under conditions of crack closure the stress field around a crack cannot be reliably described in terms of K and is also not a unique measure of the stress/strain state at the crack tip which governs crack growth. Nevertheless, ΔK_{eff} (based mainly on compliance data) has been used successfully for over two decades to describe many fatigue crack growth phenomena.

The caustic measurements outlined in this thesis show that the notion of ΔK_{eff} universally applied in fatigue is not based on the Irwin's (1958) original definition of K as a

stress field but is simply a phenomenological measure of the condition at the crack tip. It is erroneous to consider ΔK_{eff} as *the portion of the stress intensity factor range which is effective in propagating the crack.* More appropriately, it should be defined as *the equivalent range of the crack tip condition to an ideal closure-free crack with an applied stress intensity factor range of* ΔK_{eff}.

7.4 COMPARISON WITH RECENT RESULTS

Recently, Bull and Hermann (1994) published results which apparently indicate successful crack closure measurements using the method of caustics. This section analyses the discrepancy between Bull and Hermann's results and those described in Chapter 6.

Bull and Hermann used a compact tension specimen of Al-3.5wt.% Cu alloy with salient dimensions of W = 50.5 mm, a = 15.9 mm and d = 10.4 mm. This specimen was subjected to a constant amplitude fatigue loading of $\Delta K = 12.5$ MPa$\sqrt{m}$ (R=0.1) throughout which caustic and compliance measurements were made. No measurements were made under any variable amplitude load sequences.

In their paper Bull and Hermann neglect to indicate the initial curve radii used in their measurements. However, it is clear that the reference plane (z_0) used was fixed throughout the fatigue cycle since their caustic detector was fixed with respect to the imaging lens during the test. As described in Section 4.2.6, 'standard' compact tension specimens cannot provide a wide range of K measurements for a fixed z_0. Applying the criteria specified in Section 4.2.5 to Bull and Hermann's (1994) specimen it can be seen that the initial curve radius should be both greater than 5.2 mm (d/2) to ensure plane stress conditions and less than 2.1 mm (0.13a) for measurements to be within a K-dominant zone. Thus, there is no region on this specimen which satisfy the criteria that caustic measurements should be taken from a plane stress, K-dominant zone. Bull and Hermann's (1994) measurements are, in effect, produced by an unusual out of plane displacement gauge.

It is clear from their results shown in Figure 7.4, however, that their curve exhibits similarities to corresponding figures in Chapter 6 (see, for example, Figures 6.3, 6.5, 6.7). However, Bull and Hermann interpreted their data in the same way as a compliance curve,

although they neglected to elucidate on the physical reasoning for this. Based on this they identify the closure load as 2.4 kN by intersecting tangents to the upper and lower parts of the curve and stated that this result was in agreement with compliance data from a back face strain gauge. Note that, had the commonly used first non-linearity point been used the curve in Figure 7.4 would have indicated a closure load of approximately 4 kN.

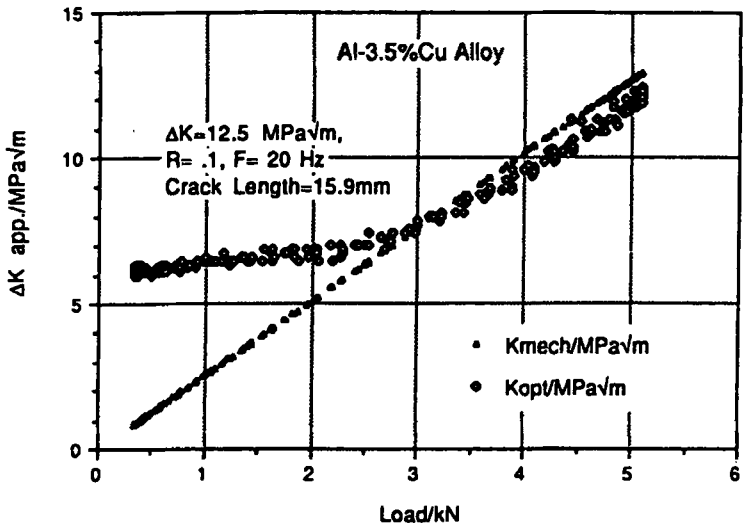

Figure 7.4 : Caustic stress intensity factor measurements over a fatigue cycle in Al-3.5wt.% Cu alloy compact tension specimen (after Bull and Hermann (1994)). (NB. The ordinate should read K not ΔK. Also K_{opt} and K_{mech} are analogous to K_{caus} and K_{theo} respectively)

Given that this material exhibits a similar level of closure to 2024-T3* it is surprising that the curve in Figure 7.4 exhibits a large and abrupt deviation from the theoretical line. This difference has motivated a study to investigate the possible effects of specimen configuration on caustic measurements.

In order to make a comparison between CCP and CT specimens a crack was grown in a centre-cracked panel under constant amplitude loading (ΔK=10 MPa$\sqrt{m}$, R=0.1). After conducting a series of caustic measurements over the fatigue cycle the specimen was cut to form two identical edge-cracked panels which were subsequently machined into compact

---

* *P_{max}≈5.1 kN and P_{min}≈0.4 kN, therefore $U=\Delta P_{eff}/\Delta P$≈0.57. This value is close to U_{Elber} and U_{Newman} (0.54 and 0.69 respectively) for 2024-T3 given by equations (7.2) and (7.3).*

tension specimen configurations (W=64.0 mm, a=39.22 mm, d=6.0 mm). The test was then repeated on one of the CT specimens. These tests were therefore conducted on successive fatigue cycles of the same crack but with the crack embedded within different specimens. In addition, a compliance measurement was taken on the compact tension specimen using a crack mouth clip gauge for comparison. The results of this experiment are shown in Figure 7.5. Note that the compliance curve is shown with the axes interchanged with respect to the schematic curve in Figure 3.7.

Figure 7.5 shows that the response of the compact tension specimen is almost identical to the centre-cracked panel but is markedly different from Bull and Hermann's (1994) results.

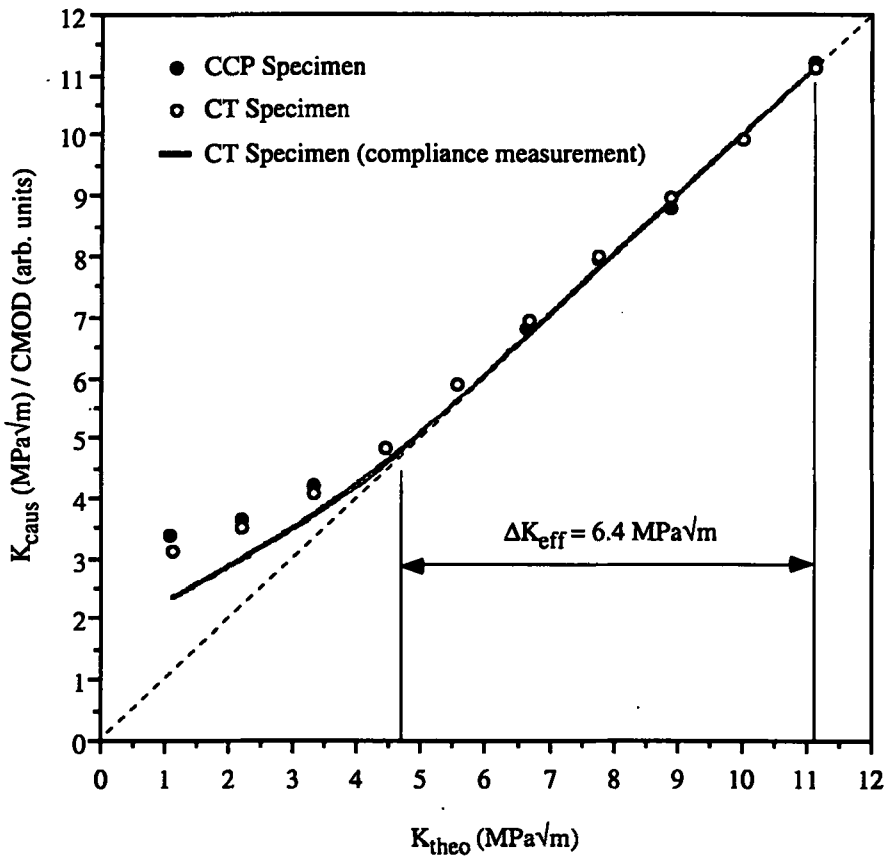

Figure 7.5 : Comparison of caustic and compliance measurements over a fatigue cycle for centre-cracked panel and compact tension specimens (2024-T3 aluminium alloy)

The compliance measurement for the compact tension specimen indicates ΔK_{eff} is 6.4 MPa$\sqrt{m}$. The resulting U_{CMOD} value (0.58) therefore compares well with U_{Elber} (equation (7.2)).

Returning to Figure 7.4, it is noticeable that around the maximum of the fatigue cycle the caustic measurements yield a consistently low K_{caus} with respect to K_{theo}. Further analysis of this curve offers a reason for the difference between Figures 7.4 and 7.5. The low K_{caus} values around K_{max} must arise as a result of caustic measurements from within the triaxial stress state region (ie. $r_0/d<0.5$). Since Bull and Hermann used a fixed camera (and therefore a fixed z_0) for the whole fatigue cycle the initial curve would have reduced further as the applied load was reduced. This means that *all* Bull and Hermann's (1994) measurements must have been made from within the triaxial stress state region. Figure 7.6 schematically shows the variation in K_{caus}/K_{theo} over a fatigue cycle and a range of initial curves derived from the results presented in Figure 6.12. Also shown are the points where Bull and Hermann must have made their measurements.

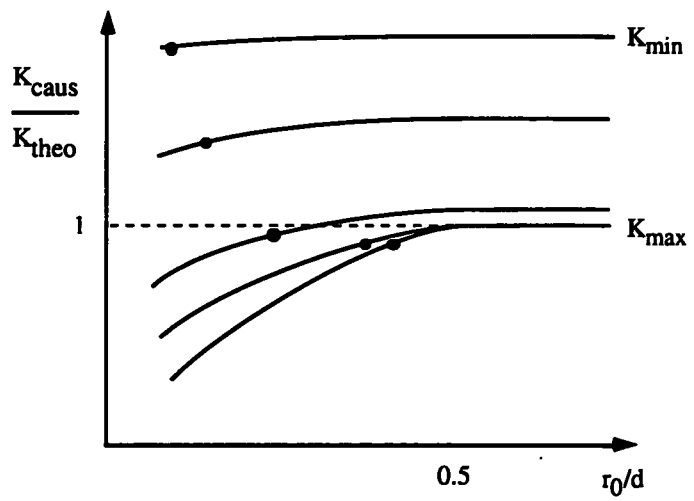

Figure 7.6 : Caustic measurements from a fixed camera over a range of K

As the load is reduced from K_{max} two opposing effects occur with measurements at a fixed camera position; the initial curve reduces and the caustic curve increases. Figure 7.6 shows that these effects can produce a K_{caus} which is consistently low around K_{max} but then rapidly increases as K_{min} is approached. If a different camera position had been selected

Bull and Hermann would have generated a different curve in Figure 7.4 and therefore calculated a different ΔK_{eff}.

These results show that a thin, long cracked specimen must first be chosen to provide a broad valid zone and that, if a wide range of stress intensity factors are to be measured, the reference plane position must be variable to maintain all measurements within the valid zone.

Chapter 8: CONCLUSIONS AND RECOMMENDATIONS FOR FUTURE WORK

8.1 CONCLUSIONS

The principal conclusions drawn from this work can be summarised as follows:

1 The optical method of reflected caustics provides a convenient means of experimental determination of stress intensity factors in flat plates containing through-thickness cracks.

2 However, the conventional application of the technique to an opaque engineering material such as aluminium alloy, particularly for the measurement of low stress intensity factors, leads to prohibitively high sensitivity to experimental errors. Errors vary inversely as the stress intensity factor and also increase dramatically with initial curve radius; a fact which is exacerbated since this radius needs to be greater than half the specimen thickness.

3 To apply the method of caustics to the investigation of fatigue necessarily requires substantial improvements to the technique so as to facilitate measurements throughout the fatigue cycle and to a resolution capable of measuring small changes in stress intensity factor. The improvements required are summarised as follows:

i) A collimated incident laser beam should be used which is produced from a high quality beam expander which is interferometrically focused.

ii) The specimen surfaces should be manufactured to be flat to conventional optical standards. That is, the surface form error should be much less than 1μm over the typical measurement area.

iii) The imaging lens should be of long focal length for high caustic magnification but is not required to be a high quality multi-element lens.

iv) A 2-dimensional array electro-optic detector, such as a CCD camera, should be used to record the caustic image so that the correct caustic diameter can be measured accounting for image diffraction.

v) The split-beam caustic modification should be utilised to automatically compensate for load induced specimen distortion.

4 Using these modifications the method of caustics can detect the presence of crack closure which manifests itself as a tensile stress ahead of the crack as a result of premature crack wake contact. This tensile field can be observed even under a far field compressive stress.

5 The quantification of crack closure using this technique is not in agreement with other experimental evidence or theoretical models.

6 Caustic measurements indicate a continual change ΔK_{eff} as a crack propagates as far as 10 mm from an electro-discharge machined notch despite an observation that the crack growth rate over this range remains constant. In addition, a single tensile overload which causes transient changes in the crack tip condition and the accompanying change in crack growth rate does not affect the stress field well outside the plastic zone. Consequently, it is concluded that under conditions of crack closure the crack tip stress field is not a measure of the stress/strain state at the crack tip and, accordingly, cannot be used to rationalise the rate of crack propagation.

7 A close examination of the stress field around a closed crack indicates that it does not exhibit a form which can be expressed as $K/\sqrt{2\pi r}$. Thus, a cracked body subjected

to fatigue loading cannot be described by a stress intensity factor for all of the fatigue cycle. Therefore, there is no physical basis to the use of the effective stress intensity factor range to correlate crack growth rates. Its powerful and successful application to fatigue crack growth is derived on purely phenomenological grounds based on experimental measurements from which ΔK_{eff} is inferred.

8.2 RECOMMENDATIONS FOR FUTURE WORK

The research described in this thesis has comprised the development of an improved method of caustics and its subsequent application to crack closure measurement under a range of loading conditions. In these studies the technique has produced some results which are potentially of great importance to the use of closure in fatigue crack growth modelling. The technique can now be further exploited in the following related areas of investigation:

1 Examination of the effects of stress ratios

Although transient near-tip closure behaviour has been found to be independent of the stress field around the crack, the effects of constant amplitude loading at a range of stress ratios is yet to be investigated. Such steady state, 'remote' closure is observed in stress field measurements at low stress ratios. Extending caustic measurements to a range of stress ratios so as to collapse da/dN versus ΔK_{eff} data may show that remote closure, as measured by the crack tip stress field using caustics, is indicative of crack tip behaviour under constant amplitude loading.

2 Investigation of different closure mechanisms

Different closure mechanisms can be examined by selecting materials of different grain sizes (to produce diferent levels of roughness induced closure), by choosing different heat treatments (to vary the material yield strength and, therefore, the extent of plasticity induced closure) and by measuring in different environments to induce crack surface corrosion. Measurements under these conditions would determine whether the different closure mechanisms occur at different locations with respect to the crack tip.

3 Mixed mode closure

The method of caustics has been widely applied to a range of mixed mode loading conditions (Kalthoff, 1982, 1987; Nishioka *et al*, 1990a,b; Theocaris and Lazopoulos, 1991; Zhang and Ravi-Chandar, 1991; Hinderliter *et al*, 1991). The effects of crack surface contact under such conditions, however, has not been investigated.

4 Crack tip shielding in ceramics

Ceramics are known to exhibit certain crack tip shielding mechanisms (Ritchie, 1988). However, to date the method of caustics has had limited application to ceramic materials due to their high Young's modulus and low fracture toughness. Osagawara *et al* (1992) have reported being unable to measure caustics at initial curve radii of greater than d/2 from the crack tip in silicon nitride. Poisson contractions around the crack tip at low stress intensity factors (~ 4 MPa$\sqrt{m}$) in materials of high Young's modulus will be exceedingly small and possibly comparable to the form error of typical specimens. However, with the improved accuracy and resolution of the method of caustics resulting from the developments described in Chapter 5, low stress intensity factors should be measurable. Using glass polishing techniques specimen form errors of at least an order of magnitude lower than in diamond machined aluminium are achievable.

5 Dynamic fracture in ceramics

Caustic investigation of dynamic fracture has been limited to PMMA and metals. For the reasons described above the improved accuracy of the technique now facilitates the study of low fracture toughness materials such as ceramics.

Although the method of caustics has been extensively improved for this research the technique could be developed to provide a level of automation to the capture of caustic images *in situ* during fatigue cycling. Synchronised video frame-grabbing could be used to automatically capture caustic images from selected parts of the fatigue cycle for later processing. A modification of the technique based on the *bifocal caustic* technique of Rosakis *et al* (1990) would be necessary to enable multiple r_0 images to be captured simulateously.

REFERENCES

Abdel Mageed, A. M., R. K. Pandey and R. Chinadurai (1992). Materials Science and Engineering **A150**, p. 43-50.

Abo-el-ez, A. E., N. Takeda and K. Takahashi (1986). Journal of Materials Science **21**, p. 1631-1636.

Ahmad, H. Y. and L. Edwards (1994). In Proc. 17th Annual Adhesion Society Meeting, Orlando, Florida USA, p. 310-313.

Ahmad, H. Y., I. R. Wallhead and L. Edwards (1994). Submitted for publication to The Journal of Adhesion, September 1994.

Airy, G. B. (1838). Cambridge Philosophical Society Transactions **6**(3), p. 378-402.

Allen, R. J., G. S. Booth and T. Jutla (1988). Fatigue and Fracture of Engineering Materials and Structures **11**(1), p. 45-69.

Allison, J. E., R. C. Ku and M. A. Pompetzki (1988). In *Mechanics of fatigue crack closure, ASTM STP 982,* J. C. Newman and W. Elber, Editors. Philadelphia, ASTM. p. 171-185.

Banerjee, S. (1984). AFWAL-TR-84-4031. A review of crack closure. Materials Laboratory, Air Force Wright Aeronautical Laboratories, Air Force Systems Command, Wright-Patterson Air Force Base, Ohio.

Beinert, J. and J. F. Kalthoff (1981). In *Mechanics of Fracture,* G. C. Sih, Editor. Mass, Martinus Nijhoff Publishers. p. 280-330.

Berry, M. V. and C. Upstill (1980). In *Progress in optics,* E. Wolf, Editor. p. 258-346.

Bertel, J. D., A. Clérivet and C. Bathias (1981). 5th International Conference on Fracture: Advances in fracture research, Cannes, France, Pergamon Press, p. 943-951.

Bowles, C. Q. and J. Schijve (1983). In *Fatigue Mechanisms: Advances in Quantitative Measurement of Physical Damage, ASTM STP 811*, Philadelphia, ASTM. p. 400-426.

Broek, D. (1974). Elementary Engineering Fracture Mechanics, Noordhoff Int. Pub., The Netherlands.

Bull, C. and R. Hermann (1994). Scripta Metallurgica **30**(10), p. 1337-42.

Chermahini, R. G., K. N. Shivakumar and J. C. Newman (1988). In *Mechanics of fatigue crack closure, ASTM STP 982,* J. C. Newman and W. Elber, Editors. Philadelphia, ASTM. p. 398-413.

Clérivet, A. and C. Bathias (1988). In *Mechanics of fatigue crack closure, ASTM STP 982,* J. C. Newman and W. Elber, Editors. Philadelphia, ASTM. p. 583-597.

Davidson, D. L. (1988). In *Mechanics of fatigue crack closure, ASTM STP 982,* J. C. Newman and W. Elber, Editors. Philadelphia, ASTM. p. 44-61.

Davidson, D. L. and J. Lankford (1979). Fatigue of Engineering Materials and Structures **1**, p. 439-446.

Dugdale, D. S. (1960). Journal of the Mechanics and Physics of Solids **8**, p. 100-104.

Elber, W. (1970). Engineering Fracture Mechanics **2**, p. 37-45.

Elber, W. (1971). In *Damage Tolerance in Aircraft Structures, ASTM STP 486.* American Society for Testing and Materials. p. 230-242.

Endo, K., K. Komai and K. Ohnishi (1969). Memo of Faculty of Engineering, Kyoto University, Vol 31, p. 25-46.

Ewalds, H. L. and R. J. H. Wanhill (1986). Fracture Mechanics. London, Edward Arnold (Publishers) Ltd.

Feddersen, C. (1967). In *ASTM STP 410*, p. 77.

Fleck, N. A. (1982). Technical Report, CUED/C/MATS/TR.89, Cambridge University Engineering Department.

Frost, N. E., L. P. Pook and K. Denton (1971). Engineering Fracture Mechanics **3**, p. 109-126.

Gallagher (1983). Damage Tolerant Design Handbook. Univerisity of Dayton Research Institute, Dayton, Ohio.

Gdoutos, E. E. and E. C. Aifantis (1986). Engineering Fracture Mechanics **23**(2), p. 423-430.

Gray, G. T., J. C. Williams and A. W. Thompson (1983). Metallurgical Transactions, **15A**, p. 421.

Güngör, S., I. R. Wallhead and L. Edwards (1992). Nondestructive Testing and Stress-Strain Measurement, FENDT '92, Tokyo, Japan, The Japanese Society for Non-Destructive Inspection, p. 598-603.

Halliday, M. D. and C. J. Beevers (1979). International Journal of Fracture **15**, p. R27-R30.

Hermann, R. (1991). Scripta Metallurgica **25**(1), p. 207-212.

Hermann, R. and N. J. H. Holroyd (1985). Materials Science and Engineering **76**, p. 119-126.

Hermann, R. and N. J. H. Holroyd (1986). Materials Science and Technology **2**(Dec), p. 1238-1244.

Herrmann, K. P. and A. Noe (1992). Engineering Fracture Mechanics. **42**, p. 573.

Herrmann, K. P. and A. Noe (1993). Theoretical and Applied Fracture Mechanics. **19**, p. 49 .

Hertzberg, R. W. (1989). Deformation and Fracture Mechanics of Engineering Materials, 3rd Edition, Wiley.

Hinderliter, G. S., R. V. Mahajan and A. S. Voloshin (1991). Engineering Fracture Mechanics **40**(2), p. 323-333.

Hudson, C. M. (1969). NASA Tech Note D-5390.

Irwin, G. R. (1958). Handbuch der Physik, Vol 6, Springer, Berlin.

Jones, J. W., D. E. Macha and D. M. Corbly (1978). International Journal of Fracture, **14**, R25.

Kalthoff, J. F. (1982). Int. Conf. on Experimental Stress Analysis, Hawaii, May 23-29, 1982, p. 1119-1126.

Kalthoff, J. F. (1987). In *Handbook on Experimental Mechanics,* A. S. Kobayashi, Editor. New Jersey, Prentice-Hall. p. 430-500.

Kalthoff, J. F., J. Beinert and S. Winkler (1979). IUTAM Symp. Opt. Methods Mech. Solids, University of Poiters, France, 10-14 Sept, 1979, Sijthoff-Noordhoff, Alphen aan den Rijn, The Netherlands, 1980, p. 497-508.

Kalthoff, J. F., W. Böhme and S. Winkler (1982). 7th Int. Conf. Exp. Stress Anal., Haifa, Israel, p. 148-160.

Kamath, S. M. and K. S. Kim (1986). Experimental Mechanics **26**(4), p. 386-393.

Klein, M. V. (1970). Optics. London, John Wiley & Sons.

Konsta-Gdoutos, M. and E. E. Gdoutos (1992). Engineering Fracture Mechanics **42**(2), p. 251-263.

Kumar, R. (1992). Engineering Fracture Mechanics **42**(1), p. 151-158.

Lee, O. S. and M. K. Han (1991). Fracture and Strength 90, p. 55-61.

Leftheris, B. P. and J. M. Papazian (1992). Journal of Engineering Materials and Technology **114**, p. 399-405.

Liaw, P. K. (1988). In *Mechanics of fatigue crack closure, ASTM STP 982,* J. C. Newman and W. Elber, Editors. Philadelphia, ASTM. p. 62-92.

Longhurst, R. S. (1966). Geometrical and Physical Optics, 2nd Edition, Longmans, Green and Co Ltd, London, p. 346-347.

Ma, C. C. (1990). Optics and Lasers in Engineering **13**(3 & 4), p. 279-304.

Manogg, P. (1964). Anwendung der Schattenoptik zur Untersuchung des Zerreissvorgangs von Platten. PhD dissertation, Freiburg, Germany.

McEvily, A. J. (1977). Fatigue 1977 Conference, University of Cambridge, England.

McEvily, A. J. (1988). In *Mechanics of fatigue crack closure, ASTM STP 982,* J. C. Newman and W. Elber, Editors. Philadelphia, ASTM. p. 35-43.

Meletis, E. I., W. Huang and E. E. Gdoutos (1991). Engineering Fracture Mechanics **39**(5), p. 875-885.

Meyn, D. A. (1992). Engineering Fracture Mechanics **43**(2), p. 185-194.

Meyn, D. A., T. W. Webb and E. C. Aifantis (1989). Engineering Fracture Mechanics **33**(6), p. 913-925.

Mouritsen, O. Ø. and B. L. Karihaloo (1993). Fatigue '93, Montréal, Canada, EMAS, Vol 3, p. 1825-1830.

Minakawa, K. and A. J. McEvily (1981). Scripta Metallurgica, **15**, p. 663-636.

Minakawa, K., G. Levan and A. J. McEvily (1986). Metallurgical Transactions A, **17A**, p. 1787.

Newman, J. C. (1981). A crack-closure model for predicting fatigue crack growth under aircraft spectrum loading. NASA-TM-81941.

Newman, J. C. (1984). International Journal of Fatigue **24**, p. R131-R135.

Newman, J. C. (1988). In *Mechanics of fatigue crack closure, ASTM STP 982,* J. C. Newman and W. Elber, Editors. Philadelphia, ASTM. p. 1.

Newman, J. C. (1994). Private communication.

Newman, J. C., C. A. Bigelow and K. N. Shivakumar (1993). Engineering Fracture Mechanics **46**(1), p. 1-13.

Nigam, H. and A. Shukla (1987). Experimental Mechanics **28**(2), p. 123-131.

Nishioka, T. and H. Kittaka (1990). Engineering Fracture Mechanics **36**(6), p. 987-998.

Nishioka, T., H. Kittaka, et al. (1990). International Journal of Pressure Vessels and Piping **44**(1), p. 17-33.

Ogasawara, T., T. Akiba, et al. (1992). Journal of the Ceramic Society of Japan **100**(8), p. 1007-1010.

Ohta, A., M. Kosuge and E. Sasaki (1978). International Journal of Fracture **14**(3), p. 251-264.

Papadopoulos, G. A. (1990). Optics and Lasers in Engineering **13**(3 & 4), p. 211-249.

Paris, P. C. and F. Erdogan (1963). Journal of Basic Engineering Transactions, ASME Series D, **85** (4), p. 528.

Rice, J. R. (1967). In *Fatigue crack propagation, ASTM STP 415*. American Society for Testing and Materials. p. 347-311.

Ritchie, R. O. (1988). Materials Science and Engineering, **A103**, p. 15-28.

Ritchie, R. O. and S. Suresh (1982). Metallurgical Transactions **13A**, p. 937-940.

Ritchie, R. O., S. Suresh and C. M. Moss (1980). Journal of Engineering Materials Technology, Transactions ASME, Series H, **102**, p. 293-299.

Rooke, D. P. and D. J. Cartwright (1976). Compendium of Stress Intensity Factors, HM's Stationery Office, London.

Rosakis, A. J. and L. B. Freund (1981). Journal of Applied Mechanics **48**, p. 302-308.

Rosakis, A. J., S. Krishnaswamy and H. V. Tippur (1990). Optics and Lasers in Engineering **13**(3 & 4), p. 183-210.

Rosakis, A. J. and K. Ravi-Chandar (1986). International Journal of Solids and Structures **22**(2), p. 121-134.

Rosakis, A. J., A. T. Zehnder and R. Narasimhan (1988). Optical Engineering **27**(8), p. 596-610.

Rosakis, A. J., S. Krishnaswamy and H. V. Tippur (1990). Optics and Lasers in Engineering **13**, 3, p. 183-210.

Rossmanith, H. P. (1983). Engineering Fracture Mechanics **18**(4), p. 903-908.

Rossmanith, H. P. and R. E. Knasmillner (1991). International Seminar on Dynamic Failure of Materials - Theory, Experiments and Numerics, Vienna, Austria, Elsevier Science Publishers Ltd, Essex, U.K., p. 260-272.

Sadananda, K., N. Louat and A. K. Vasudevan (1993). Fatigue 93, the Fifth International Conference on Fatigue and Fatigue Thresholds, May 3-7, Montréal,Quebec, Canada, EMAS (Publ) Ltd., Warley, England, Vol 1, p 571-576.

Schijve, J. (1988). In *Mechanics of fatigue crack closure, ASTM STP 982,* J. C. Newman and W. Elber, Editors. Philadelphia, ASTM. p. 5-34.

Sharpe, W. N. (1982). Optical Engineering **21**(3), p. 483-488.

Shigeru, A. and K. Tadashi (1991). International Seminar on Dynamic Failure of Materials - Theory, Experiments and Numerics, Vienna, Austria, Elsevier Science Publishers Ltd, Essex, U.K., p. 204-218.

Shimizu, K. and S. Takahashi (1990). JSME International Journal, Series I - Solid Mechanics Strength of Materials **33**(4), p. 490-496.

Sih, G. C. M. (1965). Handbook of Stress Intensity Factors, Lehigh University.

Smith, R. H. and L. B. Freund (1991). Optics and Lasers in Engineering **14**(2), p. 85-99.

Sneddon (1946). Proceedings of the Physical Society, London, **186** p. 229-260.

Stavroudis, O. N. (1972). The Optics of Rays, Wavefronts and Caustics. London, Academic Press Inc. (London) Ltd.

Sukere, A. A. (1986). Proceedings of the 8th International Conference on Experimental Stress Analysis, Amsterdam, The Netherlands, May 12-16, Martinus Nijhoff Publishers, p. 417-428.

Sukere, A. A. (1987). Engineering Fracture Mechanics **26**(1), p. 65-74.

Suresh, S. and R. O. Ritchie (1982). Metallurgical Transactions **13A**, p. 1627.

Suresh, S., G. F. Zamiski and R. O. Ritchie (1981). Metallurgical Transactions **12A**, p. 1435.

Suresh, S., D. M. Parks and R. O. Ritchie (1982). Fatigue Thresholds, EMAS, Warley, England.

Tada, H., P. C. Paris and G. R. Irwin (1973). The Stress Analysis of Cracks Handbook. Del Research Corporation.

Theocaris, P. S. (1970). Journal of Applied Mechanics **37**, p. 409-415.

Theocaris, P. S. (1971). Applied Optics **10**(10), p. 2240-2247.

Theocaris, P. S. (1981). In *Mechanics of Fracture,* G. C. Sih, Editor. Mass, Martinus Nijhoff Publishers. p. 189-252.

Theocaris, P. S. (1988). Journal of Elasticity **19**(2), p. 163-178.

Theocaris, P. S. (1989). Engineering Fracture Mechanics **33**(4), p. 553-559.

Theocaris, P. S. (1989). Acta Mechanica **80**(1 & 2), p. 1-38.

Theocaris, P. S. (1991). Engineering Fracture Mechanics **39**(1), p. 71-81.

Theocaris, P. S. (1991). Engineering Fracture Mechanics **38**(1), p. 37-54.

Theocaris, P. S. and C. Lazopoulos (1991). Engineering Fracture Mechanics **39**(1), p. 83-92.

Theocaris, P. S. and L. Petrou (1987). International Journal of Fracture **35**(4), p. 269-282.

Theocaris, P. S. and L. Petrou (1989). Acta Mechanica **76**(3 & 4), p. 133-159.

Theocaris, P. S. and T. P. Philippidis (1987). Engineering Fracture Mechanics **27**(3), p. 299-314.

Theocaris, P. S. and C. I. Razem (1981). International Journal of Mechanical Science **23**, p. 275-284.

Thompson, N., N. J. Wadsworth and N. Luat (1956). Philosophical Magazine, **1** p. 113.

Vasudevan, N. and W. G. Knauss (1988). International Journal of Fracture **36**(2), p. 121-135.

Vasudevan, A. K., K. Sadananda and N. Louat (1993). Fatigue 93, the Fifth International Conference on Fatigue and Fatigue Thresholds, May 3-7, Montréal,Quebec, Canada, EMAS (Publ) Ltd., Warley, England, Vol 1, p 565-570.

von Euw, E. F. J., R. W. Hertzberg and R. Roberts (1972). In *Stress Analysis and Growth of Cracks, Proceedings of the 1971 National Symposium on Fracture Mechanics, Part I, ASTM STP 513*. American Society for Testing and Materials. p. 230-259.

Wallhead, I. R. and L. Edwards (1993). Engineering Fracture Mechanics **46**(3), p. 537-540.

Wallhead, I. R., S. Güngör and L. Edwards (1994). Optics and Lasers in Engineering **20**, p. 109-133.

Westergaard, H. M. (1939). Journal of Applied Mechanics, **61**, p A49.

Wheeler, O. E. (1972). Journal of Basic Engineering, **94**, p. 181-186.

Willenbourg, J. R., M. Engle and H. A. Wood (1971). AFFDL-TM-FBR-71-1.

Williams, M. L. (1957). Journal of Applied Mechanics, **24**, p. 109-114.

Zaiken, E. and R. O. Ritchie (1984). Scripta Metallurgica **18**, p. 847-850.

Zaiken, E. and R. O. Ritchie (1985). Engineering Fracture Mechanics **22**(1), p. 35-48.

Zehnder, A. T. and A. J. Rosakis (1986). International Journal of Fracture **30**, p. R43-R48.

Zehnder, A. T. and A. J. Rosakis (1990). Journal of Applied Mechanics **57**(3), p. 618-626.

Zhang, Y. and K. Ravi-Chandar (1991). Optics and Lasers in Engineering **14**(2), p. 71-83.

Zhilkin, V. A., V. P. Tyrin and L. A. Sheffer (1990). Industrial Laboratory-USSR **56**(12), p. 1484-1488.